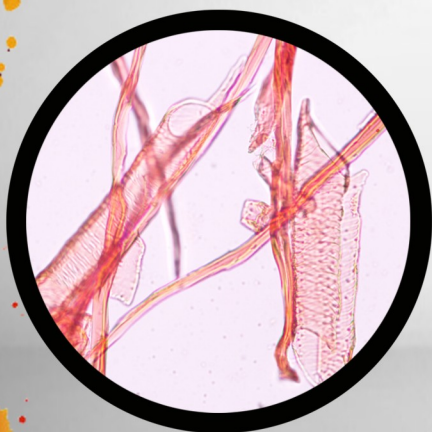


Efectos del **déficit hídrico** sobre el **flujo de savia**  
y la **conductancia estomática** en frutales



TITULO: *Efectos del déficit hídrico sobre el flujo de savia y la conducta estomática en frutales.*

AUTOR: *Álvaro López Bernal*

---

© Edita: Servicio de Publicaciones de la Universidad de Córdoba. 2015  
Campus de Rabanales  
Ctra. Nacional IV, Km. 396 A  
14071 Córdoba

[www.uco.es/publicaciones](http://www.uco.es/publicaciones)  
[publicaciones@uco.es](mailto:publicaciones@uco.es)

---

**UNIVERSIDAD DE CÓRDOBA**  
**DEPARTAMENTO DE AGRONOMÍA**



UNIVERSIDAD DE CORDOBA

Programa de doctorado

**Biociencias y ciencias agroalimentarias**

TESIS DOCTORAL

**Efectos del déficit hídrico sobre el flujo de savia y la conductancia  
estomática en frutales**

Effects of water deficits on sap flow and stomatal conductance in fruit trees

Autor

**Álvaro López Bernal**

Dirigido por

**Dr. Francisco J. Villalobos Martín**

Tesis financiada por el programa de formación de personal investigador “Junta para la Ampliación de Estudios” (subprograma JAE-predoc) del Consejo Superior de Investigaciones Científicas (CSIC)

Instituto de Agricultura Sostenible – CSIC

**Marzo 2015**





**TÍTULO DE LA TESIS:** Efectos del déficit hídrico sobre el flujo de savia y la conductancia estomática en frutales

**DOCTORANDO/A:** Álvaro López Bernal

**INFORME RAZONADO DEL/DE LOS DIRECTOR/ES DE LA TESIS**

(se hará mención a la evolución y desarrollo de la tesis, así como a trabajos y publicaciones derivados de la misma).

El Dr. **Francisco J. Villalobos Martín**, Catedrático de la Universidad de Córdoba, adscrito al Instituto de Agricultura Sostenible del CSIC, como director de la Tesis Doctoral titulada “EFECTOS DEL DÉFICIT HÍDRICO SOBRE EL FLUJO DE SAVIA Y LA CONDUCTANCIA ESTOMÁTICA EN FRUTALES” realizada por **Álvaro López Bernal**,

**INFORMA QUE:**

- Dicha Tesis Doctoral ha sido realizada bajo mi dirección
- Ha tenido como principal objetivo estudiar la potencialidad de los sistemas de medida del flujo de savia para el estudio de las relaciones hídricas en árboles frutales, identificando limitaciones metodológicas de dichos sistemas y desarrollando nuevas metodologías que complementan la información que aportan sobre el estado hídrico.
- Tanto la aproximación experimental, los resultados y las conclusiones que se derivan son de relevancia para los usuarios de los sistemas de medida del flujo de savia.

- En su etapa predoctoral, Álvaro López Bernal ha colaborado en numerosas líneas de trabajo, algunas desarrolladas expresamente en su Tesis Doctoral y otras en otros Proyectos de Investigación del grupo en los que él se ha incorporado. De estos trabajos se han derivado las siguientes publicaciones, indicándose con asterisco las directamente relacionadas con los objetivos de su Tesis Doctoral:

Revistas incluidas en el Science Citation Index:

1. **López-Bernal A**, Alcántara E, Testi L, Villalobos FJ (2010) Spatial sap flow and xylem anatomical characteristics in olive trees under different irrigation regimes. *Tree Physiol* 30:1536-1544.
- 2\*. **López-Bernal A**, Testi L, Villalobos FJ (2012) Using the compensated heat pulse method to monitor trends in stem water content in standing trees. *Tree Physiol* 32:1420-1429.
3. Villalobos FJ, Testi L, Orgaz F, García-Tejera O, **López-Bernal A**, González-Dugo MV, Ballester-Lurbe C, Castel JR, Alarcón-Cabañero JJ, Nicolás-Nicolás E, Girona J, Marsal J, Fereres E (2013) Modelling canopy conductance and transpiration of fruit trees in Mediterranean areas: a simplified approach. *Agric For Meteorol* 171:93-103.
- 4\*. **López-Bernal A**, Alcántara E, Villalobos FJ (2014) Thermal properties of sapwood of fruit trees as affected by anatomy and water potential: errors in sap flux density measurements based on heat pulse methods. *Trees* 28:1623-1634.
5. Tejado I, Vinagre BM, Torres D, **López-Bernal A**, Villalobos FJ, Testi L, Podlubny I. Fractional approach for estimating sap velocity in trees. *Fract Calc Appl Anal* 18:479-494.
- 6\*. **López-Bernal A**, García-Tejera O, Testi L, Orgaz F, Villalobos FJ. Low winter temperatures induce a disturbance of water relations in field olive trees. *Trees*, en impresión.

7\*. **López-Bernal A**, García-Tejera O, Vega V, Hidalgo JC, Testi L, Orgaz F, Villalobos FJ. Using sap flow measurements to estimate the effects of water stress on net assimilation in fruit orchards. *Irrig Sci*, en revision.

Aportaciones a Congresos Internacionales:

8. Villalobos FJ, Alcántara E, Testi L, **López-Bernal A** (2010) Spatial sap flow and xylem anatomical characteristics in olive trees under different irrigation regimes. *XXVIII International Horticultural Congress*, Lisbon, Portugal, 22-27 August 2010.

9\*. **López-Bernal A**, Testi L, Villalobos FJ (2012) Using the compensated heat pulse method to monitor the stem water content in standing trees. *XII Congress of the European Society for Agronomy*, Helsinki, Finland, 20-24 August 2012.

10. Villalobos FJ, Tejado I, **López-Bernal A**, Torres D, Testi L, Vinagre BM, Podlubny I (2013) Measurement of sapwood water content using the compensated heat pulse technique. *IXth International Workshop on Sap Flow*, Ghent, Belgium, 4-7 June 2013.

11. **López-Bernal A**, Testi L, Villalobos FJ (2013) Oscillations in transpiration in young potted olive trees. *IXth International Workshop on Sap Flow*, Ghent, Belgium, 4-7 June 2013.

12. Tejado I, HosseinNia SH, Torres D, Vinagre BM, **López-Bernal A**, Villalobos FJ, Testi L, Podlubny I (2014) Fractional models for measuring sap velocities in trees. *International Conference on Fractional Differentiation and its Applications (ICFDA14)*, Catania, Italy, 23-25 June 2014.

13. García-Tejera O, **López-Bernal A**, Orgaz F, Villalobos FJ, Testi L (2014) Root distribution under different irrigation regimes. *XIIIth Congress of the European Society for Agronomy*, Debrecen, Hungary, 20-24 August 2014.

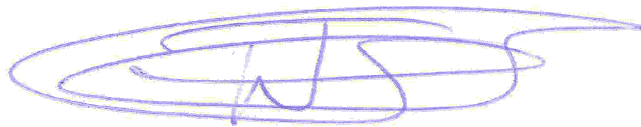
14. **López-Bernal A**, García-Tejera O, Orgaz F, Testi L, Villalobos FJ (2014) Olive bud dormancy is induced by low temperatures. *XIIIth Congress of the European Society for Agronomy*, Debrecen, Hungary, 20-24 August 2014.

- Considero que el trabajo realizado cumple con los requisitos necesarios para su presentación y lectura.

Por todo ello, se autoriza la presentación de la Tesis Doctoral.

Córdoba, 18 de Marzo de 2015

Firma del director



Fdo.: Francisco Javier Villalobos Martín



## Tesis por compendio de artículos

Esta tesis cumple el requisito establecido por la Universidad de Córdoba para su presentación como compendio de artículos, consistente en un mínimo de 3 artículos publicados o aceptados en revistas incluidas en los tres primeros cuartiles de la relación de revistas del ámbito de la especialidad y referenciadas en la última relación publicada por el Journal Citations Report (SCI):

1. **López-Bernal A**, Testi L, Villalobos FJ (2012) Using the compensated heat pulse method to monitor trends in stem water content in standing trees. *Tree Physiol* 32:1420-1429

Datos de 2012 (JCR): índice de impacto 2.853, índice de impacto de los últimos 5 años 3.131, posición 2/62 y 1º cuartil en el área temática de *Forestry*.

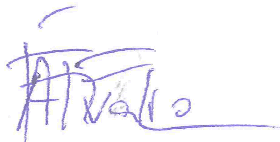
2. **López-Bernal A**, Alcántara E, Villalobos FJ (2014) Thermal properties of sapwood of fruit trees as affected by anatomy and water potential: errors in sap flux density measurements based on heat pulse methods. *Trees* 28:1623-1634.

Datos de 2013 (JCR): índice de impacto 1.869, índice de impacto de los últimos 5 años 2.154, posición 11/64 y 1º cuartil en el área temática de *Forestry*.

3. **López-Bernal A**, García-Tejera O, Testi L, Orgaz F, Villalobos FJ. Low winter temperatures induce a disturbance of water relations in field olive trees. *Trees*, en impresión.

Datos de 2013 (JCR): índice de impacto 1.869, índice de impacto de los últimos 5 años 2.154, posición 11/64 y 1º cuartil en el área temática de *Forestry*.

El doctorando



Fdo.: Álvaro López Bernal



## **Agradecimientos**

Mis primeras palabras de agradecimiento van para mi director, Francisco Villalobos, por introducirme en el mundo de la ciencia, por darme la oportunidad de realizar la presente tesis doctoral bajo su tutela, por ser capaz de encontrar nuevos enfoques e ideas incluso cuando parecía encontrarme en “callejones sin salida” y por infundirme optimismo y tranquilidad. Sin sus contribuciones y confianza, este trabajo habría sido imposible.

Una mención especial merecen, Francisco Orgaz y Luca Testi, que han actuado como "codirectores virtuales", ayudándome en el diseño de los experimentos, la discusión de resultados y el revisión de los escritos. Esteban Alcántara realizó también aportaciones muy importantes en uno de los capítulos, y siempre me ha guardado un sitio en su laboratorio para realizar determinaciones anatómicas.

Para Ignacio Calatrava, José Luis Vázquez y Rafael del Río sólo tengo palabras de alabanza por su trabajo técnico impecable, valiosos consejos, ayuda en los trabajos de campo y por los buenos momentos juntos. Además José Luis Vázquez es el artífice de la portada de este trabajo.

Omar García también tiene, por derecho propio, un lugar importante en estas líneas. Por desempeñar un papel fundamental en las medidas de campo, por su inquietud a la hora de compartir ideas y por su buena disposición a colaborar siempre que ha estado en su mano, Omar se ha convertido en el mejor compañero posible y en un gran amigo.

Aparte de los arriba nombrados, son muchos los compañeros y amigos que, como Rocío Calderón, Elías Fereres, Carmen Ruz, Alberto Hornero, Victorino Vega, Juan Carlos Hidalgo, José Manuel Cabezas u Oscar Pérez, han puesto su granito de arena para ayudarme o hacerme las cosas más fáciles en algún momento.

Además, no quiero dejar de mencionar el valor intangible que para mí ha tenido el buen ambiente en el entorno en el que he trabajado, aspecto que además de a los arriba mencionados debo agradecer a muchas personas, destacando a Marga García, Manuela Medina, Luis Ahumada, Pablo Elorza, Manolo López, Manolo González, David Moldero, María Burguet, Lola García, Carlos Lemus, Manuel Morales, Mercedes Maldonado,

Mónica Espadafor, Thais Aznar, Rafaela Gutiérrez, Tadeo Bellot, Alfredo Gómez, Carmen Ozuna, Mariluz Guillén y Facundo Vita. Finalmente, quiero agradecer el apoyo incondicional de mis amigos ajenos al IAS, así como el de mis padres y el de mis dos hermanos; muy especialmente a estos últimos por el "kidney power".

## Table of contents

List of figures .....	i
List of tables .....	vi
List of symbols .....	viii
List of abbreviations .....	xi
Summary .....	xii
Resumen .....	xiii
Chapter 1: General introduction .....	1
1.1. Why sap flow sensors can be useful in an agronomical context ..	2
1.2. An overview of sap flow methods and their working principles..	5
1.3. Theoretical and practical limitations of heat pulse sap flow methods .....	10
1.4. Water stress detection using sap flow sensors.....	12
1.5. Using sap flow sensors to assess the occurrence of chilling stress in field trees .....	14
1.6. Objectives and outline of the thesis.....	15
References .....	18
Chapter 2: Using sap flow measurements to estimate the effects of water stress on net assimilation in fruit orchards .....	26
Summary .....	27
2.1. Introduction .....	28
2.2. Materials and methods.....	29
2.2.1. Theoretical framework .....	29
2.2.2. Experimental site .....	30

2.2.3. Sap flow measurements .....	32
2.2.4. Comparison with eddy covariance measurements .....	34
2.2.5. Other measurements and calculations.....	35
2.3. Results.....	36
2.3.1. Seasonal changes in weather conditions and irrigation applied.....	36
2.3.2. Comparison with eddy covariance measurements .....	37
2.3.3. Responses of $A$ and classical water status indicators to long- term deficit irrigation .....	38
2.4. Discussion.....	42
2.4.1. Methodological issues: sensitivity to changes in $C_a$ and water stress.....	42
2.4.2. Comparisons with eddy covariance measurements and literature data .....	45
2.4.3. Comparison with classical indicators of water status .....	47
2.4.4. Final remarks .....	48
Acknowledgements.....	49
References.....	50

Chapter 3: Using the compensated heat pulse method to monitor trends in stem water content in standing trees .....	54
Summary .....	55
3.1. Introduction.....	57
3.2. Material and Methods .....	59
3.2.1. Theoretical framework of VSH-CHP.....	59
3.2.2. Lab experiments.....	62
3.2.3. Field experiments.....	64
3.3. Results.....	66

3.3.1. Lab experiments .....	66
3.3.2. Field experiments .....	70
3.4. Discussion .....	73
3.4.1. Lab experiments .....	73
3.4.2. Influence of anisotropy on VSH-CHP methodology .....	76
3.4.3. Field experiments .....	78
3.5. Conclusions .....	80
Acknowledgments .....	81
References .....	82

Chapter 4: Thermal properties of sapwood of fruit trees as affected by anatomy and water potential: errors in sap flux density measurements based on heat pulse methods .....	86
Summary .....	87
4.1. Introduction .....	88
4.2. Materials and methods.....	90
4.2.1. Experiment 1 .....	91
4.2.1.1. Measurements of basic density ( $\rho_d$ ), $F_s$ , $F_w$ and $F_g$ .....	91
4.2.1.2. Determination of thermal properties.....	91
4.2.1.3. Anatomical measurements.....	94
4.2.2. Experiment 2 .....	95
4.2.2.1. Desorption curves.....	95
4.2.2.2. Theoretical analysis of errors in $J$ measurements by CHP, CAG and Sapflow+ as a function of $\Psi$ .....	96
4.2.2.3. Theoretical analysis of errors in $J$ measurements by HR as a function of $\Psi$ .....	97
4.2.2.4. Theoretical analysis of errors in $J$ measurements by Tmax as a function of $\Psi$ .....	98

4.2.2.5. Application to a field case.....	98
4.3. Results.....	100
4.3.1. Experiment 1 .....	100
4.3.2. Experiment 2 .....	105
4.4. Discussion.....	110
4.4.1. Characterisation of thermal properties and their determining factors.....	110
4.4.2. Contrast of methodologies for determining sapwood thermal properties.....	111
4.4.3. Experiment 2: Implications of sapwood water potential variations for sap flux density measurements .....	113
4.5. Conclusions.....	116
Acknowledgements.....	118
References.....	119

Chapter 5: Low winter temperatures induce a disturbance of water relations in field olive trees.....	122
Summary .....	123
5.1. Introduction.....	124
5.2. Materials and methods .....	126
5.2.1. Experimental site.....	126
5.2.2. Measurements .....	127
5.2.3. Determination of stomatal conductance.....	129
5.2.4. Determination of hydraulic resistances.....	129
5.2.5. Water balance.....	130
5.3. Results.....	131
5.4. Discussion.....	140



5.5. Conclusions .....	146
Acknowledgements .....	148
References .....	149
Chapter 6: General discussion and final remarks .....	156
6.1. General discussion.....	157
6.2. Conclusions .....	165
References .....	168
Other scientific contributions .....	174



## List of figures

**Figure 2.1.** Daily values of reference evapotranspiration ( $ET_0$ , black line) and rainfall (grey bars) (panels **A-C**) and evolution of the cumulative irrigation applied to the treatments (CI = control, FI = farm irrigation, RDI = deficit irrigation) (panels **D-F**) during the three years of experiment.

**Figure 2.2.** Seasonal course of net ecosystem exchange (NEE, black solid line), estimated net assimilation ( $A$ , gray solid line) and vapour pressure deficit (VPD, dotted line) for the summer of 2011. NEE was determined with an eddy covariance system placed in the centre of the orchard while values of  $A$  were deduced from the sap flow records of the two farm trees in the separate experimental plot. In all cases values correspond to daytime means.

**Figure 2.3.** Plot of estimated net assimilation ( $A$ ) versus net ecosystem exchange (NEE), deduced from sap flow and eddy covariance systems, respectively. Data correspond to daily values from 24 June 2011 (DOY 175) to 27 September 2011 (DOY 175). Dotted line indicates the 1:1 line.

**Figure 2.4.** Time course of predawn (closed symbols) and midday (open symbols) shoot water potential ( $\Psi$ , panels **A-C**), calibrated transpiration ( $E_p$ , panels **D-F**), estimated net assimilation ( $A$ , panels **G-I**) and maximum trunk diameter (MXTD, panels **J-L**) for the three irrigation treatments (CI = control, FI = farm irrigation, RDI = deficit irrigation) during the three years of experiment (left, middle and right panels correspond to 2011, 2012 and 2013, respectively).

**Figure 2.5.** Course of net assimilation ( $A$ ) estimated for the deficit irrigation (RDI) and the farm treatments (FI) in relation to that of the

control (CI) throughout the three years of experiment (i.e. ratio of either RDI or FI values to those of CI).

**Figure 2.6.** Diurnal time course (4 August 2011, DOY 216) of air CO<sub>2</sub> concentration ( $C_a$ , dotted line) and estimated net assimilation ( $A$ ) calculated either assuming (grey solid line) or not (black solid line) a variable  $C_a$ . In the former case a fixed value of 380  $\mu\text{mol mol}^{-1}$  was assumed for  $C_a$ . Data on  $A$  correspond to the average of the two control trees.

**Figure 3.1.** Evolution of sapwood water content values estimated by VSH-CHP methodology ( $F_{w,est}$ , solid line) and those gravimetrically obtained ( $F_{w,obs}$ , dashed line) during the drying process. The results correspond to one of the monitored wooden blocks of fig (Block 6).  $F_{w,est}$  values show a step reduction in parallel with those of  $F_{w,obs}$  followed by an stabilization which is not found for the gravimetric data.

**Figure 3.2.** Comparisons between sapwood water content values calculated by VSH-CHP methodology ( $F_{w,est}$ ) and those gravimetrically obtained ( $F_{w,obs}$ ) for each lab experiment showing the variability among individual sensors. Dashed line correspond to the 1/1 line and each symbol represent a sensor.

**Figure 3.3.** Apparent dielectric constant versus gravimetric wood water content ( $F_{w,obs}$ ). Data were obtained from the olive wooden blocks 16, 17, 18 and 19 which were equipped with TDR probes.

**Figure 3.4.** Temporal variation in the estimated stem water content ( $F_{w,est}$ ) in olive tree trunks under different irrigation regimes (CI: control, solid line; CDI: continuous deficit irrigation, dotted line; RDI: regulated deficit irrigation, dashed line) based on the VSH-CHP methodology. Data correspond to the mean of four trees for CDI and RDI treatments, and of

two for the control one. All trees were monitored by two sensors each at a height of 30 cm over the soil.

**Figure 3.5.** Temporal variation in the relative tree  $F_{w,est}$  (top) and sap flow (bottom) of CDI (solid line) and RDI (dotted line) olive tree trunks referred to the control (i.e. the ratio between the value of either the CDI or RDI treatments and that of the control one) based on the VSH-CHP methodology. The values employed to obtain this graph include data from 4 CI, 6 CDI and 6 RDI trees which were monitored by two sensors each at a height of 30 cm over the soil.

**Figure 4.1. A** Volumetric fraction of sapwood occupied by solid ( $F_s$ ), liquid ( $F_w$ ) and gas ( $F_g$ ) for the studied species. **B** Volumetric fraction of sapwood occupied by fibres, rays, axial parenchyma and vessels for the studied species. Oe=olive, Pd=almond, Cs=sweet orange, Ca=bitter orange, Pg=pomegranate, Dk=kaki, Fc=fig.

**Figure 4.2. A** Axial and tangential thermal conductivities ( $K_x$  and  $K_y$ ), **B** anisotropy ratio ( $R_K$ ) and volumetric specific heat ( $\rho c$ ) for the studied species. Values were estimated following the Vandegehuchte and Steppe (2012) approach. Error bars showing standard errors are present for those species in which several trees were studied. Oe=olive, Pd=almond, Cs=sweet orange, Ca=bitter orange, Pg=pomegranate, Dk=kaki, Fc=fig.

**Figure 4.3.** Plot of axial and tangential thermal conductivities ( $K_x$ , closed symbols and  $K_y$ , open symbols) estimated by both Siau (1971) (Eqs. 4.3 and 4.4),  $T_{max}$  (combining Eqs. 4.7 and 4.8) and Knight et al. (2012) approaches versus those obtained from Eqs. 4.5 and 4.6 (Vandegehuchte and Steppe 2012) (**A**, **B** and **C** panels, respectively). Each point represents one experimental tree. Dotted line indicates the 1:1 line.

**Figure 4.4.** Desorption curves for sapwood of olive (**A**), sweet orange (**B**), almond (**C**) and fig (**D**) trees. Closed symbols correspond to points in which water potential ( $\Psi$ ) was measured using a WP4-T dewpoint potentiometer while open symbols were obtained from measurements of  $\Psi$  at predawn and midday in non transpiring shoots with a pressure chamber. Sample water content ( $F_w$ ) was always gravimetrically determined (in the latter case from cores extracted at the same time that  $\Psi$  was measured).

**Figure 4.5.** Relative error in sap flux density ( $E_j$ ) of compensated heat pulse (CHP), calibrated average gradient (CAG), sapflow+ (those three in solid line), heat ratio (HR, dashed line) and Tmax (dotted line) methods in the sapwood of olive (**A**), sweet orange (**B**), almond (**C**) and fig (**D**) as a function of water potential ( $\Psi$ ).

**Figure 4.6. A** Seasonal course of midday sapwood water potential ( $\Psi$ ) for the control (CI, closed symbols) and deficit irrigation (RDI, open symbols) treatments. **B** Seasonal relative errors in sap flux density ( $E_j$ ) in relation to heat pulse method (circles for CHP and CAG, and triangles for HR) and irrigation treatment. The water applied to RDI was 30 % of that of CI from DOY 182 to DOY 243 and the same as CI for the rest of the season.

**Figure 5.1.** Maximum ( $T_{max}$ ) and minimum ( $T_{min}$ ) daily temperatures and daily precipitation recorded by a meteorological station during the experiments in 2011-2012 (**A**) and 2012-2013 (**B**) winters.

**Figure 5.2.** Patterns of midday vapor pressure deficit (VPD; solid line) and relative soil water content (RSWC; dotted line with circles) (**A** and **B**), predawn (closed symbols) and midday (open symbols) stem water potentials ( $\Psi$ ; **C** and **D**), sap flow rate normalized by cross-sectional sapwood area ( $Q_n$ ; **E** and **F**), midday bulk canopy stomatal conductance ( $G_s$ ; **G** and **H**), and calculated hydraulic resistances ( $R$ ; **I** and **J**) for the days

of measurement in both the winters 2011-2012 (left panels) and 2012-2013 (right panels). The complete time course is presented for both  $G_s$  and  $D$  panels excluding those days with rainfall  $>0.3$  mm. In  $\Psi$ ,  $Q_n$  and  $R$  panels, data are means  $\pm$  standard errors ( $n=5$  in 2011-2012 and  $n=4$  in 2012-2013) of all monitored trees. Lowercase letters in panels A, B, C, D, I and J denote statistically significant ( $P < 0.05$ ) differences between dates.

**Figure 5.3.** Daily shoot water potential ( $\Psi$ ) as a function of sap flow rate normalized by cross-sectional sapwood area ( $Q_n$ ) for the five days of measurement in the 2012-2013 season. The points represent the averaged values of the four instrumented trees for each simultaneous measurement of  $Q_n$  and  $\Psi$ . Vertical and horizontal error bars correspond to standard errors.

**Figure 5.4.** Diurnal course of shoot water potential ( $\Psi$ ; **A**), sap flow rate normalized by cross-sectional sapwood area ( $Q_n$ ; **B**) and bulk canopy stomatal conductance ( $G_s$ ; **C**) for both a winter (29-January-2013, closed symbols) and a spring date (12-April-2013, open symbols). Values are the averaged values of the four instrumented trees. Standard errors are represented by the error bars in the case of **A** and avoided in the rest for the sake of clarity.

**Figure 5.5.** Temporal variation of both the whole soil-plant continuum hydraulic resistance ( $R$ ; solid lines, closed symbols) and the soil-to-trunk hydraulic resistance ( $R_{root}$ ; dashed lines, open symbols) in 2011-2012 (circles) and 2012-2013 (triangles) seasons. In the former season the results correspond to the average of the two trees in which measurements of  $\Psi$  were performed in non-transpiring shoots.

**Figure 5.6.** Time course of apparent root sap viscosity ( $\eta$ , solid line) and midday soil temperature (dotted line) through the 2012-2013 season.

## List of tables

**Table 1.1.** Overview of heat-pulse sap flow methods, indicating the range of flows in which they are applicable and some relevant comments

**Table 3.1.** Species, installed devices and drying temperature for each of the wooden blocks examined in lab experiments.

**Table 3.2.** Linear regressions relating the sapwood water content calculated by VSH-CHP methodology to that gravimetrically estimated considering only the first phase of the drying process. Accordingly, only the data with  $F_{w,obs}$  greater than 0.75 of the initial value of  $F_{w,obs}$  were taken into account.

**Table 3.3.** Range of  $F_{w,obs}$ ,  $F_{w,est}$  and  $F_{w,corr}$  between the extremes considered in the linear regression analysis for each sample. The values of  $\delta$  needed to calculate  $F_{w,corr}$  are also shown and they were estimated using the equations of Siau (1971) and Vandegehuchte and Steppe (2012c).

**Table 4.1.** Values of thermal properties (axial and tangential thermal conductivities,  $K_x$  and  $K_y$ ; anisotropy ratio,  $R_K$ ; volumetric specific heat,  $\rho c$ ; axial and tangential thermal diffusivities,  $D_x$  and  $D_y$ ) in relation to the methodology applied. All values correspond to the average of all experimental trees.

**Table 4.2.** Predawn and midday water potentials ( $\Psi$ ) on a sunny day of midsummer (DOY 234) for the control (CI) and deficit irrigation treatments (RDI). Relative errors in sap flux density ( $E_J$ ) at daily scale are estimated for different heat-pulse based methods taking the estimated predawn values of  $F_w$  and  $D_x$  as references (Eqs. 4.9 and 4.10).

**Table 5.1.** Maximum increases in hydraulic resistance ( $\Delta R$ , in n-folds increases) observed in the literature for woody species exposed to different



temperature treatments. Equation 5.1 was applied to deduce the viscosity increments ( $\Delta\eta$ , in n-folds). Data from the present study are presented in the last two rows allowing comparisons. Values of  $\eta$  for the 2012-2013 season were estimated from midday soil temperature measurements

**Table 6.1.** Strengths and weaknesses of the available methods for estimating  $F_w$  using sap flow sensors.

## List of symbols

$a$	Empirical coefficient
$A$	Bulk net assimilation
$b$	Empirical coefficient
$C_a$	CO <sub>2</sub> concentration in the leaf boundary layer
$C_i$	CO <sub>2</sub> concentration in the substomatal cavity
$c_s$	Specific heat capacity of the wood matrix
$c_w$	Specific heat capacity of water
$D$	Thermal diffusivity
$D_x$	Thermal diffusivity in the axial (flow) direction
$D_y$	Thermal diffusivity in the tangential (lateral) direction
$E_J$	Relative error in the determination of $J$
$E_p$	Plant transpiration
$E_{p,est}$	Modeled transpiration
$ET$	Evapotranspiration
$ET_0$	Reference evapotranspiration
$f$	Fraction of intercepted PAR
$F_g$	Volumetric fraction of gas in sapwood
$F_s$	Volumetric fraction of solids in sapwood
$F_{V,FSP}$	Volumetric sapwood water content at fiber saturation point
$F_w$	Volumetric fraction of liquid in sapwood
$F_{w,corr}$	$\theta_c$ corrected by anisotropic effects
$F_{w,est}$	Stem water content estimated with VSH-CHP
$F_{w,obs}$	Gravimetric stem water content
$G_c$	Bulk stomatal conductance to CO <sub>2</sub>
$G_s$	Bulk stomatal conductance to H <sub>2</sub> O
$H$	Heat input from heat pulse
$I$	Irrigation applied
$J$	Sap flux density
$k$	Empirical coefficient
$K$	Thermal conductivity
$K_x$	Thermal conductivity in the axial (flow) direction
$K_w$	Thermal conductivity of water
$K_y$	Thermal conductivity in the tangential (lateral) direction
$L_i$	Distance to the heater in the “i” direction
$P$	Atmospheric pressure

$P_{\text{eff}}$	Effective precipitation
$Q$	Sap flow rate
$Q_n$	Sap flow rate normalized by cross-sectional xylem area
$R$	Hydraulic resistance of the water pathway from soil to shoots
$R_K$	Ratio of axial to tangential thermal conductivity
$R_{\text{root}}$	Hydraulic resistance of the water pathway from soil to trunk
$R_{\text{sd}}$	Total daily solar radiation
$t$	Time from heat pulse emission
$T$	Temperature
$t_0$	Time from heat pulse emission until $\Delta T$ returns to its initial value
$T_1$	Temperature in the downstream probe of a CHP sensor
$T_2$	Temperature in the upstream probe of a CHP sensor
$t_m$	Time for the maximum temperature rise after heat pulse emission
$t_n$	Time for $\Delta T$ to reach the minimum value from heat pulse emission
$t_p$	Heat pulse duration
$V$	Fresh volume
$v_h$	Convective heat pulse velocity
$w_d$	Dry weight
$w_f$	Fresh weight
$x$	Axial distance from a temperature probe to the heater
$x_1$	Distance from the downstream probe to the heater in a CHP sensor
$x_2$	Distance from the upstream probe to the heater in a CHP sensor
$\beta$	Ratio of $C_i$ to $C_a$
$\delta$	Square root of $R_K$
$\Delta R$	Seasonal change in $R$ estimated in relative terms as the ratio of winter values to those of spring
$\Delta R_{\text{root}}$	Seasonal change in $R_{\text{root}}$ estimated in relative terms as the ratio of winter values to those of spring
$\Delta T$	Temperature difference between down- and up-stream probes
$\Delta T_a$	Averaged $\Delta T$ in the 170 s following a heat pulse

$\Delta\eta$	Seasonal change in $\eta$ estimated in relative terms as the ratio of winter values to those of spring
$\Delta\Psi$	Water potential gradient
$\varepsilon$	Apparent dielectric constant
$\eta$	Viscosity of xylem sap
$\rho_{cw}$	Basic density of cell walls
$\rho_d$	Basic density of sapwood
$\rho_w$	Basic density of liquid water
$\rho c$	Volumetric specific heat
$\Psi$	Water potential
$\Psi_{ref}$	Reference water potential
$\Psi_{soil}$	Soil water potential
$\Psi_{trunk}$	Trunk xylem water potential

## List of abbreviations

CAG	Calibrated average gradient
CDI	Continuous deficit irrigation treatment
CHP	Compensated heat pulse
CI	Control irrigation treatment aimed to supply enough water to keep maximum <i>ET</i>
DI	Deficit irrigation
DOY	Day of year
FI	Farm irrigation treatment
GMT	Greenwich Mean Time
HFD	Heat field deformation
HR	Heat ratio
LVDT	Linear variable differential transducer
MXTD	Daily maximum trunk diameter
NEE	Net ecosystem exchange
PAR	Photosynthetically active radiation
RDI	Regulated deficit irrigation treatment
RSWC	Relative soil water content
SHB	Stem heat balance method
SPAC	Soil plant atmosphere continuum
SWC	Soil water content
TD	Thermal dissipation
TDR	Time domain reflectometry
TDV	Trunk diameter variation
THB	Trunk sector heat balance
Tmax	Tmax method
VPD	Vapor pressure deficit
VSH-CHP	Volumetric specific heat – Compensated heat pulse method

## **Summary**

Sap flow sensors based on heat pulse techniques enable a semi-continuous estimation of transpiration, which makes them promising devices for studying water relations in woody species. Furthermore, high expectations have been created for the role that these sensors might play in the development of irrigation scheduling strategies in fruit trees. The general objective of this thesis is to contribute to explore the full potential and limitations of heat pulse techniques, illustrating how they can yield information both about water relations and the effects of water stress on tree functioning. As first outputs, new methodologies to estimate net assimilation at the canopy level and xylem water content dynamics from sap flow measurements are presented. The validity of such methodologies was tested on several experiments, some of them carried out in mature olive orchards under different irrigation regimes. Besides, this thesis assesses the extent to which the accuracy of heat pulse techniques are compromised both by changes in xylem water content and by the method applied to determine its thermal properties. Finally, based on sap flow and water potential measurements conducted in a mature olive orchard during two consecutive winters, it is evidenced that chilling temperatures lead to a disturbance in water relations similar to those occurring under drought stress conditions in that species.

## **Resumen**

Los sensores de flujo de savia basados en técnicas de pulso de calor permiten obtener estimas casi continuas de la transpiración, lo que los convierte en dispositivos prometedores para el estudio de relaciones hídricas en especies leñosas. Además, se han creado grandes expectativas sobre el papel que estos sistemas podrían jugar en el desarrollo de estrategias de programación de riego en árboles frutales. El objetivo general de esta tesis es contribuir a explorar el máximo potencial y las limitaciones de las técnicas de pulso de calor, ilustrando como éstas pueden proporcionar información sobre las relaciones hídricas y el efecto del déficit hídrico en el funcionamiento de los árboles. Como primeras aportaciones, se presentan dos nuevas metodologías que permiten estimar la asimilación neta a nivel de cubierta y la dinámica del contenido de agua del xilema a partir de medidas de flujo de savia. La validez de dichas metodologías fue analizada en varios experimentos, algunos de ellos llevados a cabo en olivares adultos bajo distintos regímenes de riego. Por otra parte, esta tesis evalúa el grado en el que la precisión de las técnicas de pulso de calor se ven comprometidas por cambios en el contenido de agua del xilema y el método aplicado para determinar sus propiedades térmicas. Finalmente, en base a medidas de flujo de savia y potencial hídrico realizadas durante dos inviernos consecutivos en un olivar adulto, se evidencia que las bajas temperaturas resultan en alteraciones en las relaciones hídricas que se asemejan a las que ocurren en condiciones de sequía en esa especie.









# **Chapter 1**

## **General introduction**

---

## **Chapter 1**

### **General introduction**

#### **1.1. Why sap flow sensors can be useful in an agronomical context**

Irrigated agriculture play an undeniable role for the sustenance of human life. Globally, food production from irrigation represents >40 % of the total and uses only about 17 % of the land area devoted to agriculture (Feres and Connor 2004). However, the improvement of crop yields associated to irrigation presents a high cost in terms of water applied, which makes irrigated agriculture being the largest single consumer of freshwater on the planet by far. Thus, in arid and semiarid zones the proportion of water allocated for agriculture is estimated to exceed 70 % of the total (Feres and Soriano 2007). In the coming decades, the forecast global population growth will not only increase the demand for food, but also will result in a higher proportion of water destined to satisfy the needs of the urban, industrial and environmental sectors. Global climate change might further exacerbate the competition for water through the likely increase in temperature and changes in annual rainfall amounts and regional distribution patterns (IPCC 2007). In view of the simultaneous expectations of increasing food demand and decreasing supplies to agriculture, there is an urgent need for a more efficient management of the water resources employed by irrigated systems.

Over the last decades, the modernization of irrigation schemes and the shift from traditional surface towards precision irrigation methods (e.g. drip irrigation) have played a major role in reducing the water requirements in agricultural crops. At the same time, these changes have emphasized the need for new methods of accurate irrigation scheduling and control. For

example, irrigation scheduling was initially developed to supply crops with sufficient water so that the full evapotranspiration requirements were met throughout the season, while in recent years it has become clear that maintaining slight water deficits allows for a more efficient use of water in many crops. The application of water below the full evapotranspiration requirements is termed deficit irrigation (DI) and its main strength lies in the fact that the yield losses associated to the unavoidable water stress-induced reductions in biomass production can be partially compensated by improvements in the partitioning of assimilates to reproductive structures (Feres and Soriano 2007).

Although DI has been satisfactorily tested in a variety of field crops, it is in fruit trees and vines where it has achieved the greatest success. This fact can be explained because the economic return in tree crops is notoriously influenced by quality attributes, which makes total production more decoupled from the farmer's profit in relation to annual crops. Furthermore, the imposition of moderate levels of water stress at certain developmental periods (referred to as regulated deficit irrigation) can result in very low or negligible reductions in yield on the one hand, and both help to control excessive growth and have a positive effect on fruit quality on the other (Uriu and Magness 1971; Chalmers et al. 1981; Goldhamer et al. 2006; Iniesta et al. 2009). Hence, the application of regulated deficit irrigation in fruit tree orchards is regarded as a promising mean to cope with the forthcoming water scarcity landscape.

The implementation of successful DI involves accurate soil moisture or plant water status sensing in order to avoid exceeding critical water stress thresholds at critical time instances. To this end, a variety of sensors and methodologies based on either soil or plant measurements have been developed. The former approaches are thought to be less appropriate than

## *General introduction*

the later because many plant physiological features respond directly to changes in the water status of plant tissues, rather than to changes in bulk soil water content (McCutchan and Shackel 1992; Jones 2004). Moreover, monitoring the rootzone water status under localized irrigation is not an easy task (Feres and Goldhamer 1990). These facts have motivated an intense search for robust plant-based approaches over the last decades.

Perhaps the measurement of leaf or stem water potential ( $\Psi$ ) using the classical pressure chamber method (Scholander et al. 1965) has become the most widely extended plant-based indicator for irrigation scheduling. In fact, it has been applied not only in experimental studies, but also by farmers in commercial orchards (Feres, personal communication). Despite being considered a reference technique for monitoring plant water status, the pressure chamber technique presents considerable limitations including its destructive nature, the high labor requirements in the operation process or the fact that results can vary slightly between users (Jones 2004). As an alternative, new techniques for water stress detection have appeared in recent years. Among them, the indices based on dendrometry, sap flow and hyperspectral and multispectral imagery seem to be the most promising.

The greatest strength of sap flow methods for irrigation scheduling lay in their capacity to provide semi-continuous estimates of sap flow rates ( $Q$ ) which can generally be considered good surrogates of plant transpiration ( $E_p$ ) (Swanson 1994).  $E_p$  is sensitive to water deficits and stomatal closure and, because the outward flow of water via stomatal openings is coupled with the inward flow of carbon dioxide,  $Q$  records indirectly provide information about biomass production. These facts are indicative of the great potential that sap flow methods present for both irrigation scheduling and studying water relations in general. For instance, measures of  $Q$  could

provide useful information to enhance our understanding about the functioning of vascular transport through the xylem (Williams et al. 2001; López-Bernal et al. 2010) or to quantify stomatal conductance to either H<sub>2</sub>O or CO<sub>2</sub> ( $G_s$  or  $G_c$ , respectively) at canopy scale (Villalobos et al. 2013). In addition, sap flow methods can be a valuable tool in the development and calibration of soil-plant-atmosphere continuum (SPAC) models (Swanson 1994; Steppe et al. 2006) or serve as a diagnostic tool for plant diseases caused by vascular pathogens (Yamoaka et al. 1990; Urban and Dvorak 2014).

## **1.2. An overview of sap flow methods and their working principles**

Although the many sap flow methods available to date present different principles, all of them are based on the use of heat as a tracer. Heat transport in the xylem occurs by convection in the flowing sap and by conduction through the sap and the stationary tissue of both sapwood and heartwood, which makes the problem of measuring  $Q$  theoretically complex. All methods deal with such difficulties and address the convective component to estimate  $Q$  (typically expressed in l h<sup>-1</sup>), but they do it through different approaches. Because in-depth information about the particularities of each sap flow method can be easily found in the literature (Swanson 1994; Smith and Allen 1996; Vandegehuchte and Steppe 2013), only a brief description summarizing the main features of the most common sap flow methods is provided below.

Sap flow methods can be classified in two categories, depending on whether the heat is applied continuously or discontinuously through short heat pulses. Both the stem heat balance (SHB, Sakuratani 1981) the trunk sector heat balance (THB, Cermak et al. 1973; 2004), thermal dissipation (TD, Granier 1985; 1987) and the heat field deformation (HFD, Nadezhdina et al. 1998; 2012) methods are included in the former group.

## *General introduction*

On the one hand, both SHB and THB directly derive  $Q$  by solving the heat balance over a continuously heated section of the plant, with the first being the only non-invasive method (and hence suitable for both herbaceous and relatively thin woody stems). Both of them exhibit some limitations as some of the components of the heat balance are difficult to estimate with accuracy (particularly the storage component in the case of large stems - THB) or require zero flow conditions (Smith and Allen 1996). On the other hand, both TD and HFD derive  $Q$  from determinations of sap flux density ( $J$ ,  $\text{cm}^3 \text{cm}^{-2} \text{h}^{-1}$ ) and their bases remain empirical. TD is probably the most widely extended sap flow method because of its simplicity and low cost, but its accuracy is compromised by a variety of issues such as the sensitivity to natural temperature gradients (Do and Rocheteau 2002) and water content variations (Vergeynst et al. 2014), the need for some reference zero flow periods (Granier 1985; 1987) and the uncertainties associated to the position of boundaries between active and inactive xylem (Vandeghuchte and Steppe 2013). HFD overcomes some of the later issues but accurate  $J$  estimates are only obtained using specific calibration equations, as in the case of TD (Vandeghuchte and Steppe 2012a).

Heat pulse methods are perhaps the most suitable for monitoring tree water use in field conditions because they have lower power requirements. Unlike the aforementioned methods, they are based on the fundamental heat conduction-convection equation for porous media presented by Marshall (1958), who was inspired by the works of Carslaw and Jaeger (1947). Many heat pulse methods have been developed over the last decades including the compensated heat pulse (CHP, Swanson and Whitfield 1981), Tmax (Cohen et al. 1981), heat ratio (HR, Burgess et al. 2001), calibrated average gradient (CAG, Testi and Villalobos 2009) and Sapflow+ (Vandeghuchte and Steppe 2012b) methods. The complexity of the instrumentation used by each of these methods varies widely, as well as the equations from which



the convective heat velocity ( $v_h$ ,  $\text{cm}^3 \text{ cm}^{-2} \text{ h}^{-1}$ ) is calculated. As heat pulse methods play a central role in the present thesis, their main features of each one have been summarized in Table 1.1 and a more detailed description is provided below.

**Table 1.1.** Overview of heat-pulse sap flow methods, indicating the range of flows in which they are applicable and some relevant comments

Method	Range	Comments
<b>Tmax</b> (Cohen et al. 1981)	Moderate to high flows	- Instrumentally simple - Needs $D_x$ estimation
<b>Heat ratio</b> (HR; Burgess et al. 2001)	Reverse to moderate flows	- Needs $D_x$ estimation
<b>Compensated heat pulse</b> (CHP; Swanson & Whitfield 1981)	Moderate to high flows	- Low flows are measurable when combined with CAG
<b>Calibrated average gradient</b> (CAG; Testi & Villalobos 2009)	Zero to moderate flows	- Applied in combination with CHP
<b>Sapflow+</b> (Vandegehuchte & Steppe 2012b)	Reverse to high flows	- Instrumentally complex - Estimates $F_w$ at low flows - Not tested in living trees

Of all heat pulse methods, Tmax is the simplest instrumentally, but at expense of a lower robustness. Sensors consist of a temperature probe located downstream from a heater probe. By measuring the time for the maximum temperature rise ( $t_m$ ) after a heat pulse,  $v_h$  can be determined provided axial diffusivity of sapwood ( $D_x$ ) is known (Cohen et al. 1981;

## *General introduction*

Green et al. 2003).  $D_x$  is typically determined from  $t_m$  records at night assuming that  $v_h$  is null before dawn but this procedure is challenged by the occurrence of nocturnal sap flow. Further uncertainties arise because the resulting temperature curves are noisy and slight errors in the determination of  $t_m$  lead to large deviations in the resulting values of  $D_x$  and  $v_h$ .

HR sensors consist of a heater and two temperature probes that are located at equal distances up- and downstream from the heater. According to Burgess et al. (2001),  $v_h$  can be calculated from the temperature increases at given times after heat pulse emission, with  $D_x$  being again present in the working equation. In this method,  $D_x$  is derived from the model of thermal properties of Siau (1971) -recently corrected by Vandegehuchte and Steppe (2012c)- using both dry density ( $\rho_d$ ) and water content ( $F_w$ ) of sapwood as inputs. Such parameters can be easily determined from core sampling measurements. Given a good estimation of  $D_x$ , the HR method has proven its robustness for measuring  $v_h$  in conditions of low or even reverse flows. By contrast, it is unreliable in practice when  $v_h$  is high (Bleby et al. 2008).

CHP systems present similar instrumentation than HR, but in this case the temperature probes are asymmetrically inserted in relation to the heater (i.e. the distance from the downstream probe to the heater is higher than that from the upstream one). Swanson and Whitfield (1981) showed that  $v_h$  is linearly related to the inverse of the time from heat-pulse emission until the temperature difference between the downstream and upstream probes ( $\Delta T$ ) returns to its initial value ( $t_0$ ). As a great advantage over HR and Tmax,  $D_x$  is not present in the working equation of CHP, which only includes  $t_0$  records and the distances from each temperature probe to the heater. Besides that, the method is reliable for measuring from moderate to high  $v_h$  and, contrary to HR, is not suitable for determining low values of  $v_h$ . This

limitation has been overcome by the development of CAG (Testi and Villalobos 2009).

The CAG method uses the same sensor configuration than CHP and is based on the fact that, at low flows,  $v_h$  is linearly correlated with the average temperature difference between the downstream and upstream probes ( $\Delta T_a$ ). Such linear relation can be empirically obtained from data on  $\Delta T_a$  when  $v_h$  is low but still measurable with the CHP working equation (Testi and Villalobos 2009). Hence, the application of CAG allows for extending the measurable domain of  $v_h$  in CHP sensors from zero to high values.

Sapflow+ is the most recently developed heat pulse method (Vandegehuchte and Steppe 2012b). The sensor configuration is that of HR with an additional temperature probe tangentially located in relation to the heater. The corrected heat conduction-convection equations of Vandegehuchte and Steppe (2012d) are fitted to the measured temperature curves enabling the simultaneous estimation of  $v_h$ , volumetric specific heat ( $\rho c$ ) and axial and tangential thermal conductivities ( $K_x$  and  $K_y$ , respectively). From these parameters, both  $F_w$ ,  $D_x$  and thermal diffusivity in the tangential direction ( $D_y$ ) can be theoretically inferred in low flow conditions, which makes the method particularly promising. However, Sapflow+ has not been tested yet in standing trees to our knowledge.

Regardless of the heat pulse method employed, flow path obstruction and wounding reactions originated by the insertion of the probes can lead to large underestimations of  $v_h$ . Generally, this problem is solved by applying polynomial wound correction equations that have been derived from finite element modelling analysis for given sensor configurations (Swanson and Whitfield 1981; Burgess et al. 2001; Green et al. 2003). Once the values of  $v_h$  are corrected, sap flux density can be calculated as:

$$J = (kF_s + F_w)v_h \quad [1.1]$$

where the factor  $k$  is assumed to be 0.441 within and between species for a temperature of 20 °C (Becker and Edwards 1999) and  $F_s$  represents the volumetric solid fraction of sapwood. Typically,  $F_w$  and  $F_s$  are determined from single gravimetric measurements in wooden cores taken at the end of the measurement period. Finally,  $Q$  can be estimated by integrating the values of  $J$  over the conductive xylem area.

### **1.3. Theoretical and practical limitations of heat pulse sap flow methods**

As heat pulse methods move beyond a research tool towards being an instrument that might have potential for irrigation scheduling, understanding the limitations of these techniques becomes essential. Apart from the aforementioned intrinsic restrictions in the measurable range of  $v_h$  that are specific for each method, there is a variety of issues that can affect their accuracy. Such issues make calibration highly recommendable, if not a prerequisite, when good estimates of  $E_p$  are needed; and they appear as a result of:

- Violation of implicit assumptions: the working equations of all heat pulse methods were deduced from the fundamental heat conduction-convection equations presented by Marshall (1958). Such equations present a variety of underlying assumptions which are to some extent unrealistic and, hence, might result in errors in the determinations of  $v_h$ . As first example, the equations of Marshall (1958) are based on the premise that sapwood is an infinite, thermally homogeneous and isotropic medium. In general, there is a general agreement that the first two are not an issue, except, perhaps, in the case of some hardwood species with very low vessel density and non-uniform distribution of xylem elements (e.g. in kiwifruit, according to Green and Clothier 1988). The third one, in turn, implies a

major flaw because sapwood thermal properties are dependent on the direction considered. Fortunately, the methods remain theoretically correct because they are based on derivations of the fundamental equation that rule out any anisotropic aspects. This was evidenced by Vandegehuchte and Steppe (2012d), who also modified Marshall (1958)'s equations to account for the anisotropic nature of sapwood. Further implicit issues arise from the assumptions of both infinitesimal probe diameter and infinitesimal heat pulse duration. While the first one is accounted for by using empirical wound correction equations (Swanson and Whitfield 1981; Green et al. 2003), the second is typically neglected, which may theoretically result in an underestimation of  $v_h$ .

- Incorrect probe installation: precise positioning of the sensor probes is of paramount importance to obtain good estimates of  $v_h$  (Vandegehuchte and Steppe 2013). Using drill-bit templates during sensor installation prevent probe misalignments, but it might still be insufficient at large sapwood depths. Apart from that, additional uncertainties arise in species with spiral patterns of sap ascent (Kozłowski and Winget 1963; Waisel et al. 1972) because flow direction can be difficult to predict.

- Ignoring temporal variations in  $F_w$ : values of  $\rho_d$  and  $F_w$  are required for the conversion of  $v_h$  into  $J$  (Eq. 1), but as they are usually determined from single wood core measurements, the natural seasonal and daily variations of  $F_w$  are disregarded. Such variations can also affect the accuracy of HR and Tmax because they result in fluctuating patterns for  $D_x$ . The magnitude of this issue is specifically addressed in the Chapter 4 of the present thesis.

- Difficulties in the scaling up from  $J$  to  $Q$  and  $E_p$ : heterogeneities in sapwood functioning complicate the estimation of sap flow from  $J$  determinations. On the one hand,  $J$  rates tend to decrease from the outer to the inner portions of xylem implying that measurements should be

performed at several depths if a reliable estimate of sap flow is to be obtained (Fernández et al. 2001; Nadezhdina et al. 2007; González-Altozano et al. 2008). Sensors incorporating several thermocouples along the temperature probes allow both to capture such radial variations and to establish the boundaries between active and inactive xylem. On the other, there is compelling evidence indicating that enormous azimuthal variations in sap flow take place in some tree species (López-Bernal et al. 2010), which challenges the reliability of heat pulse methods for yielding realistic estimates of  $Q$  when a small number of sensors per monitored tree are used. As a final remark, the instant  $Q$  rates are not perfectly coupled with the  $E_p$  ones because stems and leaves are capable to extract/release water from/to the transpiration stream. This complication can be neglected if either sap flow is determined over a sufficiently long period to negate changes in storage (Swanson 1994).

#### **1.4. Water stress detection using sap flow sensors**

The use of sap flow systems as a tool for assessing water status is founded on the grounds that  $G_s$  and  $E_p$  are tightly coupled. Thus, as water stress develops stomata tend to close inducing a decrease in  $G_s$ , which in turn triggers a reduction in  $E_p$  that can be monitored with sap flow methods. However, the direct use of  $E_p$  measurements in irrigation scheduling is challenged because accurate values are only obtained through calibration and due to the strong influence of environmental conditions and canopy size on the resulting records. Both issues complicate the definition of water stress thresholds for triggering irrigation (Jones 2004; Ballester et al. 2013). Given that, the most common approach followed to detect the occurrence of water stress with sap flow methods consist of comparing the course of  $E_p$  in target trees with that of similar plants receiving enough irrigation to ensure no soil water limitations. Such an approach has been successfully applied in

a variety of fruit tree species (Tognetti et al. 2004; Ortuño et al. 2006; Ballester et al. 2013; Cuevas et al. 2013) and even implemented in experimental irrigation scheduling programs (Conejero et al. 2007; Fernández et al. 2008). Nonetheless, using over-irrigated reference trees might not be suitable in commercial orchards because excessive vegetative growth may occur on these plants over time. In addition, overwatering could lead to nutrient deficiencies due to excessive leaching losses. As an alternative to the use of well-irrigated trees, reference  $E_p$  rates can be calculated from simulation models (Pereira et al. 2006; Orgaz et al. 2007; Villalobos et al. 2013). The main difficulty in the implementation of those models lay in the fact that they require detailed microclimate data, as well as user-friendly techniques to determine plant leaf area or radiation interception.

Besides the aforementioned approaches, several indirect strategies have been reported in order to evaluate water status from sap flow methods. For example, Fernández et al. (2001) and Nadezhdina et al. (2007) found subtle changes in the radial  $J$  profiles in response to variations in soil water content. In the light of those observations, the ratio of  $J$  in the inner/outer xylem was proposed as a water stress indicator. Nevertheless, subsequent research (Fernández et al. 2008) showed evidence on the unreliability of such an indicator. Another indirect water stress indicator is the nocturnal-to-diurnal sap flow ratio. Both López-Bernal et al. (2010) and Ballester et al. (2013) showed that such ratio tends to increase with water stress severity. The validity of the nocturnal-to-diurnal sap flow ratio as a water status indicator is based on the premise that the nighttime refilling of internal water stores depleted during the previous day is higher in water stress plants. However, when soil water content is very low and/or actual nighttime  $E_p$  is high, these nocturnal refilling processes could be impeded, which limits the robustness of the indicator.

### **1.5. Using sap flow sensors to assess the occurrence of chilling stress in field trees**

Given the potential of heat pulse methods to provide insight into water relations, one of the chapters (Chapter 5) of the present thesis was devoted to their characterization in the particular case of field olive trees in winter. Previous studies conducted under controlled conditions with young plants of a number of species (including olive) has shown that the exposure to low (non-freezing) soil temperatures usually results in water stress symptoms, even in conditions of non-limited water supply to roots (Kramer 1940; Running and Reid 1980; Pavel and Fereres 1998; Wan et al. 2001). However, reported evidence on the so-called ‘chilling stress’ occurring at field conditions are still lacking to date.

Chilling-induced disturbance in water relations is originated by an increase in the hydraulic resistance of the soil-plant continuum ( $R$ ) which triggers temporal imbalances between root water uptake and actual  $E_p$ , which in turn lead to the development of shoot water deficits (Aroca et al. 2001; Wan et al. 2001).  $R$  can be determined from:

$$R = \frac{\Delta\Psi}{Q} \quad [1.2]$$

with  $\Delta\Psi$  representing the water potential gradient between the soil and the plant. Plant  $\Psi$  can be measured in leaves or shoots with the pressure chamber method while soil  $\Psi$  can be either estimated using soil sensors (e.g. tensiometers) or inferred from measurements of plant  $\Psi$  at predawn under the assumption that it will be equilibrated with soil  $\Psi$  by that time (Dichio et al. 2013). However, the determination of instantaneous  $E_p$  in situ poses a greater challenge, which may partly explain the aforementioned absence of literature data beyond the observations in young plants growing under controlled conditions (e.g. greenhouse, growth chambers, and



artificially heated/chilled pots). At this point, sap flow methods seem a promising tool for evaluating the occurrence and extent of chilling stress in field-grown tree species. Yielding  $Q$  estimates, sap flow methods allow to assess the effects of low temperatures on both  $R$  (Eq. 2),  $G_s$  (Villalobos et al. 2013) and the own  $Q$ .

## 1.6. Objectives and outline of the thesis

The general aim of this thesis is to contribute to explore the full potential of heat pulse sap flow systems, illustrating how such devices can be employed as a tool for monitoring the effects of deficit irrigation on tree functionality and to improve our understanding of water relations in fruit tree species. The specific objectives are:

- (i) To develop a simple methodology to estimate bulk net assimilation in fruit tree species from measurements conducted with sap flow systems.
- (ii) To develop a methodology that allows the monitoring of sapwood water content variations along with sap flux density using compensated heat pulse sensors
- (iii) To assess the potential impact of natural changes in sapwood water content on the accuracy of heat pulse methods
- (iv) To characterize water relations in winter for field olive trees using compensated heat pulse sensors

The thesis is presented as chapters, which have the structure used by peer-reviewed publications (the third and fourth chapters have been already published). Each chapter deals with one of the previously mentioned specific objectives.

Chapter 2 describes a simple methodology based on the use of the imposed evaporation equation to derive bulk stomatal conductance to  $\text{CO}_2$  and net

assimilation values from meteorological and calibrated sap flow records at the canopy scale. The reliability of such methodology was tested in a long-term field experiment including different irrigation treatments established in a mature hedgerow olive orchard in which the estimates of net assimilation were compared with both net ecosystem exchange, water potential and trunk diameter variations measurements.

Chapter 3 reports a methodology that allows the estimation of relative variations in sapwood water content using compensated heat pulse sensors. The method, referred to as VSH-CHP, was tested in lab and field experiments, analyzing its feasibility to detect changes in water status.

Chapter 4 attempts to characterize potential errors in sap flux density determinations with heat pulse methods that might arise when the natural variations in sapwood water content are disregarded. This objective was addressed by constructing desorption curves from sapwood samples of several fruit tree species, allowing to replace sapwood water content by water potential in the working equations of each heat pulse method. In doing so, data on diurnal and seasonal changes in water potential were used to assess the accuracy of sap flux density determinations in relation to species and heat pulse method. Besides that, a characterization of thermal properties was conducted for a wider number of fruit tree species and using several methodologies (including those typically applied when the heat ratio and  $T_{max}$  heat pulse techniques are employed). The differences in thermal properties are analyzed in relation to the anatomical traits of each species and the several methodologies employed in the determinations.

Finally, Chapter 5 is devoted to characterizing the course of field olive trees water relations in winter. To this end, measurements of water potential and sap flow were performed throughout two consecutive winters, deriving values of hydraulic resistance to sap ascent from soil to shoots and bulk

stomatal conductance to H<sub>2</sub>O. Their winter values were compared with those of spring, enabling us to assess the occurrence and extent of chilling stress in field trees.

**References**

- Aroca R, Tognoni F, Irigoyen JJ, Sánchez-Díaz M, Pardossi A (2001) Different root low temperature response of two maize genotypes differing in chilling sensitivity. *Plant Physiol Bioch* 39:1067-1073.
- Ballester C, Castel J, Testi L, Intrigliolo DS, Castel JR (2013) Can heat-pulse sap flow measurements be used as continuous water stress indicators of citrus trees)? *Irrig Sci* 31:1053-1063.
- Becker P, Edwards WRN (1999) Corrected heat capacity of wood for sap flow calculations. *Tree Physiol* 19:767-768.
- Bleby TM, McElrone AJ, Burgess SSO (2008) Limitations of the HRM: great at low flow rates, but not yet up to speed? 7<sup>th</sup> Sap Flow Workshop, Seville (2008).
- Burgess SSO, Adams MA, Turner NC, Beverly CR, Ong CK, Khan AA, Bleby TM (2001) An improved heat pulse method to measure low and reverse rates of sap flow in woody plants. *Tree Physiol* 21:589-598.
- Carlsaw HS, Jaeger JC (1947) *Conduction of heat in solids*, 2<sup>nd</sup> edn. Oxford University Press, London.
- Cermak J, Deml M, Penka M (1973) A new method of sap flow rate determination in trees. *Biol plantarum* 15:171-178.
- Cermak J, Kucera J, Nadezhdina N (2004) Sap flow measurements with some thermodynamic methods, flow integration within trees and scaling up from sample trees to entire forest stands. *Trees* 18:529-546.
- Chalmers DJ, Mitchell PD, van Heek L (1981) Control of peach tree growth and productivity by regulated water supply, tree density and summer pruning. *J Am Soc Hort Sci* 106:307-312.
- Cohen Y, Fuchs M, Green GC (1981) Improvement of the heat pulse method for determining sap flow in trees. *Plant Cell Environ* 4:391-397.

- Conejero W, Alarcón JJ, García-Orellana Y, Nicolás E, Torrecillas A (2007) Evaluation of sap flow and trunk diameter sensors for irrigation scheduling in early maturing peach trees. *Tree Physiol* 27:1753-1759.
- Cuevas MV, Martín-Palomo MJ, Díaz-Espejo A, Torres-Ruiz JM, Rodríguez-Dominguez CM, Perez-Martin A, Pino-Mejías R, Fernández JE (2013) Assessing water stress in a hedgerow olive orchard from sap flow and trunk diameter measurements. *Irrig Sci* 31: 729-746.
- Dichio B, Montanaro G, Sofo A, Xiloyannis C (2013) Stem and whole-hydraulics in olive (*Olea europaea*) and kiwifruit (*Actinidia deliciosa*). *Trees* 27: 183-191.
- Do F, Rocheteau A (2002) Influence of natural temperature gradients on measurements of xylem sap flow with thermal dissipation probes. 1. Field observations and possible remedies. *Tree Physiol* 22:641-648.
- Fereres E, Connor DJ (2004) Sustainable water management in agriculture. In: Cabrera E, Cobacho R, eds. *Challenges of the new water policies for the XXI century*. Lisse, The Netherlands: AA Balkema, 157-170.
- Fereres E, Goldhamer DA (1990) Deciduous fruit and nut trees. In: Stewart BA, Nielsen DR, eds. *Irrigation of agricultural crops*, Agronomy 30. Madison, WI: ASA, CSSA, SSSA, 987-1017.
- Fereres E, Soriano MA (2007) Deficit irrigation for reducing agricultural water use. *J Exp Bot* 58:147-159.
- Fernández JE, Palomo MJ, Díaz-Espejo A, Clothier BE, Green SR, Girón IF, Moreno F (2001) Heat-pulse measurements of sap flow in olives for automating irrigation: tests, root flow and diagnostics of water stress. *Agric Water Manag* 51:99-123.
- Fernández JE, Green S, Caspari HW, Díaz-Espejo A, Cuevas MV (2008) The use of sap flow measurements for scheduling irrigation in olive, apple and Asian pear trees and in grapevines. *Plant Soil* 305:91-104.

- Goldhamer DA, Viveros M, Salinas M (2006) Regulated deficit irrigation in almonds: effects of variations in applied water and stress timing on yield and yield components. *Irrig Sci* 24:101-114.
- González-Altozano P, Pavel EW, Oncins JA, Doltra J, Cohen M, Paço T, Massai R, Castel JR (2008) Comparative assessment of five methods of determining sap flow in peach trees. *Agric Water Manag* 95:503-515.
- Granier A (1985) Une nouvelle method pour la mesure du flux de sève brute dans le tronc des arbres. *Ann Sci For* 42:193-200.
- Granier A (1987) Mesure du flux de sève brute dans le tronc du Douglas par une nouvelle méthode thermique. *Ann Sci For* 44:1-14.
- Green S, Clothier BE (1988) Water use of kiwifruit vines and apple trees by the heat-pulse technique. *J Exp Bot* 39:114-123.
- Green S, Clothier B, Jardine B (2003) Theory and practical application of heat pulse to measure sap flow. *Agron J* 95: 1371-1379.
- Iniesta F, Testi L, Orgaz F, Villalobos FJ (2009). The effects of regulated and continuous deficit irrigation on the water use, growth and yield of olive trees. *Eur J Agron* 30:258-265.
- IPCC (2007) Climate change 2007: the physical science basis. In: Solomon S, Quin D, Manning M, Chen Z, Marquis M, Averyt KB, Tignor M, Miller HL (eds) Contribution of Working Group I to the fourth assessment report of the intergovernmental panel on climate change. Cambridge University Press, Cambridge, 996 pp.
- Jones HG (2004) Irrigation scheduling: advantages and pitfalls of plant-based methods. *J Exp Bot* 55:2427-2436.
- Kozlowski TT, Winget CH (1963) Patterns of water movement in forest trees. *Bot Gaz* 124:301-311.
- Kramer PJ (1940) Root resistance as a cause of decreased water absorption by plants at low temperatures. *Plant Physiol* 15: 63-79.

- López-Bernal A, Alcántara E, Testi L, Villalobos FJ (2010) Spatial sap flow and xylem anatomical characteristics in olive trees under different irrigation regimes. *Tree Physiol* 30:1536-1544.
- Marshall DC (1958) Measurement of sap flow in conifers by heat transport. *Plant Physiol* 33:385-396.
- McCutchan H, Shackel KA (1992) Stem water potential as a sensitive indicator of water stress in prune trees (*Prunus domestica* L. cv. French). *J Am Soc Hort Res* 117:606-611.
- Nadezhdina N, Cermak J, Nadezhdin V (1998) Heat field deformation method for sap flow measurements. In: Cermak J, Nadezhdina N (eds) Proceedings of the 4<sup>th</sup> international workshop on measuring sap flow in intact plants. Publishing House of Mendel University, Brno, Czech Republic, pp 72-92.
- Nadezhdina N, Nadezhdin V, Ferreira MI, Pitacco A (2007) Variability with xylem depth in sap flow in trunks and branches of mature olive trees. *Tree Physiol* 27:105-113.
- Nadezhdina N, Vandegehuchte M, Steppe K (2012) Sap flux density measurements based on the heat field deformation method. *Trees* 26:1439-1448.
- Orgaz F, Villalobos FJ, Testi L, Fereres E (2007) A model of daily mean canopy conductance for calculating transpiration in olive canopies. *Funct Plant Biol* 34:178-188.
- Ortuño MF, García-Orellana Y, Conejero W, Ruiz-Sánchez MC, Alarcón JJ, Torrecillas A (2006) Stem and leaf water potentials, gas exchange, sap flow, and trunk diameter fluctuations for detecting water stress in lemon trees. *Trees* 20:1-8.
- Pavel EW, Fereres E (1998) Low soil temperatures induce water deficits in olive (*Olea europaea*) trees. *Physiol plantarum* 104: 525-538.
- Pereira AR, Green SR, Villa Nnova NA (2006) Penman-Monteith reference evapotranspiration adapted to estimate irrigated tree transpiration. *Agric Water Manag* 83:153-161.

## *General introduction*

- Testi L, Villalobos FJ (2009) New approach for measuring low sap velocities in trees. *Agric For Meteorol* 149:730-734.
- Sakuratani T (1981) A heat balance method for measuring water flux in the stem of intact plants. *J Agric Meteorol* 37:9-17.
- Running SW, Reid CP (1980) Soil temperature influences on root resistance of *Pinus contorta* seedlings. *Plant Physiol* 65: 635-640.
- Scholander PF, Bradstreet ED, Hemmingsen EA, Hammel HT (1965) Sap pressure in vascular plants: negative hydrostatic pressure can be measured in plants. *Science* 148:339-346.
- Siau JF (1971) Flow in wood. In: Côté WA (ed) *Syracuse wood science series*. Syracuse University Press, New York, pp 131.
- Smith DM, Allen SJ (1996) Measurement of sap flow in plant stems. *J Exp Bot* 47:1833-1844.
- Steppe K, De Pauw DJW, Lemeur R, Vanrolleghem PA (2006) A mathematical model linking tree sap flow dynamics to daily stem diameter fluctuations and radial stem growth. *Tree Physiol* 26:257-273.
- Swanson RH (1994) Significant historical development in thermal methods for measuring sap flow in trees. *Agric For Meteorol* 72:113-132.
- Swanson RH, Whitfield WA (1981) A numerical analysis of heat pulse velocity. Theory and practice. *J Exp Bot* 32: 221-239.
- Tognetti R, d'Andria R, Morelli G, Calandrelli D, Fragnito F (2004) Irrigation effects on daily and seasonal variations of trunk sap flow and leaf water relations in olive trees. *Plant Soil* 263:249-264.
- Urban J, Dvorak M (2014) Sap flow-based quantitative indication of progression of Dutch elm disease after inoculation with *Ophiostoma novo-ulmi*. *Trees* 28:1599-1605.
- Uriu K, Magness JR (1967) Deciduous tree fruits and nuts. In: Hagan RM, Haise HR, Edminster TW (eds) *Irrigation of agricultural lands*,



- Agronomy Monograph 11. American Society of Agronomy, Madison, WI, pp 686-703.
- Vandegehuchte MW, Steppe K (2012a) Interpreting the heat field deformation method: erroneous use of thermal diffusivity and improved correlation between temperature ratio and sap flux density. *Agric For Meteorol* 162:91-97.
- Vandegehuchte MW, Steppe K (2012b) Sapflow+: a four-needle heat pulse sap flow sensor enabling nonempirical sap flux density and water content measurements. *New Phytol* 196:306-317.
- Vandegehuchte MW, Steppe K (2012c) Improving sap flux density measurements by correctly determining thermal diffusivity, differentiating between bound and unbound water. *Tree Physiol* 32:930-942.
- Vandegehuchte MW, Steppe K (2012d) Use of the correct heat conduction-convection equation as basis for heat-pulse sap flow methods in anisotropic wood. *J. Exp. Bot.* 63: 2833-2839.
- Vandegehuchte MW, Steppe K (2013) Sap-flux density measurement methods: working principles and applicability. *Funct Plant Biol* 40:213-223.
- Vergeynst LL, Vandegehuchte MW, McGuire MA, Teskey RO, Steppe K (2014) Changes in stem water content influence sap flux density measurements with thermal dissipation probes. *Trees* 28:949-955.
- Villalobos FJ, Testi L, Orgaz F, García-Tejera O, López-Bernal A, González-Dugo MV, Ballester-Lurbe C, Castel JR, Alarcón-Cabañero JJ, Nicolás-Nicolás E, Girona J, Marsal J, Fereres E (2013) Modelling canopy conductance and transpiration of fruit trees in Mediterranean areas: a simplified approach. *Agric For Meteorol* 171:93-103.
- Waisel Y, Liphshitz N, Kuller Z (1972) Patterns of water movement in trees and shrubs. *Ecology* 53:520-523.

*General introduction*

Wan X, Zwiazek JJ, Lieffers VJ, Landhäuser SM (2001) Hydraulic conductance in aspen (*Populus tremuloides*) seedlings exposed to low root temperatures. *Tree Physiol* 21: 691-696.

Williams M, Bond BJ, Ryan MG (2001) Evaluating different soil and plant hydraulic constraints on tree function using a model and sap flow data from ponderosa pine. *Plant Cell Environ* 24:679-690.

Yamaoka Y, Swanson R, Hiratsuka Y (1990) Inoculation of lodgepole pine with four blue-stain fungi associated with mountain pine beetle, monitored by a heat pulse velocity (HPV) instrument. *Can J For Res* 20:31-36.



## **Chapter 2**

### **Using sap flow measurements to estimate the effects of water stress on net assimilation in fruit orchards**

---

## Chapter 2

### Using sap flow measurements to estimate the effects of water stress on net assimilation in fruit orchards

#### Summary

The measurement of bulk net assimilation ( $A$ ) in fruit tree species is hindered by the need for sophisticated and complex instrumentation despite it would be a target indicator for evaluating the effect of deficit irrigation on biomass production. The aim of this study is to present a simple alternative for estimating  $A$  from sap flow measurements and meteorological records. The proposed methodology was tested in a mature hedgerow olive orchard of 11.4 ha. Within the orchard an irrigation experiment was established in a small plot including three treatments: a full irrigated control (CI), a regulated deficit irrigation (RDI) and one additional treatment mimicking the customary orchard irrigation management (FI). Determinations of sap flow, water potential ( $\Psi$ ) and trunk diameter variations (TDV) were conducted in the three treatments for three years. Also, measurements of net ecosystem exchange (NEE) were performed with an eddy covariance system in the centre of the orchard for the first season. On the one hand, our results showed a close agreement between the pattern of  $A$  in the FI treatment and that of NEE, indicating that our approach yields sound values and is suitable to monitor seasonal variations in  $A$ . On the other, we found differences in  $A$  between irrigation treatments which were generally coherent with the differences in irrigation applied, transpiration ( $E_p$ ),  $\Psi$  and TDV, suggesting that the methodology was reliable to capture changes in  $A$  in response to mild water stress. Potential limitations arising from methodological assumptions are discussed.

## **2.1. Introduction**

At the present, and more so in the future, irrigated fruit tree culture in arid and semi-arid areas takes place under water scarcity. This context has driven to the development of deficit irrigation strategies (DI) with successful results for a wide number of fruit tree species (Mitchell and Chalmers 1982; Goldhamer and Viveros 2000; Moriana et al. 2003; Fereres and Soriano 2007). The correct application of DI requires an accurate knowledge of the effects of water shortage on tree performance, which has led to the search for robust and sensitive water stress indicators derived from plant-based measurements. Determinations of water potential ( $\Psi$ ), canopy temperature, sap flow and trunk diameter variations are among the ones that have received more attention because of their clear physiological interpretation and/or ease of implementation and data recording (Jones 2004; Fernández and Cuevas 2010). In an agronomical context, however, the ideal water stress indicator should go beyond physiological terms and show the direct effects of DI over biomass production and, ultimately, yield. In this regard, net assimilation rate ( $A$ ) should be a target indicator, but its determination remains challenging.

Leaf cuvette gas analyzers have been widely used to measure  $A$  in mature trees (Moriana and Fereres 2002), but scaling up such observations to the canopy level can lead to important errors. The use of large canopy chambers overcomes this deficiency (Pérez-Priego et al. 2010), but requires sophisticated instrumentation. Moreover, both approaches are labour-intensive and non-automatable. The eddy covariance technique can also yield useful information at the orchard scale, provided the measurements are performed within large uniform flat plots. Unlike the formers, this approach is suitable for automation, which allows the user to obtain continuous estimates of the Net Ecosystem Exchange (NEE). However

NEE is not only dependent on  $A$  but also on the soil respiration of the plot, which in turn is affected by soil moisture and temperature (Law et al. 2002).

The objective of this study is to present and test a simple alternative methodology for estimating  $A$  from tree transpiration ( $E_p$ ), whose estimation can be achieved by sap flow sensors allowing automatable and continuous recording. Besides that, the proposed approach was applied to a three year experiment in a super-intensive olive orchard with several irrigation treatments in order to assess its performance in relation to both eddy covariance measurements of NEE and the seasonal patterns of other classical water stress indicators.

## 2.2. Materials and methods

### 2.2.1. Theoretical framework

Net assimilation ( $A$ ) can be expressed as a function of the stomatal conductance to CO<sub>2</sub> ( $G_c$ ,  $\mu\text{mol m}^{-2} \text{s}^{-1}$ ) as:

$$A = G_c(C_a - C_i) \quad [2.1]$$

where  $C_a$  is the CO<sub>2</sub> concentration in the leaf boundary layer (set to 380  $\mu\text{mol mol}^{-1}$ ) and  $C_i$  is the CO<sub>2</sub> concentration in the substomatal cavity. In the case of ventilated canopies, such as fruit orchards, the magnitude of bulk aerodynamic conductance is very low in relation to  $G_c$ , which results in a tight coupling of canopies to the atmosphere. Under these circumstances,  $G_c$  can be expressed as a function of  $E_p$  by inverting the imposed evaporation equation:

$$G_c = \frac{E_p P}{1.6 \text{ VPD}} \quad [2.2]$$

Where VPD is vapour pressure deficit,  $P$  is atmospheric pressure (kPa) and 1.6 is the ratio between the diffusion coefficients of CO<sub>2</sub> and H<sub>2</sub>O in air.

In this study,  $C_i$  was calculated as a constant fraction of  $C_a$  (termed  $\beta$ ), so the working equation to deduce an equivalent of  $A$  from  $E_p$  can be written as:

$$A = \frac{E_p P}{1.6 \text{ VPD}} C_a (1 - \beta) \quad [2.3]$$

In the case of olive (*Olea europaea* L.) trees, many studies show that  $\beta$  values typically range between 0.5 and 0.6 (Centritto et al. 2005; Díaz-Espejo et al. 2006; Bacelar et al. 2007). We adopted the averaged value ( $\beta=0.58$ ) reported by Díaz-Espejo et al. (2006) for mature olive trees growing under similar environmental conditions to those in our experiments. By assuming constant values for both  $C_a$  and  $\beta$ , the method only requires meteorological and sap flow records as inputs, achieving a maximum ease of implementation. Such assumptions, however, might affect the accuracy of the methodology. The magnitude of these likely errors is assessed below on the basis of field measurements and literature data.

### **2.2.2. Experimental site**

The methodology was tested in a three year (2011, 2012, 2013) experiment performed in a 21.5 ha hedgerow olive (cv. ‘Arbequina’) orchard of 11.4 ha in ‘La Harina’ farm, which is located in Córdoba, Spain (37.8 °, 4.8 °W, 170 m altitude). The orchard was planted in 2005 with 4 x 1.5 m spacing. During the course of the experiments, the height of the canopy was  $\approx 3.2$  m and presented an average leaf area index of 1.5 m<sup>2</sup> m<sup>-2</sup>. The soil was classified as a Vertisol (FAO classification) and the climate was Mediterranean, with 600 mm of average annual rainfall and around 1400



mm of average annual reference evapotranspiration ( $ET_0$ ). The particular patterns of meteorological variables (rainfall, temperature, relative humidity, wind speed and solar radiation) during the experiments were monitored at 10 min intervals with an automated weather station placed close to one of the orchard borders.

Most of the experimental measurements were conducted in a 0.29 ha area that was established in one of the orchard corners. Such experimental area was arranged as a randomized complete block with four replications. Within each replication, three irrigation treatments were applied to separate plots of 40 trees in 4 adjacent rows. The treatments were:

1. Control irrigation (CI): aimed to supply enough water to keep maximum evapotranspiration ( $ET$ ) during all the irrigation season. To this end, irrigation doses were estimated as the difference between  $ET$  and rainfall, computing  $ET$  from the product of  $ET_0$  and the crop coefficient. The later was set to 0.75, a value that was considered high enough to avoid water stress as evidenced by measurements of shoot  $\Psi$  (described below).
2. Regulated deficit irrigation (RDI): the same water amounts as in CI were applied except for a midsummer period (typically July-August) when it ranged from 30 to 50 % of that of CI, depending on the year.
3. Farm management (FI): irrigation amount and frequency was that of the orchard habitual management.

In all cases, irrigation was applied by three 2.2 L/h drippers per tree with a maximum frequency of three times a week. Further details concerning the water amounts and the irrigation periods for each treatment can be found in Figure 2.1.

### **2.2.3. Sap flow measurements**

Within one of the replication blocks, two of the central trees of each irrigation treatment were instrumented with sap flow sensors (one per tree) based on the compensated heat pulse method (Swanson and Whitfield 1981) throughout the three irrigation seasons. The probes used were designed and produced in the IAS-CSIC laboratory in Córdoba, Spain and consist of a 4.8 W stainless steel heater of 2 mm diameter and two temperature sensors of the same diameter located 10 and 5 mm down- and upstream of the heater, respectively (Testi and Villalobos 2009). Each temperature probe has four embedded Type E (chromel–constantan wire) thermocouple junctions, spaced 10 mm along the needle, that were sampled separately to obtain heat-pulse velocities at 5, 15, 25 and 35 mm below the cambium at 15-min intervals. Sensors were installed at 50 cm height from the soil and the system was controlled by a datalogger (CR1000, Campbell Scientific Inc., Logan, UT, USA). Heat-pulse velocities were corrected for wounding effects according to Green et al. (2003) and converted to sap flux densities from water fractions that were obtained from core-sampling at the end of each measurement season. In addition, the ‘calibrated average gradient’ procedure (Testi and Villalobos 2009) was applied to calculate low sap velocities. Finally, sap flow values were deduced by integrating sap flux densities first across the trunk radius (using the radial velocity profile curve given by the probe) and then around the azimuth angle (Green et al. 2003).

To avoid errors associated to the natural azimuthal variability in sap flow rates (López-Bernal et al. 2010), the sap flow records were calibrated using the model of Villalobos et al. (2013), which allows the estimation of the daily transpiration ( $E_{p,est}$ , mm d<sup>-1</sup>) as a function of total daily solar radiation ( $R_{sd}$ , MJ m<sup>-2</sup> d<sup>-1</sup>):

$$E_{p,est} = 37.08 \cdot 10^{-3} \frac{f R_{sd}}{a+b} \frac{VPD}{P} \quad [2.4]$$

where  $f$  is the fraction of photosynthetically active radiation (PAR) intercepted by the canopy (dimensionless) and the coefficient  $37.08 \cdot 10^{-3}$  incorporates the conversion of units for Joules of solar radiation to  $\mu\text{mol}$  quanta and from mol to kg of  $\text{H}_2\text{O}$ . The parameters  $a$  ( $\mu\text{E mol}^{-1}$ ) and  $b$  ( $\mu\text{E mol}^{-1} \text{ kPa}^{-1}$ ) were taken from Villalobos et al. (2013) and they are related to the radiation use efficiency and the species-specific response to VPD, respectively. Radiation interception was computed using the model of Mariscal et al. (2000). This model calculates the PAR transmittance, at any given time, in the nodes of a three-dimensional grid inside a prism. The prism, of selectable height and grid density is delimited by four adjacent trees. By spatial and time integration, the PAR intercepted during any given period can be calculated taking separately into account direct-beam radiation, diffuse radiation and scattering. Leaf area density, which is a required input for the model, was estimated from measurements of canopy transmittance conducted with a plant canopy analyzer (LAI-2000, Li-Cor, Lincoln, NE, USA). As the trees were regularly pruned each winter and the measurements of canopy transmittance were typically performed at the end of spring (before or soon after differences in irrigation between treatments were imposed), the estimated values of leaf area density were averaged and, hence, the same radiation interception was assumed for all the treatments.

As the model is only valid for unstressed canopies, Equation 2.4 was applied for one single sunny day per season in which measurements of  $\Psi$  ensured no differences between treatments and good water status. Calibration coefficients for each tree were then computed as the ratio of measured sap flow values to  $E_{p,est}$ . Finally, the calibrated sap flow values from sunrise to sunset were used as estimates of  $E_p$  for the calculations of  $A$  with Eq. 2.3.

#### **2.2.4. Comparison with eddy covariance measurements**

The net ecosystem exchange (NEE,  $\mu\text{mol CO}_2 \text{ m}^{-2} \text{ s}^{-1}$ ) of the orchard was measured with an eddy covariance system, installed at 6.0m height atop a mast (EC tower). The mast was placed far from the treatments sector, near the centre of the orchard, to ensure a minimum of 200 m and a maximum of 285 m of fetch in the direction of the more frequent winds and no interference from the sector where the experimental blocks were located. The system consisted of a three-dimensional sonic anemometer (model CSAT3, Campbell Scientific Inc., Logan, Utah, USA) and an open path  $\text{CO}_2/\text{H}_2\text{O}$  analyzer (model LI7500, LI-COR Biosciences, Lincoln, Nebraska, USA), and took continuous measurements from 24 June 2011 (DOY 175) to 27 September 2011 (DOY 270). Measurements of air temperature and relative humidity were taken close to the anemometer with a combined probe (model HMP45C, Vaisala, Helsinki, Finland). All the sensors were connected to a data logger (model CR1000, Campbell Scientific Inc., Logan, Utah, USA) that recorded all the measurements with a sampling rate of 10 Hz.  $C_a$  concentration was measured at two heights (0.3 and 3.0 m) with a closed-path  $\text{CO}_2$  analyzer (model LI-820, LI-COR Biosciences, Lincoln, Nebraska, USA) during the night to calculate  $\text{CO}_2$  storage.

The raw data were processed using Turbulent Knight 3 software (Mauder and Foken 2011) to calculate the NEE for 30-minute periods. All the relevant corrections were applied: coordinate rotation, spectral corrections, WPL corrections (Foken et al 2012). Finally, the NEE of daytime hours (filtered by net radiation  $> 50 \text{ W m}^{-2}$ ) were integrated to obtain daily values in  $\text{g CO}_2 \text{ m}^{-2} \text{ d}^{-1}$  which were compared with the estimates of  $A$  corresponding to FI trees in the separated experimental plot.

### **2.2.5. Other measurements and calculations**

Water potential ( $\Psi$ ) was determined using a pressure chamber (Soil Moisture Equipment Corp., Santa Barbara, CA, USA). Values of predawn and midday  $\Psi$  were recorded twice a month from June to October for the three years. In each measurement, four sun-exposed shoots from the canopy top (with 1 to 3 leaf pairs attached) were sampled per treatment (shoots were always taken from one of the trees instrumented with sap flow probes).

Trunk diameter variations (TDV) were monitored in 2011, 2012 and 2013 with Linear Variable Differential Transducer dendrometers (LVDT; Model DF 2.5, Solartron Metrology, West Sussex, UK) mounted in a holder built of aluminium and 'INVAR'. One tree per irrigation treatment (one of the two instrumented with sap flow probes) was instrumented. In 2012 trunk diameter variations were only recorded in two trees (CI and RDI). The sensors were attached in locations free of scars at about 0.4 m from the soil. The contact point of each dendrometer was glued to the surface of the living tissues of the bark with standard mastic for pruning wounds. Measurements were taken every 5 min and the system was controlled by a datalogger (CR1000, Campbell Scientific Inc., Logan, UT, USA). The daily values of maximum trunk diameter (MXTD) were used to give insight into the seasonal dynamics of trunk growth.

The statistical treatment of the data (ANOVA and Tukey HSD test) was performed with the Statistix program (Statistix 9 for Windows, Analytical Software, Tallahassee, FL, USA).

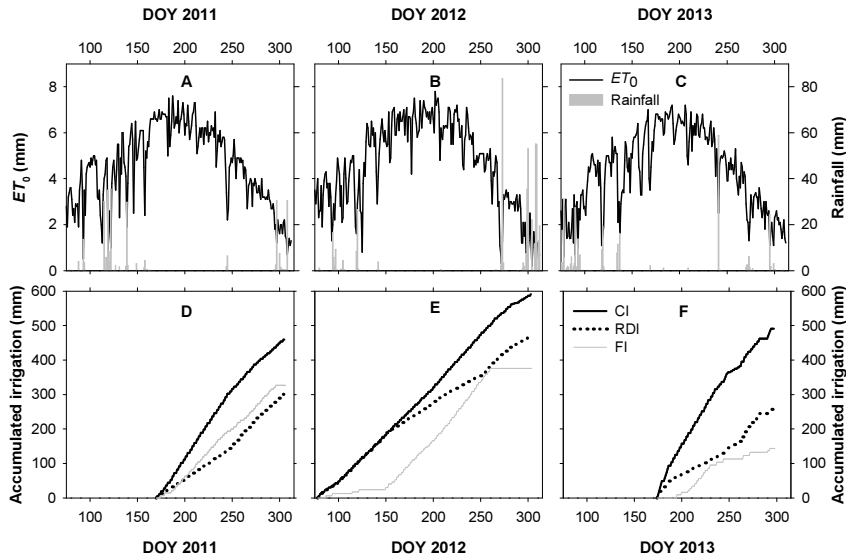


**Figure 2.1.** Daily values of reference evapotranspiration ( $ET_0$ , black line) and rainfall (grey bars) (panels A-C) and evolution of the cumulative irrigation applied to the treatments (CI = control, FI = farm irrigation, RDI = deficit irrigation) (panels D-F) during the three years of experiment.

## 2.3. Results

### 2.3.1. Seasonal changes in weather conditions and irrigation applied

In 2011 and 2013 the study site was characterized by moderate to high precipitation in the period before starting differential irrigation between CI and RDI (367 mm in January-June, respectively), whereas rainfall was very scarce in 2012 (90 mm in January-June). In all cases the summer was dry and hot (almost null precipitation and mean  $ET_0$  of  $6.2 \text{ mm d}^{-1}$  in July-August; Fig. 2.1). Seasonality and amounts of irrigation for each treatment are reported in Figure 2.1D-F. In the CI treatment, the total irrigation volume was comparable between 2011 and 2013 and higher in the case of 2012, as a result of the early start of irrigation in the later. The remaining

treatments received lower irrigation doses than CI, with variability in the periods and severity of water restrictions depending on both each particular treatment and the year considered (see Figure 2.1D-F for further details).

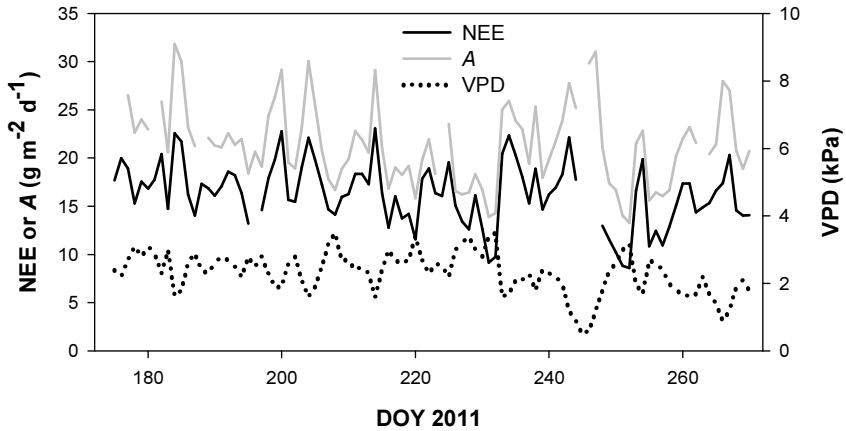


**Figure 2.2.** Seasonal course of net ecosystem exchange (NEE, black solid line), estimated net assimilation ( $A$ , gray solid line) and vapour pressure deficit (VPD, dotted line) for the summer of 2011. NEE was determined with an eddy covariance system placed in the centre of the orchard while values of  $A$  were deduced from the sap flow records of the two farm trees in the separate experimental plot. In all cases values correspond to daytime means.

### 2.3.2. Comparison with eddy covariance measurements

Figure 2.2 presents the time series of daily NEE and  $A$  deduced from eddy covariance and sap flow measurements, respectively, as well as those of VPD. Both values of  $A$  and NEE showed moderately fluctuating patterns, with the former being always slightly higher than those of NEE. In general, the highest values of both  $A$  or NEE coincided with cloudy days with low VPD whereas the minimum ones occurred in sunny days of high VPD.

Considering the whole period, the averaged values of  $A$  and NEE were 21.5 and 16.3 g CO<sub>2</sub> m<sup>-2</sup> d<sup>-1</sup>, respectively. The values of  $A$  are plotted versus those of NEE in Figure 2.3, evidencing that both variables were tightly coupled. A linear regression analysis was performed, yielding both a good fit ( $r^2 = 0.819$ ), a slope close to the unit and a positive intercept.

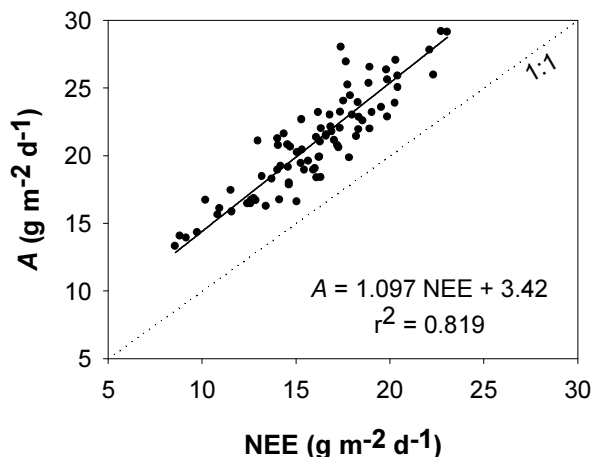


**Figure 2.3.** Plot of estimated net assimilation ( $A$ ) versus net ecosystem exchange (NEE), deduced from sap flow and eddy covariance systems, respectively. Data correspond to daily values from 24 June 2011 (DOY 175) to 27 September 2011 (DOY 175). Dotted line indicates the 1:1 line.

### **2.3.3. Responses of $A$ and classical water status indicators to long-term deficit irrigation**

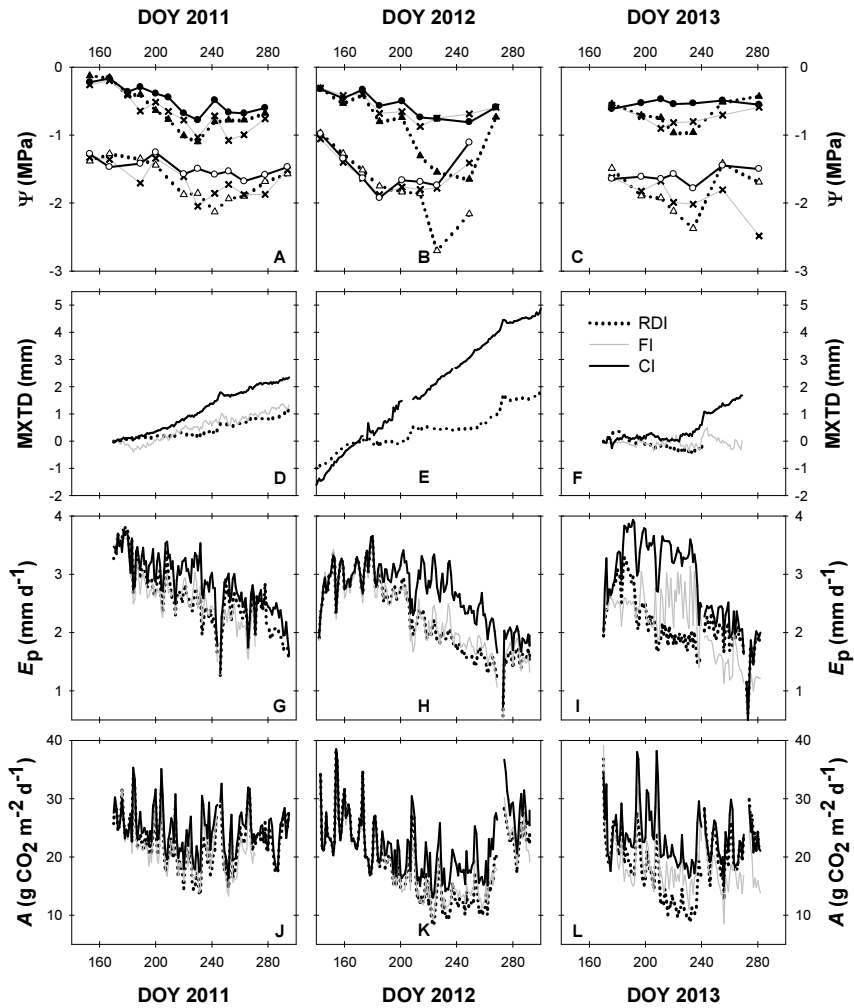
The CI treatment showed mean values of  $\Psi$  around -0.5 and -1.6 MPa at predawn and midday, respectively, with little variation between years (Fig. 2.4A-C). By contrast, the patterns of  $\Psi$  in both the FI and RDI varied in relation to the season, with 2011 being the year with the lowest differences between treatments. In relation to CI,  $\Psi$  generally decreased in RDI at



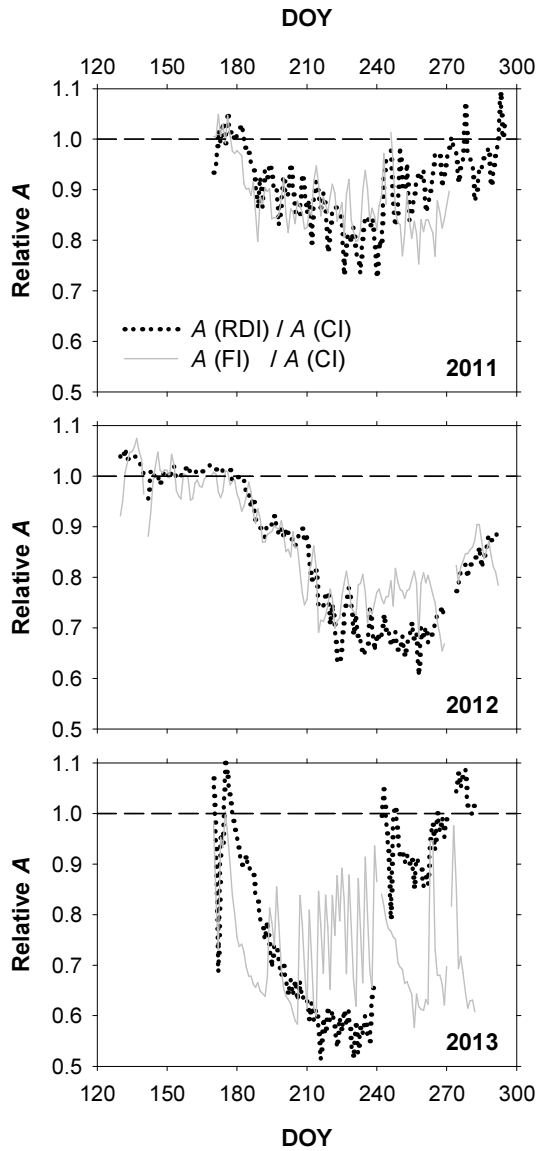
midsummer, reaching midday values of -2.1, -2.7 and -2.4 MPa in 2011, 2012 and 2013, respectively. With regard to FI, the  $\Psi$  values were similar to those of RDI in 2011 and typically intermediate, ranging between those measured for RDI and CI, in 2012 and 2013.

Figure 2.4D-F depicts the time course of MXTD for each treatment and year, relative to the values recorded at dawn of DOY 170, considering these as zero. After differential irrigation was applied, the MXTD patterns rapidly varied between treatments with CI exhibiting the highest values. Meanwhile, water deprivation resulted in lower trunk growth for RDI and FI and even in moderate shrinkage during the summer of 2013. Besides that, both CI and RDI presented higher cumulative trunk growth in 2012 in relation to 2011 and 2013. For instance, CI grew 2.0, 4.0 and 1.7 mm in the period from DOY 170 to DOY 270 of 2011, 2012 and 2013, respectively.

The seasonal course of  $E_p$  in CI trees (Fig. 2.4G-I) presented peaked patterns, with the values reaching a maximum between mid-June and mid-July (DOY 165-200,  $E_p$  around 3.5-4.0 mm d<sup>-1</sup>) which was followed by a progressive decrease towards autumn. By contrast,  $A$  presented more erratic patterns (Fig. 2.4J-L), with the highest values (30-40 g CO<sub>2</sub> m<sup>-2</sup> d<sup>-1</sup>) in spring and autumn, as well as in some summer days with low evaporative demand. Considering the period from 19 June (DOY 170) to 27 September (DOY 270), the averaged  $A$  values resulted 24.8, 19.9 and 23.3 g CO<sub>2</sub> m<sup>-2</sup> d<sup>-1</sup> in 2011, 2012 and 2013, respectively. With regard to the other treatments, they presented similar values of  $E_p$  and  $A$  to those of CI early in the season and lower ones coinciding with the periods of water deprivation.



**Figure 2.4.** Time course of predawn (closed symbols) and midday (open symbols) shoot water potential ( $\Psi$ , panels A-C), calibrated transpiration ( $E_p$ , panels D-F), estimated net assimilation ( $A$ , panels G-I) and maximum trunk diameter (MXTD, panels J-L) for the three irrigation treatments (CI = control, FI = farm irrigation, RDI = deficit irrigation) during the three years of experiment (left, middle and right panels correspond to 2011, 2012 and 2013, respectively).



**Figure 2.5.** Course of net assimilation ( $A$ ) estimated for the deficit irrigation (RDI) and the farm treatments (FI) in relation to that of the control (CI) throughout the three years of experiment (i.e. ratio of either RDI or FI values to those of CI).

The effects of deficit irrigation over  $A$  are better illustrated in Figure 2.5 by presenting the ratio of  $A$  values for each treatment to those of CI. In the first season, similar patterns of  $A$  were found both for FI and RDI, with the values decreasing to 75-85 % in relation to those of CI at midsummer. In 2012, higher relative reductions were found, particularly in the case of RDI, which reached values around 60-70 % of those of CI prior to the irrigation recovery phase of September. Finally, in 2013 the relative  $A$  for RDI decreased gradually, reaching the lowest values in August (55-65 % of those of CI). Meanwhile, in FI the highest relative reductions appeared in early summer and September (around 60-65 % of CI).

## **2.4. Discussion**

### **2.4.1. Methodological issues: sensitivity to changes in $C_a$ and water stress**

The approach presented in this study is based on two theoretical assumptions which may compromise its validity. As a first issue, the proposed methodology assumes a constant  $C_a$ , neglecting its natural variations. It is known, for instance, that the diurnal courses of  $C_a$  present a sinusoid pattern, with the highest values prior to sunrise and the lowest during daytime as a result of the intrinsic photosynthetic activity of terrestrial vegetation (Baldocchi et al. 1981). In this regard, Figure 2.6 illustrates the evolution of  $C_a$  (measured by the eddy covariance system at 3 m height) throughout the daytime of a typical summer day (4 August 2011, DOY 216) in our experimental conditions.  $C_a$  ranged from 392  $\mu\text{mol mol}^{-1}$  at dawn to 373  $\mu\text{mol mol}^{-1}$  in the late afternoon. The same figure shows the course of  $A$  in the CI treatment estimated by either considering or not such measured  $C_a$  variation, evidencing very slight differences between them.

The daily values of  $A$  deduced by integrating the whole daytime yielded 19.7 and 19.9 g CO<sub>2</sub> m<sup>-2</sup> d<sup>-1</sup> assuming a variable and a constant  $C_a$ , respectively. Furthermore, even if the eddy covariance measurements of  $C_a$  throughout the period between DOY 175 and DOY 270 are considered, the accumulated values of  $A$  only results 1.22 % higher than those obtained with a fixed  $C_a$  of 380  $\mu\text{mol mol}^{-1}$  (22.4 versus 22.2 t CO<sub>2</sub> ha<sup>-1</sup>). All this body of evidence indicates that assuming a sound constant  $C_a$  leads to negligible errors in the estimation of  $A$ .

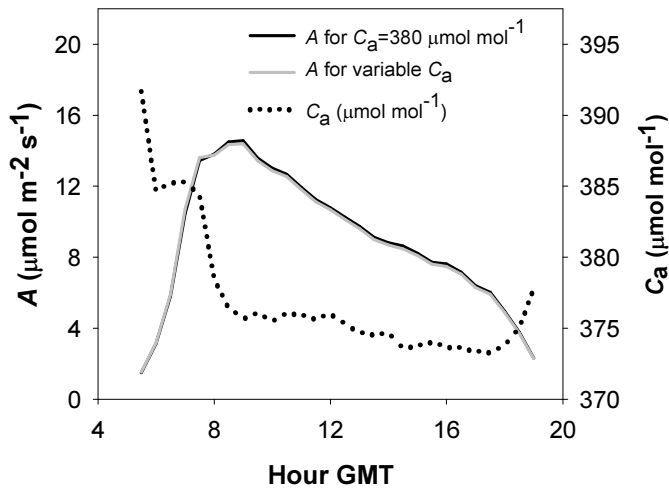


**Figure 2.6.** Diurnal time course (4 August 2011, DOY 216) of air CO<sub>2</sub> concentration ( $C_a$ , dotted line) and estimated net assimilation ( $A$ ) calculated either assuming (grey solid line) or not (black solid line) a variable  $C_a$ . In the former case a fixed value of 380  $\mu\text{mol mol}^{-1}$  was assumed for  $C_a$ . Data on  $A$  correspond to the average of the two control trees.

The second issue arises as a consequence of adopting a fixed value for  $\beta$  in Eq. 2.3. In particular, decreases in  $\beta$  in response to water stress have been

reported in many species (Brodribb 1996; Rosati et al. 2006) because stomatal closure is expected to produce a CO<sub>2</sub> “supply” limitation of photosynthesis by causing C<sub>i</sub> to become depleted (Kramer and Boyer 1995). From a theoretical point of view, Eq. 2.3 predicts that ignoring the consequent  $\beta$  variations would result in an underestimation of the  $A$  estimates under water stress conditions. This implies that the methodology might lose accuracy under changing water status but also that it would still be of some interest for detecting reductions in  $A$  in response to water deficits because the errors would tend to magnify the differences between well-watered and water-stressed conditions. However, the paradigm of  $\beta$  decreasing with water stress is not free of controversy and many studies argue that plants have evolved feedback and feedforward mechanisms to keep the importation and depletion of CO<sub>2</sub> in balance, so that either C<sub>i</sub> or  $\beta$  are conservative provided that the stress conditions develop gradually (Wong et al. 1979; Steduto et al. 2007). There has been considerable evidence showing that  $\beta$  tends to remain constant in fruit tree species such as almond (DeJong 1983; Marsal et al. 1997; Romero et al. 2004), hazelnut (Marsal et al. 2007) and orange trees (Pérez-Pérez et al. 2008), but exceptions can also be found (e.g. walnut, Rosati et al. 2006).

In the particular case of olive trees, there are many reports showing  $\beta$  stability. For instance, Centritto et al. (2005) compared the effects of partial rootzone drying on gas exchange, reporting non-significant differences in  $\beta$  between two control treatments replacing the 100 % of the crop evapotranspiration (one of them applying partial rootzone drying) and a partial rootzone drying one irrigated with 50 % of the water supplied to the controls. Similarly, Bacelar et al. (2007) conducted a study in which  $\beta$  was measured in field olive trees irrigated with 100, 60, 30 and 0 % (rainfed) of the estimated local evaporative demand at several periods of a summer day. Their results showed no significant differences between irrigated treatments

with the exception of the 30 % treatment, which exhibited lower values at midday. On the contrary, rainfed trees showed lower values in the morning but not at midday. Finally, Villalobos et al. (2012) performed simultaneous measurements of gas exchange with large canopy chambers in well and deficit irrigated trees and found that the instant transpiration efficiency (i.e. the ratio of  $A$  to  $E_p$ ) was always similar or only slightly higher for the later. As the differences in instant transpiration efficiency should be proportional to the differences in  $\beta$  (according to Eq. 2.3), the results of Villalobos et al. (2012) again suggest that, at most, water stress lead to very slight declines in  $\beta$  in the case of olive trees. Hence, applying Eq. 2.3 with a fixed  $\beta$  value should not result in a significant loss of accuracy under mild water stress conditions. Anyway, a better characterization of the relations between  $\beta$  and water status in relation to species and water stress severity deserves further research.

#### **2.4.2. Comparisons with eddy covariance measurements and literature data**

The close agreement between NEE and  $A$  patterns observed in Figure 2.2 as well as the good fit ( $r^2=0.82$ ) and the parallelisms with the 1:1 line presented in Figure 2.3 are indicative of the reliability of the proposed methodology to monitor  $A$  under field conditions. The higher values found for  $A$  were already expected, as NEE integrates the rates of  $A$  as well as those of soil and woody-organs respiration. Our results suggest that such respiration rates, deduced as the difference between  $A$  and NEE, were on average  $\approx 5 \text{ g CO}_2 \text{ m}^{-2} \text{ d}^{-1}$ , with slightly lower values appearing at midsummer (Fig. 2.2). In an irrigated olive (cv. ‘Arbequina’) orchard under similar environmental conditions, Testi et al. (2008) measured soil respiration both in the alley and in the permanently wet zones near the drippers in a summer day. The average values were 1.1 and 5.7  $\mu\text{mol CO}_2$

$\text{m}^{-2} \text{s}^{-1}$  in the alley and beneath the canopy, respectively, both being rather constant throughout the day. If these values are weighted considering the soil wetted fraction and integrated along the daytime, a rate of soil respiration of  $2.9 \text{ g CO}_2 \text{ m}^{-2} \text{ d}^{-1}$  can be calculated. Although lower than our average estimates, the discrepancy can be perfectly attributed to the lower values of apparent respiration at midsummer in our experiment, to the fact that wood respiration is included into the NEE in Testi et al. (2008) and/or to differences in respiration rates between both orchards ( $400 \text{ trees ha}^{-1}$  in Testi et. al, vs.  $1667 \text{ trees ha}^{-1}$  in this experiment). In any case, this comparison points out that our methodology yields, at least, fairly reasonable estimates of  $A$ .

Searching for data on  $A$  rates to compare with our estimates is not an easy task. In the literature many works can be found reporting measurements of  $A$  conducted with leaf gas exchange analyzers in olive trees. Nevertheless, they are of little help because such measurements are frequently performed in sunlit leaves and the values expressed on a leaf area basis while our estimates correspond to the canopy level and are expressed on a soil area basis. Fortunately, determinations of bulk  $A$  based on the use of large canopy-chambers are also available for olive trees. Thus, Villalobos et al. (2012) used this technique for measuring  $A$  in a two year experiment in a mature olive orchard (cv. 'Arbequina') with two irrigation treatments: a full irrigated control and a deficit irrigated treatment applying 25 % of the control irrigation at midsummer. In the period of maximum differences in water status (i.e. DOY 215-250), the average diurnal values of  $A$  in the control were  $12.0 \text{ g CO}_2 \text{ m}^{-2} \text{ d}^{-1}$  in the first season and  $19.0 \text{ g CO}_2 \text{ m}^{-2} \text{ d}^{-1}$  in the second; and around  $6.5$  and  $13.4 \text{ g CO}_2 \text{ m}^{-2} \text{ d}^{-1}$  in the deficit irrigated treatment. The authors attributed the higher values in the second season to the renewal of leaves caused by pruning or/and to changes in the distribution of radiations patterns within the canopy. Returning to our data



and considering the period DOY 215-240 of 2013 (when our RDI treatment were the most similar to the aforementioned ones in terms of irrigation applied), our average daily  $A$  estimates ( $20.5 \text{ g CO}_2 \text{ m}^{-2} \text{ d}^{-1}$  for CI and  $12.0 \text{ g CO}_2 \text{ m}^{-2} \text{ d}^{-1}$  for RDI, Fig. 2.4L) were not far from those obtained by Villalobos et al. (2012) in their second measurement season.

### 2.4.3. Comparison with classical indicators of water status

The seasonal patterns of  $\Psi$ , MXTD,  $E_p$  and  $A$  showed marked differences between treatments (Fig. 2.4 & 2.5) which were generally coherent with the amount and temporal distribution of irrigation (Fig. 2.1D-F). Thus, the irrigation applied to RDI during the summer period was much higher in 2011 than in 2012 and 2013, and this led to higher  $\Psi$ ,  $E_p$  and  $A$  in the former year. Moreover, 2013 was the year with the largest differences between treatments in the distribution and amount of irrigation, which also had a clear impact on the trends of  $\Psi$ ,  $E_p$  and  $A$ . For instance, the delayed start of irrigation in early summer and the water deprivation imposed in autumn for FI (Fig. 2.1F) resulted in low values of  $\Psi$ ,  $E_p$  and  $A$  in relation to those of CI in these periods, while the greatest relative declines in RDI were observed by midsummer, just prior to the recovery phase in September. The general agreement found between the course of  $A$  and that of the other water stress indicators supports the feasibility of the proposed methodology to assess the effects of deficit irrigation on gas exchange and biomass accumulation. Besides that, the seasonal dynamics of MXTD were also affected by the imposed irrigation treatments: as the summer progressed, values of MXTD in the deficit treatments diverged from those of CI indicating a reduction in trunk growth (Fig. 2.4D-F). These results seem to be in accordance with several studies indicating the possibility of using the difference in MXTD between full and RDI trees as an early indicator of water stress (Fernández et al. 2011; Cuevas et al. 2013).

#### **2.4.4. Final remarks**

This study presents a new simple methodology for estimating  $A$  in irrigated fruit trees using  $E_p$  and meteorological data as inputs. By deriving  $E_p$  from sap flow measurements, our approach overcomes some of the weaknesses associated to the traditional methods for measuring  $A$ : it is suitable for automation, the values are representative of the whole canopy and the use of instrumentation as complex and expensive as both canopy chambers and eddy covariance techniques is avoided. As a practical limitation, determining proper estimates of  $A$  requires either a large number of sensors per monitored tree (López-Bernal et al. 2010) or sap flow records to be calibrated, which require additional field measurements. Besides that, the reliability of the methodology might be compromised by some of the theoretical assumptions undertaken for simplicity and ease of implementation. In particular, by adopting a fixed value for  $\beta$ , Eq. 2.3 is prone to errors in those species with marked variations in  $C_i$  in response to changing water status. Nevertheless, that issue is not perfectly characterized and, as it tends to magnify the differences between well-irrigated and water-stressed trees, the methodology still remains valid for detecting the occurrence of decreases in  $A$  associated to limited water availability. The results of our field experiments demonstrate the suitability of the methodology to yield, at least, rough estimates of  $A$  as well as to capture its variations under mild water stress conditions in mature olive trees. Last but not least, it is worthy to stress that the use of  $A$  for assessing responses to DI in fruit trees poses a valuable asset which complements the information provided by other classical water stress indicators: as  $A$  represents a measure of biomass accumulation, it presents a direct agronomical interpretation.

### **Acknowledgements**

This work was funded by the Andalusian Regional Government (Junta de Andalucía, project P10-AGR-6456) and the Spanish Ministry of Economy and Competitiveness (MINECO, project AGL-2010-20766) and European Regional Development Fund (ERDF). In addition, we thank the Spanish Research Council (CSIC) predoctoral JAE program and again the aforementioned project AGL-2010-20766 for providing the Ph.D. scholarship granted to the first and second author, respectively. Besides that, the authors also acknowledge the excellent technical support provided by Mr Rafael del Río, Mr Ignacio Calatrava and Mr José Luis Vazquez.

## **References**

- Bacelar EA, Santos DL, Moutinho-Pereira JM, Lopes JI, Gonçalves BC, Ferreira TC, Correia CM (2007) Physiological behavior, oxidative damage and antioxidative protection of olive trees grown under different irrigation regimes. *Plant Soil* 292:1-12.
- Baldocchi DD, Verma AB, Rosenberg NJ (1981) Seasonal and diurnal variation in the CO<sub>2</sub> flux and CO<sub>2</sub>-water flux ratio of alfalfa. *Agr Meteorol* 23:231-244.
- Brodribb T (1996) Dynamics of changing intercellular CO<sub>2</sub> concentration (c<sub>i</sub>) during drought and determination of minimum functional c<sub>i</sub>. *Plant Physiol* 111:179-185.
- Centritto M, Wahbi S, Serraj R, Chaves MM (2005) Effects of partial rootzone drying (PRD) on adult olive tree (*Olea europaea*) in field conditions under arid climate II. Photosynthetic responses. *Agr Ecosyst Environ* 106:303-311.
- Cuevas MV, Martín-Palomo MJ, Díaz-Espejo A, Torres-Ruiz JM, Rodríguez-Domínguez CM, Pérez-Martín A, Pino-Mejías R, Fernández JE (2013) Assessing water stress in a hedgerow olive orchard from sap flow and trunk diameter measurements. *Irrig Sci* 31:729-746.
- DeJong TM (1983) CO<sub>2</sub> assimilation characteristics of five *Prunus* tree fruit species. *J Am Soc Hortic Sci* 108:303-307.
- Díaz-Espejo A, Walcroft AS, Fernández JE, Hafidi B, Palomo MJ, Girón IF (2006) Modeling photosynthesis in olive leaves under drought conditions. *Tree Physiol* 26:1445-1456.
- Fereres E, Soriano MA (2007) Deficit irrigation for reducing agricultural water use. *J Exp Bot* 58:147-159.
- Fernández JE, Cuevas MV (2010) Irrigation scheduling from stem diameter variations: a review. *Agric For Meteorol* 150:135-151.
- Fernández JE, Torres-Ruiz JM, Díaz-Espejo A, Montero A, Álvarez R, Jiménez MD, Cuerva J, Cuevas MV (2011) Use of maximum trunk

- diameter measurements to detect water stress in mature ‘Arbequina’ olive trees under deficit irrigation. *Agric Water Manag* 98:1813-1821.
- Foken T, Leuning R, Oncley SP, Mauder M, Aubinet M (2012) Corrections and data quality. In: M Aubinet et al. (eds) *Eddy covariance: A Practical Guide to Measurement and Data Analysis*, Springer, Dordrecht, Heidelberg, London, New York, pp 85-131.
- Goldhamer DA, Viveros M (2000) Effects of preharvest irrigation cutoff durations and postharvest water deprivation on almond tree performance. *Irrig Sci* 19:125-131.
- Green S, Clothier B, Jardine B (2003) Theory and practical application of heat pulse to measure sap flow. *Agron J* 95:1371-1379.
- Jones HG (2004) Irrigation scheduling: advantages and pitfalls of plant-based methods. *J Exp Bot* 407:2427-2436.
- Kramer PJ, Boyer JS (1995) *Water relations of plants and soils*. Academic Press, Inc. San Diego, CA, pp 321-323.
- Law BE, Falge E, Gu L, et al (2002) Environmental controls over carbon dioxide and water vapor exchange of terrestrial vegetation. *Agric For Meteorol* 113:97-120.
- López-Bernal A, Alcantara E, Testi L, Villalobos FJ (2010) Spatial sap flow and xylem anatomical characteristics in olive trees under different irrigation regimes. *Tree Physiol* 30:1536-1544.
- Mariscal MJ, Orgaz F, Villalobos FJ (2000) Modelling and measurement of radiation interception by olive canopies. *Agric Forest Meteorol* 100:183-197.
- Marsal J, Girona J, Mata M (1997) Leaf water relation parameters in almond compared to hazelnut trees during a deficit irrigation period. *J Am Soc Hortic Sci* 122:582-587.
- Mauder M, Foken T (2011) *Documentation and instrumentation manual of the eddy-covariance software package TK3*. Universität Bayreuth, Bayreuth.

- Mitchell PD, Chalmers DJ (1982) The effect of reduced water supply on peach tree growth and yields. *J Am Soc Hort Sci* 107: 853-856.
- Moriana A, Fereres E (2002) Plant indicators for scheduling irrigation of young olive trees. *Irrig Sci* 21: 83-90.
- Moriana A, Orgaz F, Pastor M, Fereres E (2003) Yield responses of mature olive orchard to water deficits. *J Am Soc Hort Sci* 123: 425-431.
- Orgaz F, Testi L, Villalobos FJ, Fereres E (2006) Water requirements of olive orchards-II: determination of crop coefficients for irrigation scheduling. *Irrig Sci* 24:77-84.
- Pérez-Pérez JG, Romero P, Navarro JM, Botía P (2008) Response of sweet orange cv 'Lane late' to deficit irrigation in two rootstocks. I: water relations, leaf gas exchange and vegetative growth. *Irrig Sci* 26:415-425.
- Pérez-Priego O, Testi L, Orgaz F, Villalobos FJ (2010) A large closed canopy chamber for measuring CO<sub>2</sub> and water vapour exchange of whole trees. *J Exp Bot* 68:131-138.
- Romero P, Navarro JM, García F, Botía P (2004) Effects of regulated deficit irrigation during the pre-harvest period on gas exchange, leaf development and crop yield of mature almond trees. *Tree Physiol* 24:303-312.
- Rosati A, Metcalf S, Buchner R, Fulton A, Lampinen B (2006) Tree water status and gas exchange in walnut under drought, high temperature and vapour pressure deficit. *J Hortic Sci Biotech* 81:415-420.
- Steduto P, Hsiao T, Fereres E (2007) On the conservative behavior of biomass water productivity. *Irrig Sci* 25:189-207.
- Swanson RH, Whitfield WA (1981) A numerical analysis of heat pulse velocity. Theory and practice. *J Exp Bot* 32: 221-239.
- Testi L, Orgaz F, Villalobos FJ (2008) Carbon Exchange and water use efficiency of a growing, irrigated olive orchard. *Environ Exp Bot* 63:168-177.

- Testi L, Villalobos FJ (2009) New approach for measuring low sap velocities in trees. *Agric For Meteorol* 149: 730-734.
- Villalobos FJ, Testi L, Orgaz F, García-Tejera O, López-Bernal A, González-Dugo MV, Ballester-Lurbe C, Castel JR, Alarcón-Cabañero JJ, Nicolás EN, Girona J, Marsal J, Fereres E (2013) Modelling canopy conductance and transpiration in fruit trees: a simplified approach. *Agric For Meteorol* 171:93-103.
- Villalobos FJ, Perez-Priego O, Testi L, Morales A, Orgaz F (2012) Effects of water supply on carbon and water exchange of olive trees. *Eur J Agron* 40:1-7.
- Wong SC, Cowan IR, Farquhar GD (1979) Stomatal conductance correlates with photosynthetic capacity. *Nature* 282:424-426.

## **Chapter 3**

### **Using the compensated heat pulse method to monitor trends in stem water content in standing trees**

---



## Chapter 3

### Using the compensated heat pulse method to monitor trends in stem water content in standing trees

#### Summary

Studying the dynamics of stem water content ( $F_w$ ) in living trees has an outstanding physiological interest but all the available techniques to measure  $F_w$  exhibit major drawbacks. In this work, we present a new methodology to estimate variations in  $F_w$  along with sap velocity using the compensated heat pulse technique (CHP). One lab experiment was performed on several wooden blocks obtained from three different tree species. Samples were slowly dried and their moisture loss was monitored by both gravimetric approaches and time-domain reflectometry (TDR) or CHP probes in order to contrast the validity of our methodology (VSH-CHP) over a range of water contents. In addition, a field experiment was conducted to monitor  $F_w$  fluctuations in standing olive trees (*Olea europaea* L. cv. 'Arbequina') growing under three different irrigation regimes. In the lab test, the actual  $F_w$  values deduced gravimetrically differed from the estimates yielded by the VSH-CHP method. However, it could successfully track relative changes in the water stored for the range of  $F_w$  expected in living wood. Furthermore, the field experiment showed a seasonal change in  $F_w$  which was similar in shape and magnitude to those reported in the literature for olive and other Mediterranean tree species. On the other hand, differences in the seasonal patterns of  $F_w$  between irrigation treatments strongly corresponded with those of sap flow and some leaf water potential measurements. The results of this work suggest that the CHP technique could be employed to monitor the dynamics of both  $F_w$  and sap flow

*Using sap flow sensors to estimate stem water content dynamics*

simultaneously in standing trees and evidence that seasonal changes in  $F_w$  might be used as a long-term water status indicator.

### 3.1. Introduction

The stem water content ( $F_w$ ) of trees has been the subject of numerous studies for decades (Waring and Running 1978, Tyree and Yang 1990, Goldstein et al. 1998, Phillips et al. 2003). There is ample evidence that trees store water in sapwood during times of low evaporative demand and consume this water in transpiration when evaporative demand exceeds root water uptake. Therefore, the water stored is withdrawn and replenished in both daily and seasonal cycles, although the magnitude of the first is small compared with the latter. Thus, several studies have reported that the annual percentage change in  $F_w$  ranges from 8 % (0.50-0.46 cm<sup>3</sup> cm<sup>-3</sup>, *Pinus sylvestris*, Irvine and Grace 1997) to 67 % (0.61-0.20 cm<sup>3</sup> cm<sup>-3</sup>, *Aesculus californica*, Constantz and Murphy 1990) depending on species and environmental conditions (Constantz and Murphy 1990, Wullschlegel et al. 1996, Irvine and Grace 1997, Hernández-Santana et al. 2008; Nadler and Tyree 2008), whereas it rarely exceeds 10 % on a daily basis (Nadler and Tyree 2008).

Water extraction from stems occurs when the soil water potential becomes progressively negative during a drought. Under these conditions the water stored allows the tree to maintain both higher transpiration and photosynthesis rates holding up stomatal closure, so it has been contended that  $F_w$  plays a biologically significant role (Goldstein et al. 1998, Cermák et al. 2007). Furthermore, some studies have proposed that measurements of  $F_w$  could be employed to detect water stress (Nadler et al. 2003, Nadler et al. 2006, Hernández-Santana et al. 2008) as the close contact between the bole and the ground led  $F_w$  to track changes in soil water potential more closely than leaf water potential (Tyree and Ewers 1991). However, measuring water content in standing trees still remains a challenging task.

The simplest technique of measuring stem water content is to collect stem cores and directly measure the water content by weighing tissue samples before and after drying. Such traditional gravimetric measurement is labor intensive, difficult to automate and harmful for the tree after repeated sampling. These shortcomings led to the development of new approaches such as gamma-ray attenuation (Edward and Jarvis 1983), nuclear magnetic resonance (Byrne et al. 1986, Van As et al. 2009), electrical conductivity (Nadler and Tyree 2008, Nadler et al. 2008) or time-domain reflectometry (TDR). The first one is not currently used because of the risk of exposure to radiation while nuclear magnetic resonance is expensive and remains difficult to apply in the field and electrical conductivity measurements present some drawbacks as the need to wait a long curing period after probe installation and the fact of being affected by salinity. Constantz and Murphy (1990) were the first using TDR in living trees and noted that the technology provided a rapid, automatable and accurate mean of measuring  $F_w$ . Since then, some authors have employed TDR methodology with different species (Wullschleger et al. 1996, Irvine and Grace 1997, Hernández-Santana et al. 2008). On the contrary, the TDR method is expensive, complicated and requires calibration, although Wullschleger et al. (1996) produced an empirical relationship which was valid for a wide range of species. During the revision process of this article, we have become aware of a work by Vandegehuchte and Steppe (2012a) developing a non-empirical heat pulse based method to determine simultaneously both sap flux density and the sapwood water content using four-needle sap flow sensors (referred to as Sapflow+). Results of both finite element modelling and lab experiments show that Sapflow+ can afford accurate estimates of sap flux density and also of water content (at least during periods of low velocities), but it was not yet tested in living trees.

In this paper we describe a new methodology to estimate  $F_w$  in standing trees using the compensated heat pulse technique (CHP). The CHP has been widely used to determine the dynamics of transpiration by measuring sap flow in conductive organs of woody plants (Swanson and Whitfield 1981) and presents a great potential for irrigation scheduling (Fernández et al. 2001, 2008). In addition, this technique can also be used to detect water stress as the decline in tree transpiration (Fernández et al. 2001, Tognetti et al. 2004, 2005) and, more recently, López-Bernal et al. (2010) have suggested that the proportion of nocturnal to diurnal sap flow (N/D index) could also be another sensitive water status indicator.

The main goals of this study are to develop a simple methodology based on the calculation of the volumetric specific heat (VSH-CHP) that allows estimating  $F_w$  along with sap velocity using CHP sensors and to test its feasibility for monitoring fluctuations in  $F_w$  of the woody parts of trees. In addition, we investigate if the  $F_w$  monitored by that method could be employed as a suitable indicator of water status in olive trees growing under different irrigation regimes.

## **3.2. Material and Methods**

### **3.2.1. Theoretical framework of VSH-CHP**

The compensated heat pulse method (CHP) is based on the measurement of the temperature difference between sensors located above and below a heater inserted in the tree trunk (Swanson 1962). Marshall (1958) established the theoretical basis for this technique by deriving an analytical solution to the diffusion equation with coupled convective transport by sap within an infinite medium which has been recently adapted for anisotropic

conditions by Vandegehuchte and Steppe (2012b). That equation may be written as:

$$\Delta T = T_1 - T_2 = \delta \frac{H}{4\pi D_x \rho c t} \left[ \exp \frac{-(x_1 - v_h t)^2}{4D_x t} - \exp \frac{-(x_2 + v_h t)^2}{4D_x t} \right] \quad [3.1]$$

where  $\Delta T$  is the temperature difference between the down- and the up-stream sensor (K),  $x_1$  and  $x_2$  are the distances from down- and up-stream to the heater respectively (m),  $H$  is heat input from heat pulse ( $\text{J m}^{-1}$ ),  $D_x$  is thermal diffusivity in the axial direction ( $\text{m}^2 \text{s}^{-1}$ ),  $t$  is time since heat pulse applied (s),  $v_h$  is heat pulse velocity ( $\text{m s}^{-1}$ ),  $\rho c$  is volumetric specific heat,  $\text{J m}^{-3} \text{K}^{-1}$ ) and  $\delta$  is the square root of the quotient between axial and tangential thermal conductivities ( $K_x$  and  $K_y$ , respectively;  $\text{W m}^{-1} \text{K}^{-1}$ ):

$$\delta = \sqrt{\frac{K_x}{K_y}} \quad [3.2]$$

Swanson and Whitfield (1981) showed that the heat pulse velocity is linearly related to the inverse of the time from the heat pulse emission until the temperature difference returns to its initial value ( $t_0$ ):

$$v_h = \frac{x_1 + x_2}{2t_0} \quad [3.3]$$

To avoid underestimations, heat-pulse velocities should be corrected for wounding effects (Swanson and Whitfield 1981, Green et al. 2003) before further calculations.

The function  $\Delta T(t)$  given by Eq. 3.1 reaches a minimum value before  $t_0$  as the upstream sensor is heated faster than the downstream one. We can calculate this minimum using the derivative of Eq. 3.1:

$$\frac{\partial \Delta T}{\partial t} = \delta \frac{H}{4\pi D_x \rho c t^2} \left[ \exp \frac{-(x_1 - v_h t)^2}{4D_x t} \left( \frac{x_1^2 - v_h^2 t^2}{4D_x t} - 1 \right) - \left[ -\exp \frac{-(x_2 + v_h t)^2}{4D_x t} \left( \frac{x_2^2 - v_h^2 t^2}{4D_x t} - 1 \right) \right] \right] \quad [3.4]$$

Eq. 3.4 is equal to zero at the time of the minimum ( $t_n$ ), so we arrive at the next equation:

$$\exp\left[\frac{x_2^2 - x_1^2 + 2v_h t_n(x_1 + x_2)}{4D_x t_n}\right] = \frac{x_2^2 - t_n^2 v_h^2 - 4D_x t_n}{x_1^2 - t_n^2 v_h^2 - 4D_x t_n} \quad [3.5]$$

Knowing  $v_h$  - from Eq. 3.3 - we can compute  $D_x$  numerically from Eq. 3.5, and inverting Eq. 3.1 we arrive to:

$$\rho c = \delta \frac{H}{4\pi D_x t_n (T_1 - T_2)_n} \left[ \exp\frac{-(x_1 - v_h t_n)^2}{4D_x t_n} - \exp\frac{-(x_2 + v_h t_n)^2}{4D_x t_n} \right] \quad [3.6]$$

At this point some remarks should be made. First, any error in  $v_h$  is taken up in Eqs. 3.5 and 3.6 so the correction for wounding effects becomes a crucial point for the accuracy of the methodology. Second, under isotropic conditions (i.e.  $K_x = K_y$  and so  $\delta = 1$ ) all the variables in Eq. 3.6 are known and  $\rho c$  can be deduced. Finally, for zero heat pulse velocity the product  $4D_x t_n$  depends only on geometrical characteristics (i.e.  $x_1$  and  $x_2$ ) as it is deduced from Eq. 3.5, so, for that condition, Eq. 3.6 can be simplified to:

$$\rho c = \delta \frac{\gamma}{(T_1 - T_2)_n} \quad [3.7]$$

where  $\gamma$  can be calculated from  $H$  and the product  $4D_x t_n$ , which is a constant that depends only on  $x_1$  and  $x_2$  (see Eq. 3.5 for  $v_h = 0$ ). For instance, when  $x_1 = 10$  mm and  $x_2 = 5$  mm,  $4D_x t_n = 22.35$  mm<sup>2</sup>.

The last step of the VSH-CHP methodology is the estimation of  $F_w$ , which can be determined from  $\rho c$  as there is a relationship between both variables (Edwards and Warwick 1984):

$$F_w = \frac{\rho c - c_s \rho_d}{\rho_w c_w} \quad [3.8]$$

where  $c_w$  is the water specific heat (J kg K<sup>-1</sup>),  $c_s$  is the solid matrix specific heat and  $\rho_d$  and  $\rho_w$  are the basic densities of wood and water respectively (kg m<sup>-3</sup>).

The presented framework is limited as there is not a basis to estimate  $\delta$  which is a prerequisite to deduce  $\rho c$  in Eq. 3.6. By contrast, the methodology allows the monitoring of  $F_w$  from  $\rho c$  estimates for isotropic conditions. In this work all the calculations of  $F_w$  assume  $\delta = 1$  and the errors arising from that assumption are discussed below.

### **3.2.2. Lab experiments**

Lab experiments were conducted employing wood samples from several plant species including olive (*Olea europaea*), plum (*Prunus domestica*) and fig (*Ficus carica*) trees. Plant material, consisting of tree stem segments of, at least, 20 cm diameter, was collected from different locations and dates (always in winter) near the city of Córdoba, Spain (37.8 °N, 4.8 °W, 110 m altitude). These segments were cut using an industrial saw to obtain wooden blocks with cubic shapes of about 10 cm x 10 cm x 10 cm preserving the bark on one of their sides. In order to prevent moisture loss during transportation from the field to the lab, the samples were kept in plastic bags within isothermal boxes and, once they reached the lab, they were kept in cold conditions (4 °C). The time from sample collection to the beginning of experiments was short (four days) for plum and fig tree samples and long (several months) for those of olive, which were immersed in water for three days before the experiment to ensure a high initial  $F_w$ .

Lab experiments consisted of a drying process in which the moisture loss of the wooden blocks was simultaneously monitored employing gravimetric procedures ( $F_{w,obs}$ ) and either the VSH-CHP methodology as detailed above ( $F_{w,est}$ ) or the TDR-technique (see Table 3.1). The water-displacement method (based on the Archimedes principle) was employed for volume measurements before installing one sensor per wooden block on the side where the bark had been preserved.

The CHP sensors were designed and produced in the IAS-CSIC laboratory in Córdoba, Spain, and consist of a 4.8 W stainless steel heater of 2 mm diameter and two temperature probes of the same diameter that are placed in holes drilled in the wood 10 and 5 mm down- and up-stream of the heater, respectively. Accurate vertical spacing and parallel drilling are achieved using a steel drill-bit guide. Each temperature probe has four



embedded Type E (chromel-constantan wire) thermocouple junctions, spaced 10 mm along the needle that were sampled separately to estimate heat-pulse velocity and volumetric specific heat at 5, 15, 25 and 35 mm below the cambium. However, only the mean of the two intermediate depths was taken into account to monitor the moisture content ( $F_{w,est}$ ) as a precautionary measure to avoid possible heterogeneities in the heat applied. The system was controlled by a datalogger (CR1000, Campbell Scientific Inc., Logan, UT, USA) which performs measurement cycles at 15-minute intervals (for more details see Testi and Villalobos 2009). On the other hand, the TDR system (TDR 100) included 5 cm length probes and was also controlled by a datalogger (CR1000, Campbell Scientific Inc., Logan, UT, USA), measuring the apparent dielectric constant every 30 minutes.

**Table 3.1.** Species, installed devices and drying temperature for each of the wooden blocks examined in lab experiments.

Blocks	Species	Technique	Temperature (°C)
1-4	Olive	CHP	30
5-8	Fig	CHP	30
9-11	Plum	CHP	30
12-15	Olive	CHP	21
16-19	Olive	TDR	21

The wooden blocks were dried for at least one week in either an oven at 30 °C or in the lab at a room temperature of 21 °C (see Table 3.1). The mass of each block (with the sensors always kept in place) was measured frequently during the tests using a precision balance of  $\pm 0.1$  g resolution, especially at the beginning, when  $F_w$  loss was higher. Finally, CHP and TDR sensors were removed and weighted and the wooden blocks were dried at 105 °C

until they achieved constant mass ( $w_d$ ). The sapwood water content  $F_{w,obs}$  was then calculated for every mass measurement as:

$$F_{w,obs} = \frac{w_f - w_d}{\rho_w V} \quad [3.9]$$

where  $V$  is the fresh sample volume ( $m^3$ ) and  $w_f$  the block weight after subtracting the sensor mass (kg). These  $F_{w,obs}$  data were fitted to the best polynomial trend to obtain values each 15 minutes and they were compared with those of sapwood water content estimated from the VSH-CHP methodology ( $F_{w,est}$ ).

### **3.2.3. Field experiments**

The feasibility of using VSH-CHP to monitor changes in moisture storage in living trees was examined by monitoring  $F_{w,est}$  values during a long-term experiment which was conducted in an experimental olive (cv. ‘Arbequina’) orchard located at the CIFA Experimental Station, Córdoba, Spain (37.8 °N, 4.8 °W, 110 m altitude) during 2006. The climate is Mediterranean and the soil is a Typic Xerofluvent of sandy loam texture exceeding 1.5 m in depth, with upper drained soil water content limit of  $0.23 \text{ m}^3 \text{ m}^{-3}$  and lower soil water content limit of  $0.07 \text{ m}^3 \text{ m}^{-3}$  (López-Bernal et al. 2010). The olive trees were planted in 1997, tree spacing was 7 m x 3.5 m and irrigation was applied five days a week by drip, with seven  $4 \text{ l h}^{-1}$  drippers per tree. From 2004 to 2006 Iniesta et al. (2009) conducted an experiment testing three different irrigation treatments, which started in 2004 and finished in 2006:

1. Control treatment (CI), which applied enough irrigation to keep the maximum estimated evapotranspiration.

2. Continuous Deficit Irrigation (CDI), which applied 25 % of water applied in the control, distributed throughout the irrigation season (typically from the end of May to the beginning of October).

3. Regulated Deficit Irrigation (RDI), which applied the same total amount of irrigation as CDI, but with a midsummer deficit period without irrigation (typically from the beginning of July to the middle of September).

Particularly, in 2006 the irrigation season started on 1 June (DOY 152) and finished on 17 October (DOY 290) and the midsummer period with no irrigation for RDI trees covered from 28 June (DOY 179) to 12 September (DOY 255).

The experimental field was arranged as a randomized complete block with three replications, and each plot consisted of 12 olive trees in three adjacent rows. Both the two central trees of each plot (except two in the CI treatment) were instrumented with two CHP sensors per tree, at a height of 30 cm over the soil (4 CI, 6 CDI and 6 RDI trees) in order to monitor the daily sap flow and  $F_{w,est}$  dynamics. As in the lab experiments, only the CHP outputs corresponding to the intermediate thermocouples junctions were taken into account in the  $F_{w,est}$  calculations. Irregularities associated with daily variations in the moisture content were avoided considering only the averaged  $F_{w,est}$  values from 0300 to 0500 GMT for each day. Mean values of  $F_{w,est}$  and sap flow were calculated for each irrigation treatment. Besides, the mean relative sap flow was calculated for deficit treatments (i.e. the ratio between either CDI or RDI sap flow and that of CI) in order to contrast differences in water status. Weather data were recorded by an automated weather station placed 500 m from the orchard and reference daily evapotranspiration was calculated following Allen et al. (1998).

### 3.3. Results

#### 3.3.1. Lab experiments

Stem segments used in all experiments showed initial  $F_{w,obs}$  ranging from  $0.590 \text{ cm}^3 \text{ cm}^{-3}$  (Block 4) to  $0.447 \text{ cm}^3 \text{ cm}^{-3}$  (Block 9) and a clear curvilinear decay throughout the tests. However, values of  $F_{w,est}$  ranged initially from  $0.642 \text{ cm}^3 \text{ cm}^{-3}$  (Block 15) to  $0.391 \text{ cm}^3 \text{ cm}^{-3}$  (Block 4) and later they were found to decrease only during a variable period of time after the beginning of the experiments (from one to four days) until a stabilization occurred. As a consequence, both values and trends of  $F_{w,obs}$  did not match closely those of  $F_{w,est}$  in the drying experiments as it is exemplified in Fig. 3.1 for one of the fig wooden blocks (Block 6).

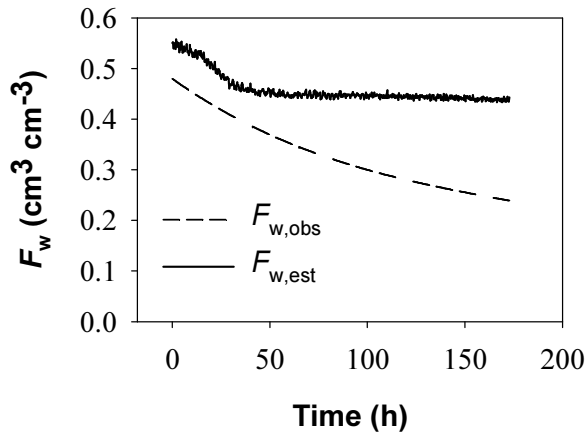


**Figure 3.1.** Evolution of sapwood water content values estimated by VSH-CHP methodology ( $F_{w,est}$ , solid line) and those gravimetrically obtained ( $F_{w,obs}$ , dashed line) during the drying process. The results correspond to one of the monitored wooden blocks of fig (Block 6).  $F_{w,est}$  values show a step reduction in parallel with those of  $F_{w,obs}$  followed by an stabilization which is not found for the gravimetric data.

The similarities and differences between the gravimetric and the calculated values of moisture content are presented in Fig. 3.2 for all samples plotting  $F_{w,est}$  against the interpolated  $F_{w,obs}$ . Although most of the sensors showed deviations from the 1/1 line (dashed line), all of them presented clear parallelisms to it for the higher moisture contents. This indicates that the relative reduction in  $F_{w,obs}$  measured during the first hours of drying was in good agreement with that detected by the VSH-CHP methodology. Fig. 3.1 also illustrates those results showing similar reductions in  $F_{w,obs}$  and  $F_{w,est}$  ( $0.102 \text{ cm}^3 \text{ cm}^{-3}$  and  $0.106 \text{ cm}^3 \text{ cm}^{-3}$  respectively) if only the first 45 h of drying test are considered.

These findings were supported by a linear regression analysis between  $F_{w,est}$  and  $F_{w,obs}$  which was performed for each sample using only pair of data with  $F_{w,obs}$  greater than 75 % of the initial value of  $F_{w,obs}$  (Table 3.2). All correlations resulted statistically significant ( $P < 0.0001$ ) with determination coefficients higher than 0.850 (except for the block 7). The slopes and the intercepts of the linear regression equations showed mean values of 0.993 and 0.003 respectively, which were very close to the theoretical optimum. On the other hand, the slope and intercept standard deviations were 0.229 and 0.107 respectively, indicating a large sensor variability which was not apparently related neither to species nor experimental conditions.

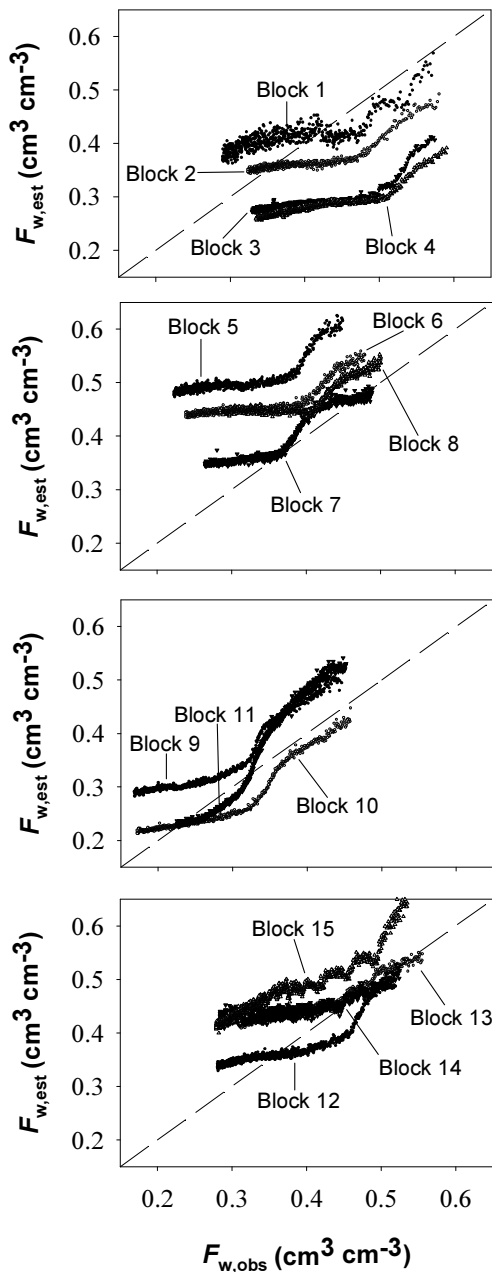


**Figure 3.2.** Comparisons between sapwood water content values calculated by VSH-CHIP methodology ( $F_{w,est}$ ) and those gravimetrically obtained ( $F_{w,obs}$ ) for each lab experiment showing the variability among individual sensors. Dashed line correspond to the 1/1 line and each symbol represent a sensor.

**Table 3.2.** Linear regressions relating the sapwood water content

calculated by VSH-CHP methodology to that gravimetrically estimated considering only the first phase of the drying process. Accordingly, only the data with  $F_{w,obs}$  greater than 0.75 of the initial value of  $F_{w,obs}$  were taken into account.

Block	Slope	Intercept	$r^2$	$\rho_d$ (g cm <sup>-3</sup> )
1	1.064	-0.073	0.893	0.67
2	0.902	-0.043	0.953	0.66
3	0.922	-0.136	0.877	0.65
4	0.769	-0.076	0.900	0.64
5	1.311	0.024	0.875	0.41
6	1.129	0.017	0.949	0.41
7	0.652	0.172	0.756	0.41
8	0.994	0.050	0.940	0.41
9	0.920	0.094	0.968	0.56
10	1.035	-0.043	0.947	0.58
11	1.291	-0.040	0.957	0.56
12	1.332	-0.193	0.933	0.62
13	0.789	0.110	0.950	0.62
14	0.610	0.186	0.872	0.63
15	1.173	-0.009	0.869	0.62
<b>Mean</b>	0.993	0.003	0.909	
<b>SD</b>	0.229	0.107	0.055	

Finally, the wooden blocks equipped with TDR sensors presented a curvilinear pattern between the monitored apparent dielectric constant ( $\epsilon$ ) and  $F_{w,obs}$  (Figure 3.3). The averaged  $\epsilon$  values decreased from 22.93 to 10.77 while those of  $F_{w,obs}$  ranged from 0.547 to 0.282 cm<sup>3</sup> cm<sup>-3</sup>. Most of the variation in  $\epsilon$  occurred when  $F_{w,obs}$  decreased from 0.55 to 0.40 cm<sup>3</sup> cm<sup>-3</sup>.

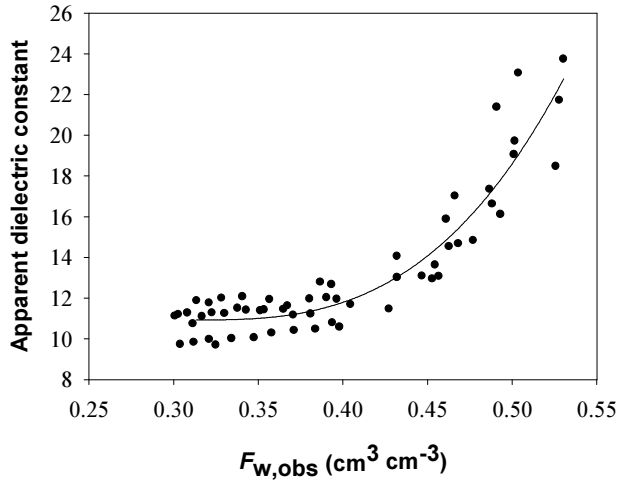


**Figure 3.3.** Apparent dielectric constant versus gravimetric wood water content ( $F_{w,obs}$ ). Data were obtained from the olive wooden blocks 16, 17, 18 and 19 which were equipped with TDR probes.

### 3.3.2. Field experiments

The mean patterns of the calculated  $F_{w,est}$  along the year 2006 are shown in Fig. 3.4. In general, the dynamics of  $F_{w,est}$  followed a sinusoid trend with a spring maximum and a late summer minimum by the end of the dry season. The mean  $F_{w,est}$  values for these extremes ranged between 0.548 and 0.488  $\text{cm}^3 \text{cm}^{-3}$  respectively and the magnitude of this interval was slightly influenced by the irrigation treatment. Thus, RDI showed the highest seasonal  $F_{w,est}$  differences (0.546 – 0.478  $\text{cm}^3 \text{cm}^{-3}$ ) followed by CDI (0.548 – 0.488  $\text{cm}^3 \text{cm}^{-3}$ ) and CI trees (0.550 – 0.497  $\text{cm}^3 \text{cm}^{-3}$ ).



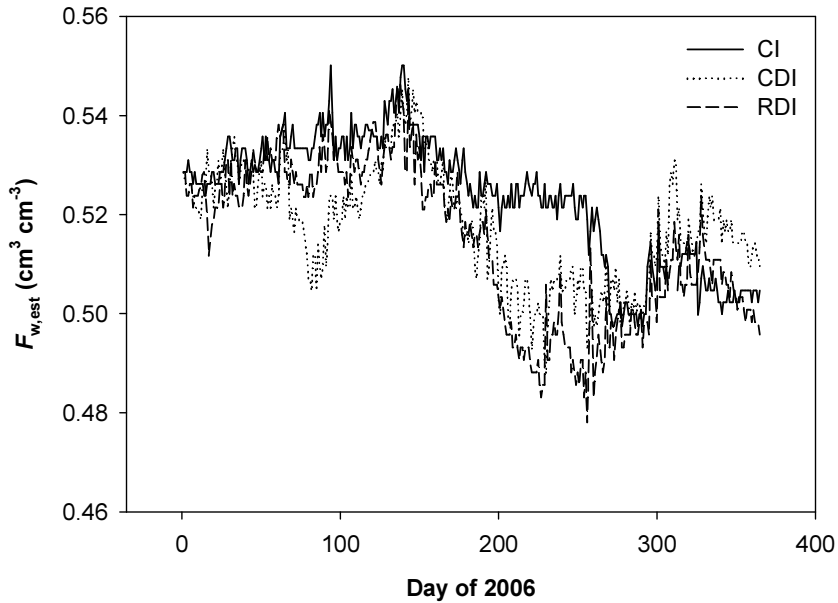


**Figure 3.4.** Temporal variation in the estimated stem water content ( $F_{w,est}$ ) in olive tree trunks under different irrigation regimes (CI: control, solid line; CDI: continuous deficit irrigation, dotted line; RDI: regulated deficit irrigation, dashed line) based on the VSH-CHP methodology. Data correspond to the mean of four trees for CDI and RDI treatments, and of two for the control one. All trees were monitored by two sensors each at a height of 30 cm over the soil.

A deeper analysis of the annual changes in moisture storage revealed decreasing trends in  $F_{w,est}$  for all irrigation treatments during summertime which were sharper for the deficit treatments (especially in RDI). By contrast, similar patterns were found in winter, spring and fall. Thus, from 28 June (DOY 179) to 12 September (DOY 255) the mean  $F_{w,est}$  values were 0.523, 0.506 and 0.498  $\text{cm}^3 \text{cm}^{-3}$  for CI, CDI and RDI respectively

while, in the rest of the season they averaged 0.524, 0.521 and 0.519 cm<sup>3</sup> cm<sup>-3</sup>.

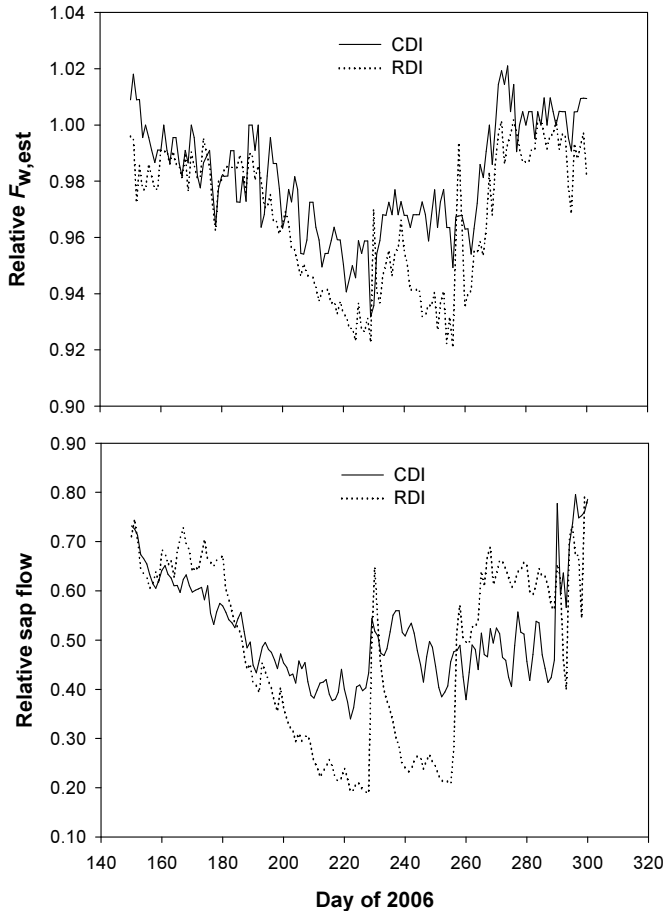


**Figure 3.5.** Temporal variation in the relative tree  $F_{w,est}$  (top) and sap flow (bottom) of CDI (solid line) and RDI (dotted line) olive tree trunks referred to the control (i.e. the ratio between the value of either the CDI or RDI treatments and that of the control one) based on the VSH-CHP methodology. The values employed to obtain this graph include data from 4 CI, 6 CDI and 6 RDI trees which were monitored by two sensors each at a height of 30 cm over the soil.

On the other hand, sap flow trends were in good agreement with those of  $F_{w,est}$ , with differences among treatments concentrated during the irrigation season when control trees maintained high values of sap flow while those of deficit treatments showed a clear decline which was sharper during the midsummer. The similarities between  $F_{w,est}$  and sap flow patterns are illustrated in relative terms in Fig. 3.5. Thus, from 28 June (DOY 179) to 12 September (DOY 255) CDI and RDI the mean sap flow values were 0.46 and 0.33 times lower in relation to CI respectively. Finally, the short and step recovering trends found for RDI and CDI from 17 August (DOY 229) were associated with a rainfall event of 47 mm.

### 3.4. Discussion

#### 3.4.1. Lab experiments

The trends in wood water stored calculated by VSH-CHP methodology did not match up the actual values of  $F_w$ . The main difference between these trends occurred as a consequence of an unexpected stabilization in  $F_{w,est}$  values (Fig. 3.1). In fact, the  $F_{w,est} - F_{w,obs}$  trends (Fig. 3.2) draw an analogy with the curvilinear relationships obtained by TDR between the apparent dielectric constant and the  $F_{w,obs}$  found in both our lab experiments (Fig. 3.3) and the literature (Constantz and Murphy 1990, Wullschleger et al. 1996, Irvine and Grace 1997). Thus, both the  $F_{w,est}$  and the apparent dielectric constant show little changes when the actual moisture contents are low. This may have been the result of heterogeneities in the drying process after losing the most part of the free water. Under these circumstances (fibre saturation point), the more strongly bound water could be leaving the outer portions of the wooden blocks faster than the inner parts (where the sensor measurements were made). However, both the

outer- and the innermost thermocouple junctions of the probes (not taken into consideration in further analysis to avoid heterogeneities in the heat applied) revealed identical  $F_{w,est}$  patterns to those of the intermediate depths (data not shown) suggesting that the drying process was spatially homogeneous throughout the volume of the blocks and, therefore, rejecting that hypothesis. An alternative explanation could be that the stabilization in  $F_{w,est}$  values might be due to changes in the local conditions of contact between wood tissue and CHP probes as wood shrinks with water withdrawal. Air may have replaced the air in the minuscule gaps between CHP probes and wood after the depletion of the free water. Such scenario would reduce the amount of heat reaching the thermocouple junctions resulting in a decrease in the maximum temperature difference between the down- and the upstream probes ( $(T_1-T_2)_h$ ) and in an overestimation of  $\rho c$  and  $F_{w,est}$  according to Eq. 3.7. As a final remark, some small cracks were originated during the drying processes indicating that changes in wood volume had taken place which may also be playing a role in the stabilization of  $F_{w,est}$ . Anyway, more research efforts are required on the subject if the causes of this phenomenon are to be clarified.

The stabilization in  $F_{w,est}$  values resulted in an underestimation of the actual drop in moisture content (given by  $F_{w,obs}$ ) during the second part of the drying tests. By contrast, the VSH-CHP methodology was able to track accurately relative variations in  $F_{w,obs}$  during the first hours of the trials which was supported by the similarity between  $F_{w,est}$  and  $F_{w,obs}$  slopes in Fig. 3.1, by the parallelisms with the 1/1 line in Fig. 3.2 and by the results of the linear regression analysis. Moreover, the slopes of the regression lines were close to 1 (Table 3.2), indicating that a decrease in the actual water content results in a reduction in  $F_{w,est}$  of the same magnitude. As mentioned in the previous section, the regression analysis included only those data with  $F_{w,obs}$  greater than 75 % of the initial value to avoid the

stabilization in  $F_{w,est}$ . This range of  $F_{w,obs}$  variation (i.e. 25 %) should cover the seasonal changes of  $F_w$  in most living trees. Standing olive trees, for example, present a seasonal range of  $F_w$  from 0.45 cm<sup>3</sup> to 0.39 cm<sup>3</sup> cm<sup>-3</sup> (i.e. 13.3 %) according to Nadler and Tyree (2008). As a consequence, it can be concluded that the VSH-CHP methodology might be useful to monitor relative  $F_w$  changes in living trees although its validity remains uncertain for those species and conditions presenting a seasonal range of  $F_w$  higher than 25 %.

On the other hand, the variability found in the regression coefficients in Table 3.2 was not found to be influenced by neither tree species, trial conditions (summarized in Table 3.1) nor basic density (Table 3.2). In other words, even samples under the same experimental conditions presented differences in the slope and intercept of the linear regression between  $F_{w,est}$  and  $F_{w,obs}$ . Differences in the heat applied by each sensor ( $H$  in Eq. 3.6) were analyzed as a possible cause for those results. For this purpose, the electrical power absorbed by each probe was individually determined by precisely measuring the voltage and current passing through them during the firing of a heat pulse. Although these measurements revealed some differences among probes (standard deviation of 0.11 W around a mean power of 4.7 W at 23 °C) their magnitude was insufficient to explain all the variability found in laboratory experiments. Small deviations with regard to the theoretical position of the thermocouple junctions may also be a source of sensor variability, although the sensors were installed using a steel drill-bit guide to ensure parallelism. Again, differences in the interface conditions between wood and sensors may be playing a major role as a source of variability in  $F_{w,est} - F_{w,obs}$  relationships, but more research efforts are required to address that point. Consequently, calibration is almost impossible, as it would require a different equation to convert the  $F_{w,est}$  estimates in actual values of  $F_w$  for each scenario of sensor – wood. Hence,

the feasibility to obtain absolute estimates of  $F_w$  by the VSH-CHP methodology is questionable.

### **3.4.2. Influence of anisotropy on VSH-CHP methodology**

All the calculations of  $F_w$  presented in this study were made assuming isotropic conditions. Such assumption is unrealistic as thermal conductivity is higher along than across the grain ( $K_x > K_y$ ) (Maku 1954, Steinhagen 1977). The origin of anisotropy lies in the histology of wood or, in other words, in the size, shape and orientation of the fibres, vessels and other cells that compose wood (Maku 1954). As a result, the degree of anisotropy should differ between species, individuals or even between stem portions of the same tree.

Considering anisotropy introduce several implications for the VSH-CHP method. First of all, the coefficient  $\delta$  in Eq. 3.6 is unknown and should present values greater than one. Consequently, the methodology is theoretically unable to determine precisely the actual  $F_w$ , and omitting anisotropy results in an underestimation of  $\rho c$  and  $F_w$ . Secondly, the degree of anisotropy depends on the moisture content with  $\delta$  increasing when wood dries (Siau 1971). Both issues should affect the feasibility of VSH-CHP to monitor the exact magnitude of changes in  $F_w$ .

**Table 3.3.** Range of  $F_{w,obs}$ ,  $F_{w,est}$  and  $F_{w,corr}$  between the extremes considered in the linear regression analysis for each sample. The values of  $\delta$  needed to calculate  $F_{w,corr}$  are also shown and they were estimated using the equations of Siau (1971) and Vandegheuchte and Steppe (2012c).

Block	$F_{w,obs}$		$F_{w,est}$		$\delta$		$F_{w,corr}$	
	Initial	Final	Initial	Final	Initial	Final	Initial	Final
1	0.57	0.43	0.54	0.40	1.15	1.24	0.65	0.54
2	0.58	0.43	0.48	0.36	1.15	1.24	0.58	0.49
3	0.57	0.43	0.41	0.29	1.15	1.24	0.50	0.41
4	0.59	0.44	0.38	0.28	1.14	1.23	0.46	0.39
5	0.44	0.33	0.61	0.49	1.23	1.30	0.78	0.68
6	0.47	0.35	0.55	0.44	1.21	1.29	0.69	0.60
7	0.48	0.36	0.48	0.36	1.21	1.28	0.61	0.50
8	0.50	0.38	0.54	0.44	1.20	1.27	0.67	0.59
9	0.44	0.33	0.50	0.39	1.23	1.30	0.66	0.56
10	0.45	0.34	0.43	0.29	1.23	1.30	0.57	0.43
11	0.45	0.34	0.52	0.40	1.23	1.30	0.68	0.57
12	0.52	0.39	0.48	0.36	1.18	1.26	0.60	0.51
13	0.55	0.41	0.54	0.44	1.16	1.25	0.66	0.60
14	0.52	0.39	0.51	0.43	1.18	1.26	0.64	0.59
15	0.53	0.40	0.64	0.49	1.18	1.26	0.79	0.67
<b>Mean</b>	0.51	0.38	0.51	0.39	1.19	1.27	0.64	0.54
<b>SD</b>	0.05	0.04	0.07	0.07	0.03	0.02	0.09	0.09

In an attempt to assess the impact of anisotropy on the results of our lab experiments the model of Siau (1971) with the corrected equations proposed by Vandegheuchte and Steppe (2012c) were applied to estimate the values of  $\delta$  from  $F_{w,obs}$  data corresponding to the extremes considered in the linear regression analysis for each sample. These  $\delta$  values were employed to deduce corrected wood water contents ( $F_{w,corr}$ ). As expected, the results of these rough calculations (summarized in Table 3.3) show that

$F_{w,corr}$  values are consistently higher than those of  $F_{w,obs}$  and  $F_{w,est}$ . Conversely, variations in  $\theta_{ck}$  in all samples are slightly higher than those of  $F_{w,obs}$  and  $F_{w,est}$  (on average  $0.15 \text{ cm}^3 \text{ cm}^{-3}$  versus  $0.12$  and  $0.12 \text{ cm}^3 \text{ cm}^{-3}$  respectively). Accordingly, if anisotropy is taken into account, the VSH-CHP method fails to accurately estimate the change in  $F_{w,obs}$  but still can afford useful information in the relative monitoring of water content variations to some extent. On the other hand, Table 3.3 show minimal differences in  $\delta$  between samples of the same species and experimental conditions indicating that the sensor variability found in the regression analysis (Table 3.2) is not a consequence of assuming  $\delta = 1$  in  $F_{w,est}$  calculations. As a final remark, conclusions arising from the above analysis should be taken with caution, as it is founded on indirect estimations of  $\delta$ . Therefore, it is obvious that anisotropy adds some uncertainty about the reliability of VSH-CHP, which deserves further research.

### **3.4.3. Field experiments**

Field experiment showed the occurrence of substantial seasonal changes in  $F_{w,est}$  for all monitored trees. Annual variations in  $F_{w,est}$  revealed a typical pattern for all irrigation treatments, with maximum values at the end of spring followed by a progressive decline during the summer and a latter recovery associated with the end of the dry season and the occurrence of autumn rainfalls (Fig. 3.4, Iniesta et al. 2009). This pattern bears a close resemblance to those previously reported in the literature and determined by TDR under similar climatic conditions (Constantz and Murphy 1990, Hernández-Santana et al. 2008). The first found an annual percentage change in  $F_w$  ranging from 15 to 70 % depending on species while the latter obtained from 10 to 17 % of  $F_w$  seasonal variation for three consecutive years in melojo oak trees (*Quercus pyrenaica*). In addition, Nadler and



Tyree (2008) reported the annual  $F_{w,est}$  variation for different species including olive, which ranged  $0.06 \text{ cm}^3 \text{ cm}^{-3}$  with a maximum value of  $0.45 \text{ cm}^3 \text{ cm}^{-3}$  (i.e. a 13.33 % of percentage change). Similarly, our results showed an average annual  $F_{w,est}$  variation of  $0.060 \text{ cm}^3 \text{ cm}^{-3}$  with a maximum average value of  $0.548 \text{ cm}^3 \text{ cm}^{-3}$  (i.e. a 9.5 % of percentage change). The good agreement found in the magnitude of the annual change in  $F_w$  is very encouraging as it indicates that the VSH-CHP methodology can successfully be employed in order to monitor  $F_w$  seasonal variations in living trees. On the contrary, the aforementioned absolute values of  $F_{w,est}$  resulted higher than those reported by Nadler and Tyree (2008) stressing again that the ability of the VSH-CHP methodology to provide actual values of  $F_w$  is uncertain at our actual stage of understanding.

Large differences were found in  $F_{w,est}$  between irrigation treatments throughout the dry season which were in good agreement with tree sap flow patterns. During the summer,  $F_{w,est}$  showed a sharper decline in CDI and RDI than in CI trees due to water shortening (Iniesta et al., 2009), being RDI the treatment which reached the lowest values and shows the widest  $F_{w,est}$  seasonal range (Fig. 3.4, 3.5). For the same period, sap flow followed a similar trend, with significant differences between CI and deficit treatments and RDI being the one reaching the lowest values (Fig. 3.5). In addition, Iniesta et al. (2009) conducted some midday leaf water potential ( $\Psi$ ) measurements for the same olive trees in 2006. Despite the scarce available data (only two measures in summer), differences between irrigation treatments can be clearly detected again, showing RDI the lowest  $\Psi$  values followed by CDI and CI. Finally, the three irrigation treatments showed no significant differences in both  $F_{w,est}$ ,  $\Psi$  and sap flow values either after or before the irrigation season (Fig. 3.4, Iniesta et al. 2009). Both the decline in sap flow,  $\Psi$  and  $F_{w,est}$  patterns during the dry season indicate differences in water status between irrigation treatments which

were in good agreement with the irrigation applied and thus with the water availability. All this body of evidence indicate that  $F_{w,est}$  could be employed as a long-term water status indicator as it has been previously suggested by other authors (Nadler et al., 2003; Nadler et al., 2006; Hernández-Santana et al., 2008).

### **3.5. Conclusions**

The present study shows a new alternative to track  $F_w$  trends in living trees by using the CHP technique. Our lab and field experiments support that the VSH-CHP method can successfully monitor relative changes in the water stored in a given sampling depth. The technique is rapid, easy to automate, provides simultaneous information about sap velocity and tree transpiration and, like TDR, is not too harmful for the tree. Nevertheless, it does not obtain actual values of  $F_w$ , calibration is not apparently possible, and its feasibility is uncertain for those trees with high seasonal changes in  $F_w$  which deserves further research. In addition, the methodology assumes that wood acts as an isotropic medium which is unrealistic and may slightly affect the accuracy of the technique. On the other hand, this work has presented new evidence on the validity of  $F_w$  as a long-term water stress indicator and has stressed that the CHP technique is a valuable tool to obtain information about the water status of trees.

**Acknowledgments**

The authors thank the excellent technical support provided by Mr. Rafael del Río, Mr. Ignacio Calatrava and Mr. José Luis Vazquez, and the constructive suggestions from both one anonymous reviewer and the editor which enabled us to improve the final version of this article. This work was funded by project AGL2010 20766 of the Spanish Ministry of Natural, Rural and Marine Environment and the predoctoral JAE program (CSIC) grants.

## **References**

- Allen RG, Pereira JS, Raes D, Smith M (1998) Crop evapotranspiration: guidelines for computing crop water requirements. Vol. 56, Food and Agriculture Organization of the United Nations, Rome, 300 pp.
- Byrne GF, Fenn MD, Burgar MI (1986). Nuclear magnetic resonance studies of water in tree sections. *Agric For Meteorol* 38:307-317.
- Cermák J, Kucera J, Bauerle WL, Phillips NG, Hinckley TM (2007) Tree water storage and its diurnal dynamics related to sap flow and changes in stem volume in old-growth Douglas-fir trees. *Tree Physiol* 27:181-198.
- Constantz J, Murphy F (1990) Monitoring moisture storage in trees using time domain reflectometry. *J Hydrol* 119:31-42.
- Edwards WRN, Jarvis PG (1983) A method for measuring radial differences in water content of intact tree stems by attenuation of gamma radiation. *Plant Cell Environ* 6:255-260.
- Edwards WRN, Warwick NWM (1984) Transpiration from a kiwifruit vine as estimated by the heat-pulse technique and the Penman-Monteith equation. *NZ J Agric Res* 27:537-543.
- Fernández JE, Palomo MJ, Diaz-Espejo A, Clothier BE, Green SR, Giron IF, Moreno F (2001) Heat-pulse measurements of sap flow in olives for automatic irrigation: tests, root flow and diagnosis of water stress. *Agric Water Manage* 51:99-123.
- Fernández JE, Green SR, Caspari HW, Diaz-Espejo A, Cuevas MV (2008). The use of sap flow measurements for scheduling irrigation in olive, apple and Asian pear trees and in grapevines. *Plant Soil* 305:91-104.
- Goldstein G, Andrade JL, Meinzer FC, Holbrook NM, Cavellier J, Jackson P, Celis A (1998) Stem water storage and diurnal patterns of water use in tropical forest canopy trees. *Plant Cell Environ* 21:397-406.
- Green SR, Clothier BE, Jardine B (2003) Theory and practical application of heat pulse to measure sap flow. *Agron J* 95:1371-1379.

- Hernández-Santana V, Martínez-Fernández J, Morán C, Cano A (2008) Response of *Quercus pirenaica* (melojo oak) to soil water deficit: a case study in Spain. *Eur J Forest Res* 127:369-378.
- Iniesta F, Testi L, Orgaz F, Villalobos FJ (2009) The effects of regulated and continuous deficit irrigation on the water use, growth and yield of olive trees. *Eur J Agron* 30:258-265.
- Irvine J, Grace J (1997) Non-destructive measurement of stem water content by time domain reflectometry using short probes. *J Exp Bot* 48:813-818.
- López-Bernal A, Alcántara E, Testi L, Villalobos FJ (2010) Spatial sap flow and xylem anatomical characteristics in olive trees under different irrigation regimes. *Tree Physiol* 30:1536-1544.
- Maku T (1954) Studies on heat conduction in wood. Kyote University, Bulletin of the Wood Research Institute No. 13. pp. 1-80. Marshall DC (1958) Measurement of sap flow in conifers by heat transport. *Plant Physiol* 33:385-396.
- Nadler A, Raveh E, Yemiyahu U, Green SR (2003) Evaluation of TDR use to monitor water content I stem of lemon trees and soil and their response to water stress. *Soil Sci Soc Am J* 67:437-488
- Nadler A, Raveh E, Yemiyahu U, Green SR (2006) Stress induced water content variations in mango stem by time domain reflectometry. *Soil Sci Soc Am J* 70:510-520.
- Nadler A, Tyree MT (2008) Substituting stem`s water content by electrical conductivity for monitoring water status changes. *Soil Sci Soc Am J* 72:1006-1013.
- Nadler A, Raveh E, Yermiyahu U, Lado M, Nasser A, Barak M, Green SR (2008) Detecting water stress in trees using stem electrical conductivity measurements. *Soil Sci Soc Am J* 72:1014-1024.
- Phillips NG, Ryan MG, Bond BJ, McDowell NG, Hinckley TM, Cermák J (2003) Reliance on stored water increases with tree size in three species in the Pacific Northwest. *Tree Physiol* 23:237-245.

- Steinhagen P (1977) Thermal conductive properties of wood, green or dry, from -40 °C to +100 °C: a literature review. Forest Product Laboratory, Forest Service, US Department of Agriculture.
- Siau JF (1971) Flow in wood. In: Côté WA (ed) Syracuse Wood Science Series. Syracuse University Press, New York, pp131.
- Swanson RH (1962) An instrument for detecting sap movement in woody plants. USDA For Serv Rocky Mountain For Rnge Exp Sta pap. No. 68.
- Swanson RH, Whitfield WA (1981) A numerical analysis of heat pulse velocity. Theory and practice. J Exp Bot 32:221-239.
- Testi L, Villalobos FJ (2009) New approach for measuring low sap velocities in trees. Agric For Meteorol 149:730-734.
- Tognetti R, d'Andria R, Morelli G, Calandrelli D, Fragnito F (2004) Irrigation effects on daily and seasonal variations of trunk sap flow and leaf water relations in olive trees. Plant Soil 263:249-264.
- Tognetti R, d'Andria R, Morelli G, Alvino A (2005) The effect of deficit irrigation on seasonal variations of plant water use in *Olea europaea* L. Plant Soil 273:139-155.
- Tyree MT, Yang S (1990) Water-storage capacity of *Thuja*, *Tsuga* and *Acer* stems measured by dehydration isotherms. Planta 182:420-426.
- Tyree MT, Ewers FW (1991) The hydraulic architecture of trees and other woody plants. New Phytol 119:345-360.
- Van As H, Scheenen T, Vergeldt FJ (2009) MRI of intact plants. Photosynth Res 102:213-222.
- Vandegehuchte MW, Steppe K (2012a) Sapflow+: a four-needle heat pulse sap flow sensor enabling nonempirical sap flux density and water content measurements. New Phytol 196:306-317.

Vandegehuchte MW, Steppe K (2012b) Use of the correct heat conduction-convection equation as basis for heat-pulse sap flow methods in anisotropic wood. *J Exp Bot* 63:2833-2839.

Vandegehuchte MW, Steppe K (2012c) Improving sap flux density measurements by correctly determining thermal diffusivity, differentiating between bound and unbound water. *Tree Physiol* 32:930-942.

Waring RH, Running SW (1978) Sapwood water storage: its contribution to transpiration and effect upon water conductance through the stems of old-growth Douglas-fir. *Plant Cell Environ* 1:131-140.

Wullschleger SD, Hanson PJ, Todd DE (1996) Measuring stem water content in four deciduous hardwoods with a time-domain reflectometer. *Tree Physiol* 16:809-815.

## **Chapter 4**

# **Thermal properties of sapwood of fruit trees as affected by anatomy and water potential: errors in sap flux density measurements based on heat pulse methods**

---



## Chapter 4

### **Thermal properties of sapwood of fruit trees as affected by anatomy and water potential: errors in sap flux density measurements based on heat pulse methods**

#### **Summary**

Sapwood thermal properties and water content ( $F_w$ ) natural variations affect the accuracy of heat pulse sap flow methods, as they are typically set as constants or calculated during zero flow conditions. In a first experiment, a characterisation of both thermal properties and some of their determining anatomical and functional factors was conducted on several fruit tree species assessing the reliability of different methodologies. Besides that, a second experiment was carried out to evaluate the errors of heat pulse methods arising from ignoring  $F_w$  variations. To do so, desorption curves were constructed, allowing the substitution of  $F_w$  changes with those of water potential ( $\Psi$ ). Results of the first experiment showed considerable differences between species in both the thermal, anatomical and functional properties of sapwood. Apart from that, discrepancies between the methods applied to determine thermal properties were also found and their implications for some heat pulse methods are discussed. The analysis conducted for the second experiment indicated that large errors in sap flux density ( $J$ ) determinations might occur when daily and seasonal variations of  $\Psi$  (and hence of  $F_w$ ) are disregarded. The extent of these errors was influenced by the species and heat pulse technique. Thus, the Heat Ratio and Tmax were, respectively, the least and most vulnerable methods to errors in  $J$  determinations associated with changes in  $F_w$ .

#### **4.1. Introduction**

Heat pulse sap flow methods have been developed to measure tree transpiration and water use, which is important in hydrology, ecophysiology, agronomy or forestry among other scientific disciplines. Given that they are based on the use of heat as a tracer, it is not surprising that sapwood thermal properties are crucial parameters for their theoretical frameworks. Despite this, little attention has been paid to characterizing thermal properties in a plant physiological context (Dupleix et al. 2013), with most available research focused on the use of dry wood as a construction material.

The main sapwood thermal properties involved in sap flow research are thermal conductivity ( $K$ ,  $\text{W m}^{-1} \text{K}^{-1}$ ), which describes its ability to transmit heat for a given temperature gradient, and volumetric specific heat ( $\rho c$ ,  $\text{J m}^{-3} \text{K}^{-1}$ ), which describes its ability to store heat. The quotient of both variables is defined as thermal diffusivity ( $D$ ,  $\text{m}^2 \text{s}^{-1}$ ):

$$D = \frac{K}{\rho c} \quad [4.1]$$

On the other hand, wood is not isotropic, as both thermal conductivity and diffusivity along the grain (i.e. in the flow direction,  $K_x$ ,  $D_x$ ) are larger than across the grain ( $K_y$ ,  $D_y$ ) (Maku 1954). The degree of anisotropy ( $R_K$ ) can be evaluated from the ratio of  $K_x$  to  $K_y$ .

Sapwood thermal properties are intimately connected with both structural and physical characteristics of the wood matrix. Thus, sapwood solid, liquid and gas fractions ( $F_s$ ,  $F_w$ ,  $F_g$ , respectively) are determining factors for thermal properties, a fact that is included in existing models (Siau 1971; Vandegehuchte and Steppe 2012a). In more depth, the  $F_s$  is mainly defined by the volume occupied by cell walls while the remaining space is divided

between  $F_w$  and  $F_g$  as a function of both the state of tension and the xylem traits determining its ability to retain water (e.g. diameter of lumen) (Tyree and Zimmermann 2002). As a result, the natural changes in stem water potential ( $\Psi$ ) occurring at both daily and seasonal scale should have an influence on  $F_w$  and, hence, on thermal properties and sap flow measurements.

The present study is focused on those sap flow methods in which sap flux density ( $J$ , i.e. the sap volume per unit area and unit of time) is determined from the velocity of a short pulse of heat moving along xylem tissue through conduction and convection ( $v_h$ ). Among them, both the compensated heat pulse (CHP), the calibrated average gradient (CAG; Testi and Villalobos 2009) and the Sapflow+ (Vandegehuchte and Steppe 2012b) methods have the advantage that thermal properties are not required a priori for  $v_h$  calculations. On the contrary, an estimate of  $D_x$  is a prerequisite for the Tmax (Cohen et al. 1981) and the heat ratio (HR, Burgess et al. 2001) methods. The latter applies a protocol to estimate  $D_x$  based on the implementation of either Siau (1971) or Vandegehuchte and Steppe (2012a) models from occasional measurements of  $F_w$  and dry density of sapwood ( $\rho_d$ ) by core sampling. In doing so, the natural variation of  $D_x$  associated to  $\Psi$  and  $F_w$  changes are disregarded. On the other hand, the Tmax method estimates  $D_x$  by applying a theoretically correct equation, but is prone to errors as it is based on single point analysis. Moreover, such an equation is only valid for zero-flow conditions, so  $D_x$  is currently computed once a day at night, neglecting its diurnal variations.

Finally, all the aforementioned methods require, once more, estimates of  $F_w$  and  $F_s$  for the conversion of  $v_h$  into  $J$ . Edwards and Warwick (1984) developed the most frequently employed equation for this purpose:

$$J = (kF_s + F_w)v_h \quad [4.2]$$

where the factor  $k$  is assumed to be 0.441 within and between species for a temperature of 20 °C (Becker and Edwards 1999).  $F_w$  and  $F_s$  are typically determined from single gravimetric measurements by core sampling which is harmful for the tree. Therefore, seasonal and daily variations in  $F_w$  are ignored although they might also induce large errors in the calculation of  $J$ . Only Sapflow+ is theoretically able to partly avoid this issue, as it allows for  $F_w$  determinations at low flow conditions (Vandegehuchte and Steppe 2012b).

The first aim of this study was to characterise sapwood thermal properties in the trunk of several fruit tree species as well as some of their determining factors, including  $F_s$ ,  $F_w$  and  $F_g$  and some anatomical traits. Thermal properties were determined by different alternative methodologies, including the most common approaches applied in the case of HR and Tmax. In doing so, comparisons between such approaches were established. The second goal of this study was to assess potential impacts of natural changes in  $\Psi$ , and hence in  $F_w$ , on the accuracy of heat pulse methods for determining  $J$ . Two different experiments were designed to address each of these objectives.

## **4.2. Materials and methods**

Experiments were conducted on mature individuals of different drip-irrigated fruit tree species growing in some experimental orchards located at the CIFA Experimental Station, Córdoba, Spain (37.8°N, 4.8°W, 110 m altitude).

### 4.2.1. Experiment 1

In June and July 2012, three trees of olive (*Olea europaea* L.; Oe), three of almond (*Prunus dulcis* (Mill) D.A. Webb; Pd), two of sweet orange (*Citrus sinensis* L.; Cs) and one of bitter orange (*Citrus aurantium* L.; Ca), pomegranate (*Punica granatum* L., Pg), kaki (*Diospyros kaki* Thunb.; Dk) and fig (*Ficus carica* L.; Fc) were selected to characterise their sapwood thermal, anatomical and functional properties.

#### 4.2.1.1. Measurements of basic density ( $\rho_d$ ), $F_s$ , $F_w$ and $F_g$

Wood cores of 2.5 cm diameter and 4 cm length were extracted from the tree trunk at breast height (one per tree) and transported to the lab in sealed plastic bags early in the morning (~06:00 GMT). Fresh weight ( $w_f$ ) and fresh volume ( $V$ ) were subsequently measured (the latter applying the water displacement method, which is founded in the Archimedes principle). Then, wood samples were oven-dried until they achieved constant weight ( $w_d$ ).  $\rho_d$  was determined as the quotient between  $w_d$  and  $V$  while  $F_w$  was calculated dividing the difference  $w_f - w_d$  by the product of  $V$  and water density (1000 kg m<sup>-3</sup>). Then,  $F_s$  was estimated as the ratio of  $\rho_d$  to the basic density of cell walls ( $\rho_{cw}$ ), which was assumed to be 1530 kg m<sup>-3</sup> (Kollmann and Côté 1968). Finally,  $F_g$  was deduced as  $1 - F_w - F_s$ .

#### 4.2.1.2. Determination of thermal properties

Four different methods were applied to estimate sapwood thermal properties:

- Siau (1971) classic model: it allows the calculation of  $K_x$  and  $K_y$  through empirical relationships from values of  $F_w$  and  $F_s$ :

$$K_x = K_w F_w + (1 - F_w) 0.04186 [21 - 20(1 - F_s - F_w)] \quad [4.3]$$

$$K_y = K_w F_w + (1 - F_w) 0.04186 [12.2 - 11.3 \sqrt{1 - F_s - F_w}] \quad [4.4]$$

where  $K_w$  is the thermal conductivity of water ( $0.5984 \text{ W m}^{-1} \text{ K}^{-1}$ ). Despite the fact that the meaning of  $F_w$  is misinterpreted in these equations (Vandegehuchte and Steppe 2012a), we have included this approach because it has been the most widely used methodology to determine thermal properties in the context of sap flow research to date. Input data were taken from the core-sampling and gravimetric measurements described above.

- Vandegehuchte and Steppe (2012a) model: this model is an improvement of the Siau (1971) classic model in which the equations are corrected, making it sound for determining  $K_x$  and  $K_y$  in living sapwood. Input data were the same as in the previous method. The equations are:

$$K_x = K_w (F_w - F_{V,FSP}) + 0.04186 (21 - 20 F_{V,FSP}) \quad [4.5]$$

$$K_y = K_w (F_w - F_{V,FSP}) + 0.04186 (12.2 - 11.3 \sqrt{F_{V,FSP}}) \quad [4.6]$$

Where  $F_{V,FSP}$  is the volumetric water content at fibre saturation point, which can be calculated as  $0.2(\rho_d/1000)^{0.5}$  according to Roderick and Berry (2001).

- Tmax method: each experimental tree was instrumented with sap flow probes (one per tree) for four days. The probes were designed and produced in the IAS-CSIC Laboratory in Córdoba, Spain, and consist of a 4.8 W stainless steel heater of 2 mm diameter and two temperature probes of the same diameter that are placed in holes drilled in the wood. Each temperature probe measured independently (once a second during cycles of 169 s) the temperature rise after a 2 s heat pulse at 5 and 15 mm below the cambium with two embedded Type E (chromel-constantan wire) thermocouple junctions. The system was controlled by a datalogger (CR1000, Campbell Scientific Inc., Logan, UT, USA) which performs measurement cycles at 15-min

intervals. Temperature probes were installed 5 mm apart from the heater in axial (vertical) and tangential (lateral) directions using a steel drill-bit guide to ensure the accuracy of the spacing and parallel drilling. The equation derived by Kluitenberg and Ham (2004), which accounts for finite pulse duration, was employed in the estimation of  $D_x$  and  $D_y$  using the time between the onset of the heat pulse and the maximum temperature rise recorded in the temperature probes ( $t_m$ ) as input:

$$D_i = \frac{L_i^2}{4t_m} \frac{t_p}{(t_m - t_p)} \left[ \ln \left( \frac{t_m}{t_m - t_p} \right) \right]^{-1} \quad [4.7]$$

Where  $t_p$  is heat pulse duration (s) and  $L_i$  the distance to the heater in the “i” direction (mm). Only the  $t_m$  records corresponding to measurement cycles from 03:00 to 4:45 GMT (both included) of four consecutive days were employed for determining  $D_x$  and  $D_y$ , as the approach is only valid for zero-flow conditions.

- Knight et al. (2012) method: these authors presented a semianalytical solution that, accounting for probe radius and heat capacity, allows the calculation of sapwood thermal properties using dual heat pulse probes following an optimization process. In other words, the semianalytical solution applies varying values of  $K$  and  $\rho c$  as inputs to produce temperature curve responses at a given distance to the heater. Thus, sapwood thermal properties can be deduced from the subset of  $K$  and  $\rho c$  values achieving the best fit to measured temperature data. To do so, the temperature curves provided by the sap flow equipment described for the Tmax method were used. As for Eq. 4.7, the semianalytical solution of Knight et al. (2012) is only valid for zero-flow conditions so, in order to minimize possible errors, again the data recorded between 03:00 and 04:45 GMT were considered for the determinations.

Except for the latter, in all approaches  $\rho c$  was determined from data on  $\rho_d$  and  $F_w$  as in López-Bernal et al. (2012):

$$\rho c = \rho_w c_w F_w + c_s \rho_d \quad [4.8]$$

with  $\rho_w$  being density of water ( $1000 \text{ kg m}^{-3}$ ) and  $c_w$  and  $c_s$  specific heat capacities of water ( $4186 \text{ J kg}^{-1} \text{ K}^{-1}$ ) and the wood matrix ( $1200 \text{ J kg}^{-1} \text{ K}^{-1}$ ), respectively. Finally, the calculated values of  $\rho c$ ,  $K_x$  and  $K_y$  were used to deduce  $D_x$  and  $D_y$  (Eq. 4.1) and  $R_K$ . Note also that in the case of the Tmax method, it was  $K_x$  and  $K_y$  which were deduced (inverting Eq. 4.1) from the estimated values of  $D_x$  and  $D_y$ .

#### **4.2.1.3. Anatomical measurements**

Anatomical traits were measured at  $\sim 5$  mm depth below the cambium from wood samples which were obtained from the exact location where sap flow probes had been installed. In other words, anatomical observations were carried out in the same wood in which thermal properties were measured with the outermost reading of sap flow probes. One sample per species was used. Transversal and tangential sections of 40-50  $\mu\text{m}$  thick were obtained with a sliding microtome, non-permanent preparations were mounted with toloum chloride and finally they were examined in an optical microscope (Nikon, Eclipse 80i, Japan).

The cross-sectional area fraction occupied by each cell type was obtained by drawing the contour of rays (in tangential sections), vessels and axial parenchyma cells (in transverse sections) over a xylem area always greater than  $3 \text{ mm}^2$  using the program NIS-Elements D 2.30 (Nikon). In order to account for the differences between earlywood and latewood in the ring porous wood of almond, the sampling area of axial elements was extended in radial direction to cover a whole growth ring. The remaining fibre



fraction was then deduced. Assuming that cell structures are perfectly oriented in the axial (fibre, vessels and axial parenchyma) or radial (rays) directions, these cross-sectional area fractions of each cell type were considered to represent the volumetric fractions in wood.

#### **4.2.2. Experiment 2**

The aim of experiment 2 was to quantify the errors in  $J$  determined by heat pulse methods associated with the natural variations in  $F_w$ . To do so, desorption curves of sapwood (i.e. relationships between  $\Psi$  and  $F_w$ ) were measured for some of the previously studied fruit tree species, allowing the prediction of  $F_w$  variations from those of  $\Psi$ . Desorption curves were employed to deduce the theoretical errors in  $J$  as a function of  $\Psi$  in relation to species and heat pulse method and some field data were used to illustrate the practical implications of ignoring  $F_w$  variations for calculating  $J$ .

##### **4.2.2.1. Desorption curves**

Desorption curves were constructed for olive, almond, fig, and sweet orange. Wood cores (2.5 cm diameter and 4 cm length) were extracted in summer 2013 from the same orchards in which measurements of thermal and anatomical properties were performed, in neighbouring trees to those previously studied. Wood samples were immersed in water immediately after their extraction for at least 24 h. Then, cores were sectioned perpendicularly to their longitudinal axis obtaining 3-4 wooden discs of about 1 cm thick whose volume was determined using the water displacement method. Hereafter a WP4-T dewpoint potentiometer (Decagon devices, Pullman, WA) was used to determine the water potential ( $\Psi$ ) of the wooden discs, which were progressively air dried. The weight of samples was recorded immediately after each  $\Psi$  measurement. Once measurements were finished, samples were oven dried at 105 °C until they

achieved constant weight to deduce both  $\rho_d$  and the  $F_w$  corresponding to each  $\Psi$  measurement. As shown below in the results section, the obtained desorption curves presented well-differentiated phases so piecewise linear equations of either 4 or 5 segments were fitted to the data pairs of  $F_w$ - $\Psi$  to obtain continuous mathematical functions linking both variables ( $F_w(\Psi)$ ).

To give insight into the validity of the desorption curves, a small set of independent and additional field measurements of  $\Psi$  at dawn and midday with a pressure chamber (Soil Moisture Equipment Corp., Santa Barbara, CA, USA) were conducted in selected shoots from the same trees where samples were taken for the construction of desorption curves (with the exception of the fig tree because we were unable to measure  $\Psi$  due to the typical exudation of latex in this species). For midday measurements, the sampled shoots were previously covered with aluminium foil (around 6 h before measurements) in order to prevent transpiration and, in all cases, they were directly attached to the tree trunk. In doing so, the measured values of  $\Psi$  were assumed to represent those in the trunk xylem. This assumption was reasonable as long as the presence of low flows through the selected shoots, which may result from night-time transpiration or refilling processes, should only lead to very slight underestimations of  $\Psi$  because of both the low magnitude of these possible flows and the short path (low hydraulic resistance) between the point of insertion into the trunk and the point of measurement.

#### **4.2.2.2. Theoretical analysis of errors in $J$ measurements by CHP, CAG and Sapflow+ as a function of $\Psi$**

For both CHP and CAG methods  $F_w$  is involved in  $J$  determinations as shown in Eq. 4.2, but its diurnal and seasonal variations are ignored. The same applies to Sapflow+ (Vandegehuchte and Steppe 2012b) with the particularity that, as it allows the determination of  $F_w$  under conditions of

low sap flow (which can be daily assumed at night), it minimizes the errors associated to seasonal variations in  $F_w$ . Equation 4.2 was rewritten using the  $F_w(\Psi)$  for each species in order to obtain piecewise expressions in which  $J$  were calculated as a function of  $\Psi$  (i.e.  $J(\Psi)$ ). Then, the relative error in the determination of  $J$  ( $E_j$ , %) was calculated as:

$$E_j = \frac{J(\Psi_{\text{ref}}) - J(\Psi)}{J(\Psi)} 100 \quad [4.9]$$

Where  $J(\Psi_{\text{ref}})$  and  $J(\Psi)$  are  $J$  calculated from either a preset value of  $\Psi$  ( $\Psi_{\text{ref}}$ ) or the actual value of  $\Psi$ , respectively. Therefore, Eq. 4.9 represents the deviations in the calculation of  $J$  that arise from assuming  $\Psi$  (and, hence  $F_w$ ) as a constant with a value of  $\Psi_{\text{ref}}$  under actually varying  $\Psi$  conditions. Hence, it is simulating what occurs in practice, as Eq. 4.2 is generally applied from single measurements of  $F_w$ . For the calculations, the value of  $\Psi_{\text{ref}}$  was assumed to be the maximum of the range covered by the desorption curves (in all species around -0.6 MPa).

#### **4.2.2.3. Theoretical analysis of errors in $J$ measurements by HR as a function of $\Psi$**

According to the HR working equation,  $v_h$  is directly related to  $D_x$ , which is typically determined by applying both Eq. 4.8 and either Eq. 4.3 or Eq. 4.5 from single destructive measurements of  $F_w$  and  $\rho_d$  (Burgess et al. 2001; Vandegheuchte and Steppe 2012a). Such values of  $F_w$  and  $\rho_d$  are also used further in Eq. 4.2 to obtain  $J$ . As  $F_w$  is involved in the calculation of  $D_x$ , an additional source of error has to be considered for the HR as compared to CHP, CAG and Sapflow+ methods. For this purpose, equations 4.8 and 4.5 were modified by substituting  $F_w$  with  $\Psi$  -again using the  $F_w(\Psi)$  relationships for each species-, allowing the calculation of  $D_x$  as a function of  $\Psi$ . Then, the working equation of Burgess et al. (2001) was rewritten to

express  $v_h$  as a function of  $\Psi$  (i.e.  $v_h(\Psi)$ ). Finally, combining the functions  $v_h(\Psi)$  with those resulting from modifying Eq. 4.2,  $E_J$  can be calculated as:

$$E_J = \frac{J(\Psi_{\text{ref}}) - J(\Psi)}{J(\Psi)} 100 = \frac{[kF_s + F_w(\Psi_{\text{ref}})]v_h(\Psi_{\text{ref}}) - [kF_s + F_w(\Psi)]v_h(\Psi)}{[kF_s + F_w(\Psi)]v_h(\Psi)} 100 \quad [4.10]$$

Where the value of  $\Psi_{\text{ref}}$  was again assumed to be the maximum of the range covered by the desorption curves.

#### **4.2.2.4. Theoretical analysis of errors in $J$ measurements by Tmax as a function of $\Psi$**

In the case of the Tmax method,  $D_x$  is again included in the working equation (Kluitenberg and Ham 2004):

$$v_h = \sqrt{\frac{4D_x}{t_p} \ln\left(1 - \frac{t_p}{t_m}\right) + \frac{x^2}{t_m(t_m - t_p)}} \quad [4.11]$$

With  $t_p$  being the heat pulse duration and  $x$  the distance between the temperature probe and the heater. The same procedure as in HR was applied to assess  $E_J$  as a function of  $\Psi$  with an exception: as  $v_h$  is not linearly related to  $D_x$  (Eq. 4.11) the assessment of  $E_J$  is dependent on the values of  $x$ ,  $t_p$  and  $t_m$ . Thus, a common configuration of  $x=10$  mm and  $t_p=1$  s and a  $t_m$  of 52 s were always assumed in the analysis, leading to  $v_h$  around  $50 \text{ cm h}^{-1}$  for the  $\Psi_{\text{ref}}$ . Lastly, note that the theoretical  $E_J$  estimated for the Tmax method applies on a daily scale, as daily calculations of  $D_x$  are theoretically possible at night-time if conditions of zero-flow can be assumed (Kluitenberg and Ham 2004).

#### **4.2.2.5. Application to a field case**

Measurements of  $\Psi$  were performed in four dates from spring to autumn in 2013 (DOYs 176, 211, 234 and 281; DOY=day of year) in a hedgerow

olive orchard located near Córdoba. The orchard had been planted in 2005 with 4 x 1.5 m spacing over a soil classified as Vertisol according to the FAO classification. Trees were drip-irrigated and two irrigation treatments were applied in separate plots of 40 trees in 4 adjacent rows:

1. Control irrigation (CI): enough water to sustain maximum evapotranspiration was supplied during all the irrigation season (from DOY 177 to DOY 295). To do so, the irrigation dose was calculated following the approach of Orgaz et al. (2006).
2. Deficit irrigation (RDI): the water applied was a 30 % of that of CI from DOY 182 to DOY 243 and the same as CI for the rest of the irrigation season.

Measurements of  $\Psi$  were performed with a pressure chamber (Soil Moisture Equipment Corp., Santa Barbara, CA, USA) at midday in non-transpiring shoots directly attached to the tree trunk or main branches (shoots were covered with aluminium foil five hours before the measurements). One central tree per treatment (the same for the four dates) and four shoots per tree were sampled. In addition, predawn  $\Psi$  was measured on DOY 234. All these measured values of  $\Psi$  were used as input data for estimating the errors in sapflow arising from both seasonal and daily variations of  $\Psi$  (and hence of  $F_w$ ) for the different methods using either Eq. 4.9 or Eq. 4.10. The required values of  $\Psi_{\text{ref}}$  were taken either from the midday  $\Psi$  corresponding to the first measurement date (DOY 176) when seasonal  $E_J$  were assessed or from the predawn  $\Psi$  on DOY 234 for the analysis of daily  $E_J$ .

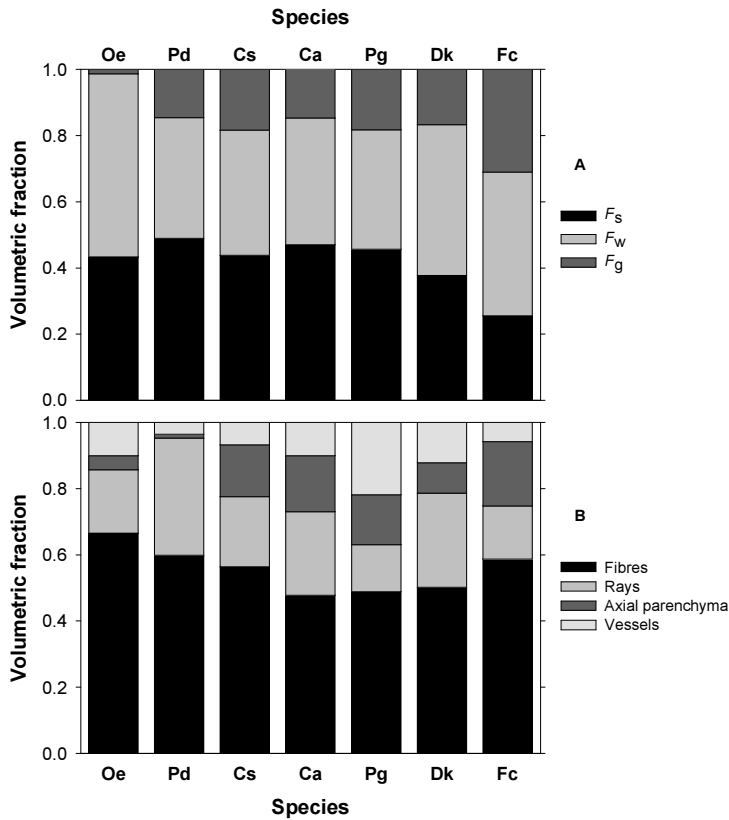
### **4.3. Results**

#### **4.3.1. Experiment 1**

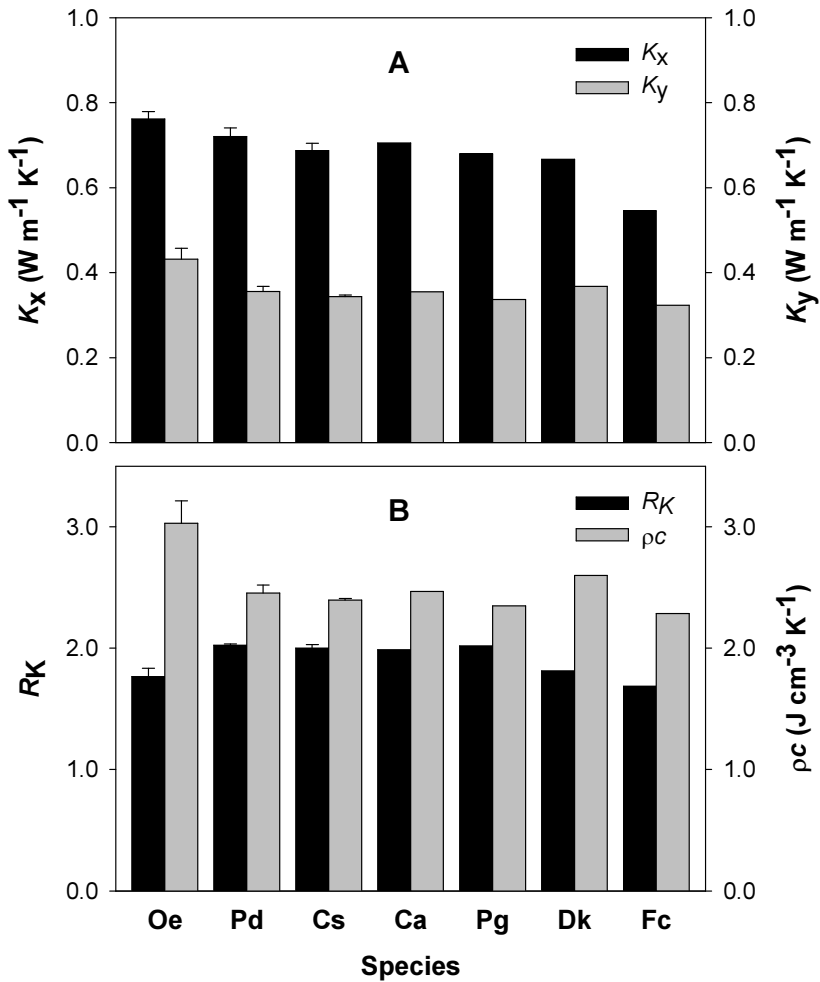
Variability between species in  $F_s$ ,  $F_w$  and  $F_g$  of sapwood is presented in Figure 4.1A.  $F_s$  accounted for slightly less than half of the sapwood volume in all species except for the lighter fig wood, in which  $F_s$  was 0.26. With regard to the remaining sapwood space,  $F_g$  was very high for fig (0.31), very low for olive (0.03) and intermediate for the rest of species (around 0.16). On the other hand, Fig. 4.1B shows the proportion of xylem occupied by each cell type for the studied species. Broadly speaking, slightly more than half of the xylem was comprised of fibre cells in all species while rays occupied between 0.16 and 0.28 of sapwood except for the case of almond, whose wide multiseriate rays accounted for 0.35. Greater differences were found in the proportions of axial parenchyma and vessels between species. Thus, the former was almost absent for almond while it occupied large xylem proportions ( $>0.15$ ) for fig and the two orange species (in these three species most axial parenchyma cells appeared grouped in tangential bands) while the vessel fraction ranged from 0.04 (almond) to 0.21 (pomegranate).

Figure 4.2 presents the thermal properties estimated following the approach of Vandegehuchte and Steppe (2012a) for the studied species. Both  $K_x$  and  $K_y$  were the highest and the lowest for olive and fig sapwood, respectively. For the rest of species,  $K_x$  was slightly below those of olive while  $K_y$  was closer to that of fig (Figure 4.2A). The resulting  $R_K$  ranged from 1.68 to 2.03, with the lowest values for fig and olive sapwood (Figure 4.2B). Apart from that, small differences between species were found in  $\rho c$  except for the much higher values in the case of olive, which were in accordance with the greater  $F_w$  in this species (Fig. 4.1A). Thus, the latter yielded  $3.03 \text{ J cm}^{-3} \text{ K}^{-1}$ , while the rest of species exhibited an average  $\rho c$  of  $2.43 \text{ J cm}^{-3} \text{ K}^{-1}$ .

For almond, pomegranate and the two orange species the estimates of  $D_x$  ranged from 0.294 to 0.286  $\text{mm}^2 \text{s}^{-1}$  and lower values were observed in the case of olive, kaki and fig trees (0.252, 0.257 and 0.239  $\text{mm}^2 \text{s}^{-1}$ , respectively). By contrast, the variability in  $D_y$  between species was negligible (values ranging from 0.141 to 0.146  $\text{mm}^2 \text{s}^{-1}$ ). Finally, within tree variability in thermal properties (represented by the error bars for olive, almond and sweet orange in Figure 4.2) was generally small as compared to that observed among species.



**Figure 4.1.** **A** Volumetric fraction of sapwood occupied by solid ( $F_s$ ), liquid ( $F_w$ ) and gas ( $F_g$ ) for the studied species. **B** Volumetric fraction of sapwood occupied by fibres, rays, axial parenchyma and vessels for the studied species. Oe=olive, Pd=almond, Cs=sweet orange, Ca=bitter orange, Pg=pomegranate, Dk=kaki, Fc=fig.



**Figure 4.2.** **A** Axial and tangential thermal conductivities ( $K_x$  and  $K_y$ ), **B** anisotropy ratio ( $R_K$ ) and volumetric specific heat ( $\rho c$ ) for the studied species. Values were estimated following the Vandegehuchte and Steppe (2012) approach. Error bars showing standard errors are present for those species in which several trees were studied. Oe=olive, Pd=almond, Cs=sweet orange, Ca=bitter orange, Pg=pomegranate, Dk=kaki, Fc=fig.



Figure 4.3 and Table 4.1 illustrate the differences in estimated thermal properties as a function of the approach employed. The former represents the values of  $K_x$  and  $K_y$  estimated by the Siau (1971) (Fig. 4.3A), Tmax (Fig. 4.3B) and Knight et al. (2012) (Fig. 4.3C) approaches plotted against those obtained following Vandegehuchte and Steppe (2012a). On average, a good agreement was found between the values of  $K_x$  yielded by Siau (1971), Knight et al (2012) and Vandegehuchte and Steppe (2012a) approaches (Table 4.1 and Fig. 4.3A and 4.3C), while the Tmax method resulted in slightly lower values (Table 4.1, Fig. 4.3B). With regard to  $K_y$ , all methods showed systematically higher values than those estimated following the Vandegehuchte and Steppe (2012a) method, as evidenced both by the large differences shown in the  $K_y$  averages of Table 4.1 and by the fact that no points were found below the 1:1 line in Fig. 4.3. These results led to higher  $R_K$  deduced from the latter approach as compared to the rest (Table 4.1). Besides, the application of the Knight et al. (2012) approach resulted in higher values of  $\rho c$  than in the rest of methodologies (all of them based on Eq. 4.8). As a consequence,  $D_x$  values were the lowest and  $D_y$  estimates were close to those of Vandegehuchte and Steppe (2012a) when Knight et al. (2012) was applied (Table 4.1).

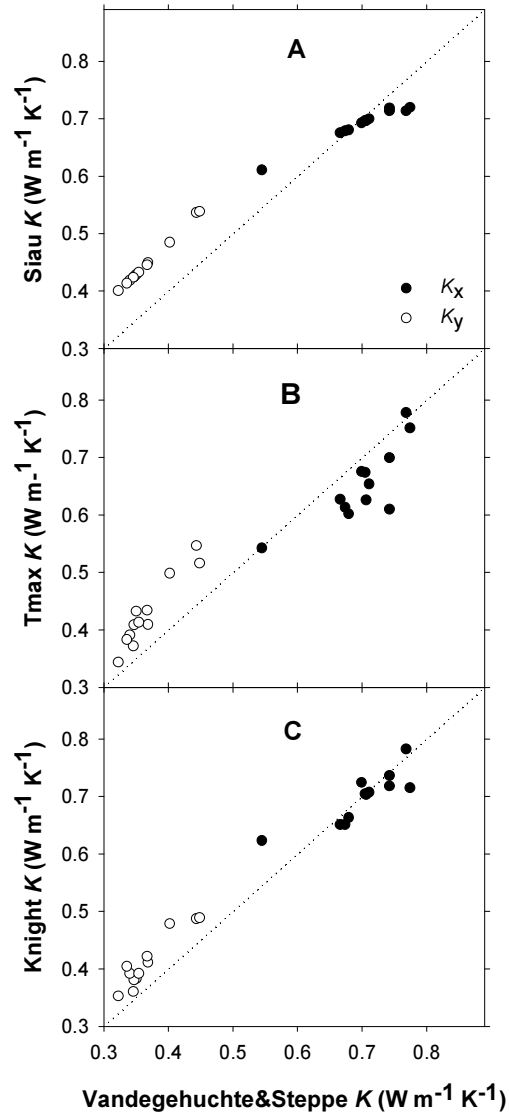


**Figure 4.3.** Plot of axial and tangential thermal conductivities ( $K_x$ , closed symbols and  $K_y$ , open symbols) estimated by both Siau (1971) (Eqs. 4.3 and 4.4), Tmax (combining Eqs. 4.7 and 4.8) and Knight et al. (2012) approaches versus those obtained from Eqs. 4.5 and 4.6 (Vandegehuchte and Steppe 2012) (A, B and C panels, respectively). Each point represents one experimental tree. Dotted line indicates the 1:1 line.

**Table 4.1.** Values of thermal properties (axial and tangential thermal conductivities,  $K_x$  and  $K_y$ ; anisotropy ratio,  $R_K$ ; volumetric specific heat,  $\rho c$ ; axial and tangential thermal diffusivities,  $D_x$  and  $D_y$ ) in relation to the methodology applied. All values correspond to the average of all experimental trees.

Method	Vandegheuchte & Steppe (2012)	Siau (1971)	Tmax	Knight et al. (2012)
$K_x$ ( $\text{W m}^{-1} \text{K}^{-1}$ )	0.702	0.691	0.654	0.698
$K_y$ ( $\text{W m}^{-1} \text{K}^{-1}$ )	0.369	0.449	0.429	0.412
$R_K$	1.90	1.54	1.52	1.69
$\rho c$ ( $\text{J cm}^{-3} \text{K}^{-1}$ )	2.58*	2.58*	2.58*	2.92
$D_x$ ( $\text{mm}^2 \text{s}^{-1}$ )	0.272	0.268	0.253	0.239
$D_y$ ( $\text{mm}^2 \text{s}^{-1}$ )	0.143	0.174	0.166	0.141

\*Values were obtained from those of  $F_w$  and  $\rho_d$  measured by core sampling.

### 4.3.2. Experiment 2

Desorption curves of olive, orange, almond and fig sapwood are shown in Figure 4.4 (panels A, B, C and D, respectively). In all cases, similar trends were observed, starting with a high capacitance region (large variations in  $F_w$  with little change in  $\Psi$ ) for the highest  $F_w$  which was followed by a phase of very low capacitance (with little change in  $F_w$  but large variations in  $\Psi$ ). Lastly, sapwood capacitance was partially recovered for  $\Psi$  values below those expected in living trees (below -4 MPa in all cases). For both olive and almond (Fig. 4.4A and 4.4C, respectively), the transition from the initial phase to the next took place sharply at  $F_w$  and  $\Psi$  around  $0.40 \text{ L L}^{-1}$  and -1.0 MPa, respectively, while the change was more gradual in the case

of sweet orange sapwood (Fig. 4.4B). The desorption curve for fig (Fig. 4.4D) was similar to those of olive and almond, but the first two phases occurred at higher  $F_w$ . Additionally, independent pairs of measurements of predawn and midday  $F_w$  and  $\Psi$  (the latter with a pressure chamber) were in good agreement with the trends observed using the WP4-T dewpoint potentiometer (see open symbols in Fig. 4.4A, 4.4B and 4.4C).

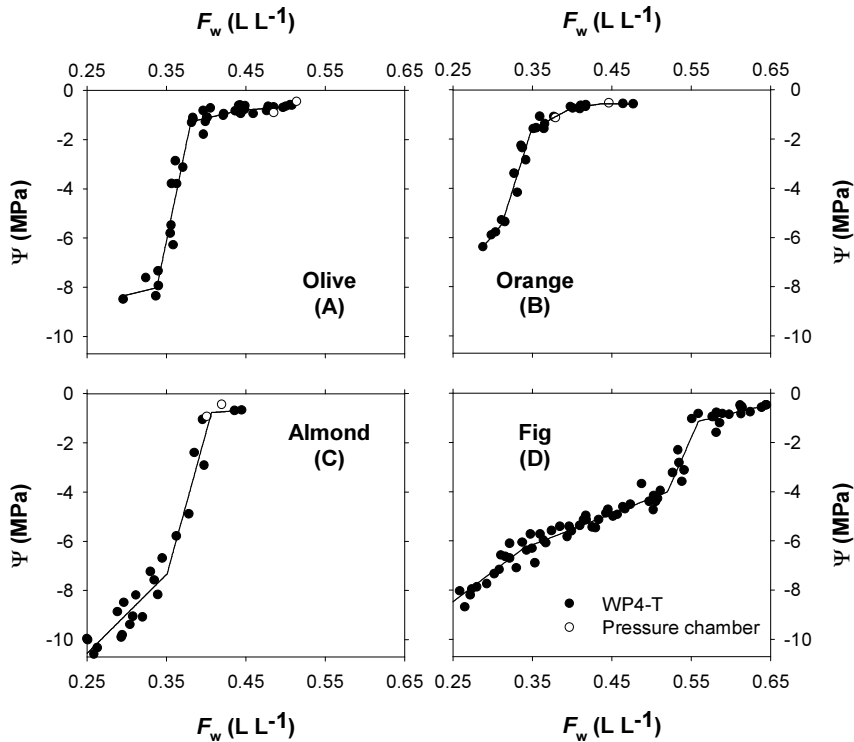


**Figure 4.4.** Desorption curves for sapwood of olive (A), sweet orange (B), almond (C) and fig (D) trees. Closed symbols correspond to points in which water potential ( $\Psi$ ) was measured using a WP4-T dewpoint potentiometer while open symbols were obtained from measurements of  $\Psi$  at predawn and midday in non transpiring shoots with a pressure chamber. Sample water content ( $F_w$ ) was always gravimetrically determined (in the latter case from cores extracted at the same time that  $\Psi$  was measured).

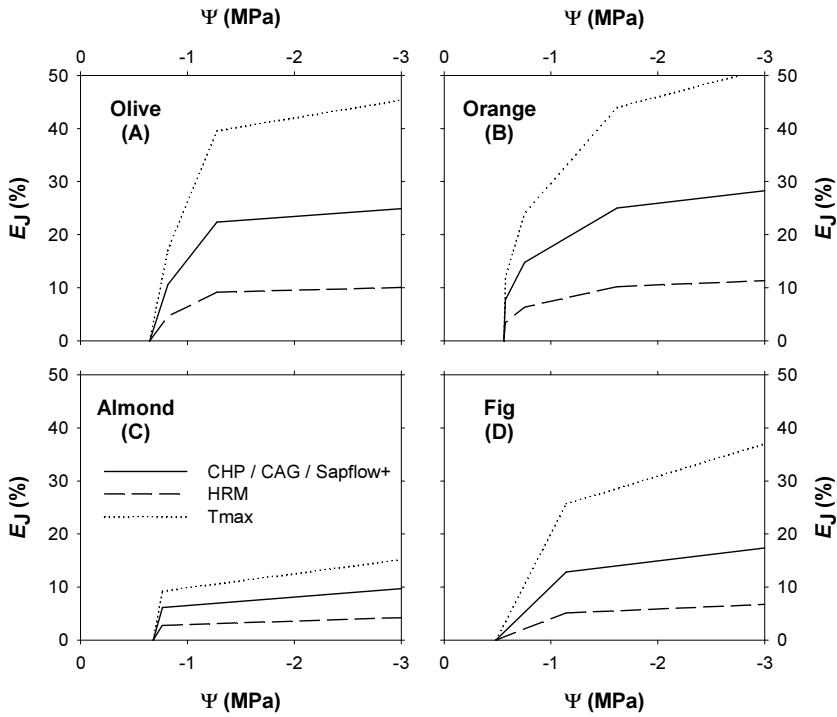


**Figure 4.5.** Relative error in sap flux density ( $E_J$ ) of compensated heat pulse (CHP), calibrated average gradient (CAG), sapflow+ (those three in solid line), heat ratio (HRM, dashed line) and Tmax (dotted line) methods in the sapwood of olive (A), sweet orange (B), almond (C) and fig (D) as a function of water potential ( $\Psi$ ).

Figure 4.5 presents the theoretical  $E_J$  as a function of  $\Psi$  in relation to heat pulse method and species. In general, all the  $E_J(\Psi)$  curves followed the same pattern, with high slopes for the higher  $\Psi$  that declined with decreasing  $\Psi$ . Differences between species were also evident, with lower  $E_J$  for almond and fig trees and higher for olive and orange. For instance, considering the CHP method and  $\Psi$  of -1 MPa,  $E_J$  was 14.9, 17.3, 6.6 and 9.7 % for olive, sweet orange, almond and fig trees, respectively. In addition, heat pulse methods also differed between them, with  $E_J$  always being the highest for Tmax and the lowest for HR throughout the  $\Psi$  range.

Thus, considering again  $\Psi$  of -1 MPa and focusing on fig curves (Fig. 4.5D),  $E_j$  were 9.7, 3.9 and 18.9 % for CHP/CAG/Sapflow+, HR and Tmax methods, respectively.

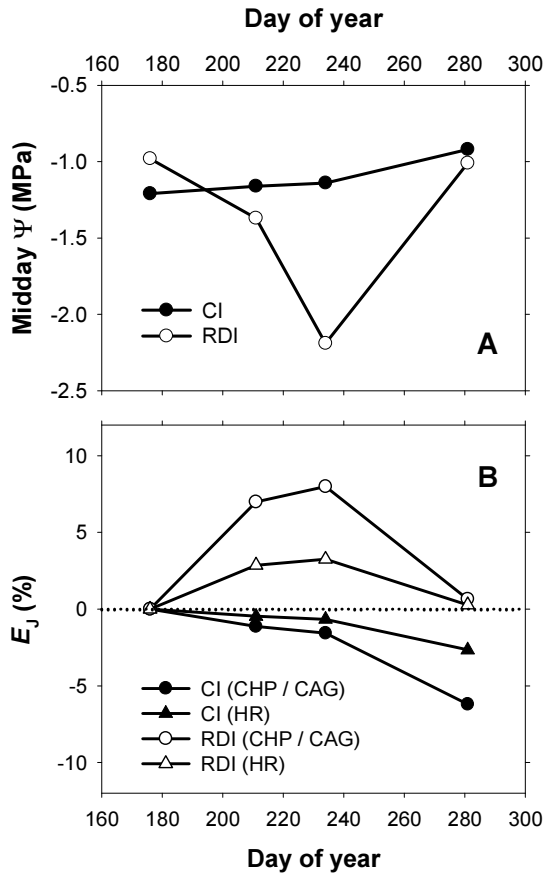


**Figure 4.6.** **A** Seasonal course of midday sapwood water potential ( $\Psi$ ) for the control (CI, closed symbols) and deficit irrigation (RDI, open symbols) treatments. **B** Seasonal relative errors in sap flux density ( $E_j$ ) in relation to heat pulse method (circles for CHP and CAG, and triangles for HR) and irrigation treatment. The water applied to RDI was 30 % of that of CI from DOY 182 to DOY 243 and the same as CI for the rest of the season.

Figure 4.6 illustrate the potential  $E_J$  for the different heat pulse methods from the field data on seasonal variations of midday  $\Psi$ . In this regard, Fig. 4.6A presents the measured values of  $\Psi$  for the two irrigation treatments showing that, while CI always maintained high midday  $\Psi$  ( $>-1.25$  MPa) with a slight tendency to increase throughout the season, it decreased during the summer for RDI reaching a minimum value of  $-2.19$  MPa on DOY 234. Such  $\Psi$  patterns were translated into the  $E_J$  trends shown in Fig. 4.6B. Thus, when considering the case of CHP/CAG,  $J$  was overestimated up to  $6.5$  % at the end of the season in the case of CI whereas RDI exhibited a peaked pattern for  $E_J$  with a maximum underestimation in  $J$  of  $8$  % on DOY 234. For both treatments, the HR would yield more accurate estimates of  $J$  than CHP/CHP as predicted  $E_J$  were always below  $3.3$  %.

**Table 4.2.** Predawn and midday water potentials ( $\Psi$ ) on a sunny day of midsummer (DOY 234) for the control (CI) and deficit irrigation treatments (RDI). Relative errors in sap flux density ( $E_J$ ) at daily scale are estimated for different heat-pulse based methods taking the estimated predawn values of  $F_w$  and  $D_x$  as references (Eqs. 4.9 and 4.10).

	CI	RDI
Predawn $\Psi$ (MPa)	-0.65	-0.96
Midday $\Psi$ (MPa)	-1.14	-2.19
$E_J$ CHP, CAG, Sapflow+ (%)	15.1	7.7
$E_J$ HR (%)	6.9	3.3
$E_J$ Tmax (%)	22.46	12.4

Finally, the effects of predawn-to-midday variations in  $\Psi$  on the accuracy of heat pulse methods are presented in Table 4.2. Despite a greater variation in  $\Psi$  measured for RDI, the higher values of  $\Psi$  in CI lead to higher  $E_J$  for all

heat pulse methods. Again the ranking of heat pulse methods accuracy remained equal independent of irrigation treatment, with the lowest and highest  $E_J$  for HR and Tmax, respectively.

#### **4.4. Discussion**

##### **4.4.1. Characterisation of thermal properties and their determining factors**

Large variability between species was found in the partitioning of sapwood porosity into  $F_w$  and  $F_g$  (Fig. 4.1A). In most species water occupied around 70 % of the porous space (i.e. the space excluding  $F_s$ ), but olive and fig trees showed a different and opposed pattern: while the former operated close to saturation values (97 %),  $F_w$  only accounted for slightly more than half of the pore fraction in the latter species (58 %). However, the considerable amount of gas spaces found in most species is not new. Gartner et al. (2004) conducted a review of published data showing that  $F_g$  ranged from 7 to 40 % (26 %, on average) across 34 hardwood species. Also, the average proportions of fibre, axial parenchyma, rays and vessels (Fig. 4.1B) were in good agreement with those reported for a wide range of shrubs species of similar  $\rho_d$  by Martínez-Cabrera et al. (2009).

Despite the central role of thermal properties for sap flow research, few efforts have been made to characterise them in living wood resulting in a surprising scarcity of reported data in the literature (Vandegheuchte and Steppe 2012a; Dupleix et al. 2013). To our knowledge, only the study of Turrell et al. (1967), in which thermal properties of several *Citrus* trees were determined by the steady-state method described in Griffiths and Kaye (1923), presents values of thermal properties for one of the species



studied here (sweet orange, Cs in Fig. 4.2). As compared to our results, these authors measured lower values for  $K_x$  (0.59 versus 0.68 W m<sup>-1</sup> K<sup>-1</sup>),  $\rho c$  (2.05 versus 2.40 J cm<sup>-3</sup> K<sup>-1</sup>) and  $R_K$  (1.38 versus 1.99). As Turrel et al. (1967) reported the same value for  $F_w$  (37 %) and slightly higher  $\rho_d$ , the most likely cause of discrepancies lays in the different measurement methodology applied.

#### **4.4.2. Contrast of methodologies for determining sapwood thermal properties**

In this study, sapwood thermal properties of seven fruit tree species were determined using various methods. Among them, the one proposed by Vandegehuchte and Steppe (2012a) (Eqs. 4.5 and 4.8) was chosen as the reference for assessing deviations in the most common protocols that have been applied for HR (Eqs. 4.3 and 4.8) and Tmax (Eqs. 4.7 and 4.8) to date.

Considering only the results for the axial direction, the Siau (1971) approach yielded on average similar results to the reference with regard to  $K_x$  and  $D_x$  (Table 4.1). Nevertheless, substantial relative deviations of up to 11 % were found for the trees with higher and lower  $K_x$  (olive and fig, Fig. 4.3A) which can be ascribed to the misinterpretation of  $F_w$  in Eq. 4.3. This fact can lead to errors of the same relative magnitude in  $J$  determinations by HR as  $D_x$  is linearly related to  $v_h$  (Burgess et al. 2001). Consequently, Eq. 4.5 instead of Eq. 4.3 should be used when working with this sap flow method, as stressed by Vandegehuchte and Steppe (2012a).

On the other hand, the estimates of  $K_x$  and  $D_x$  corresponding to the Tmax method were even further from those predicted by Vandegehuchte and Steppe (2012a) equations (up to 18 %, Fig. 4.3B). There might be several factors contributing to explain these large deviations including either the sensitivity of this method to scatter in the temperature data, small

misalignments of probes or even actual differences in thermal properties (the  $F_w$  and  $\rho_d$  required in Vandegehuchte and Steppe (2012a) protocol were taken 5 cm apart from the place in which probes had been installed). Moreover, Eq. 4.7 was derived under the assumptions of both zero probe radius and absence of heat convection (Kluitenberg and Ham 2004), so finite dimensions of the probes and nocturnal sap flow can also lead to deviations. The second assumption, however, should only result in small overestimations of  $D_x$  and  $D_y$  (and hence in  $K_x$  and  $K_y$ ). In fact, inverting Eq. 4.11 considering a nocturnal  $v_h$  of 10 cm/h and our sensor specifications ( $x = 5$  mm,  $t_p = 2$  s), relative errors in  $D_x$  and  $D_y$  are always below 5 % for the range of  $t_m$  observed in this study (25 to 40 s).

Apart from that, thermal properties were also determined from a semianalytical solution derived for dual heat pulse probes (Knight et al. 2012), being the first time that this approach was applied in sapwood. The main strengths of this methodology are two: it accounts for finite probe radius and heat capacity, overcoming some of the incorrect assumptions implicit in the Tmax method, and it theoretically allows the determination of  $F_w$  making core sampling unnecessary. The application of such semianalytical solution yielded promising results (especially as compared to those of Tmax) on one hand, as relative deviations in  $K_x$  from the estimates of Eq. 4.5 were below 7 % except for one individual (Fig. 4.3C). However, the Knight et al. (2012) estimates of  $\rho_c$  were always slightly higher (13 %, on average) than those deduced from core sampling and Eq. 4.8, leading as well to lower values for  $D_x$  (Table 4.1). Again, small misalignments of probes, low nocturnal sap flow rates or actual differences in thermal properties might be involved in the discrepancies found between the Knight et al. (2012) approach and the reference values.

As far as the tangential direction is concerned, all methods yielded higher values for  $K_y$  than those obtained following Vandegehuchte and Steppe (2012a) (Table 4.1, Fig. 4.3). This could be associated with any of the aforementioned theoretical and/or methodological problems that both the Siau (1971), Tmax and Knight et al. (2012) approaches present. However, the fact that all of them systematically overestimated  $K_y$  might also raise concerns about the accuracy of Eq. 4.6 for predicting  $K_y$ . Despite the fact that prediction of  $K_y$  or  $D_y$  is irrelevant for most heat pulse methods, it is still of some interest for some applications. For instance, the reliability of the VSH-CHP method (VSH is the acronym of Volumetric Specific Heat; i.e.  $\rho c$ ), which allows CHP to estimate relative variations in  $\rho c$  and hence in  $F_w$ , is dependent on  $R_K$  and its variations with  $F_w$  (López-Bernal et al. 2012). As a result, ascertaining the origin of discrepancies in  $K_y$  between the methods deserves further research.

#### **4.4.3. Experiment 2: Implications of sapwood water potential variations for sap flux density measurements**

Heat pulse methods require values of  $F_s$  and  $F_w$  as they are involved in the calculation of both  $J$  (Eq. 4.2) and  $D_x$ , the latter only in the case of HR and Tmax (Burgess et al. 2001; Kluitenberg and Ham 2004). Although  $F_s$  should remain constant for a specific region of sapwood,  $F_w$  is known to vary periodically, with annual and daily changes of up to 70 and 18 %, respectively, depending on species and environmental conditions (Constant and Murphy 1990; Scholz et al. 2007). Despite this,  $F_w$  is usually measured once because of the harmful nature of core sampling, which implies that large errors might occur in  $J$  determinations. In the present study, we have assessed the impacts of natural changes in  $F_w$  on the accuracy of heat pulse methods by constructing desorption curves for four fruit tree species (Fig. 4.4). In doing so, the prediction of  $E_j$  is expressed in relation to  $\Psi$  (Fig.

4.5), whose measurement pose lesser problems and is more extended and repeatable.

For the typical range of  $\Psi$  found in living trees, our desorption curves presented an initial phase of high capacitance followed by a decline at moderate  $\Psi$  (on average around -1 MPa) in all cases (Fig. 4.4). These trends were similar to those previously found in other species and, moreover, our estimates of sapwood capacitance in both phases ( $0.33 \text{ kg L}^{-1} \text{ MPa}^{-1}$  and  $0.010 \text{ kg L}^{-1} \text{ MPa}^{-1}$ ) were close to the values reported in the literature (Griffin 1977; Tyree and Yang 1990). Besides that, the reliability of desorption curves was reinforced by the agreement with the independent set of measurements with pressure chamber and core sampling (Fig. 4.4A, 4.4B and 4.4C).

The high capacitance of the initial phase of desorption curves had a profound impact on the results of the analysis of errors as it resulted in large variations of  $F_w$  in the normal operating range of  $\Psi$  of trees with adequate water supply. For instance, this explains the fact that the  $E_J$  shown in Table 4.2 was higher for CI than for RDI trees, independently of the heat pulse method. Note, however, that this observation should not lead to the incorrect conclusion that error is always lower for water stressed trees as compared to well irrigated ones. If a monitored tree undergo periods of both good water status (high predawn  $\Psi$ ) and water stress (low midday  $\Psi$ ) its seasonal maximum  $E_J$  will be higher than that of a tree with a maintained good water status (high predawn  $\Psi$  and high midday  $\Psi$ ) throughout the same period. Thus, in our field example, the overall seasonal  $E_J$  for CHP (calculated assuming a maximum predawn  $\Psi$  of -0.65 MPa for both treatments and the lowest midday  $\Psi$  shown in Fig. 4.6) yields 17 and 19 % for the CI and RDI tree, respectively.

As compared to the rest, Tmax and Sapflow+ present the advantage of allowing the determination of  $D_x$  and  $F_w$  (respectively) in conditions of zero flow. In this way, the errors arising from seasonal variations of  $F_w$  are, at least, partly neutralised. Nevertheless, both are vulnerable to daily variations in  $F_w$ , which still might lead to considerable deviations in the calculation of  $J$  as exemplified in Table 4.2. The case of Tmax is even trickier, as Eq. 4.7 led to additional errors in  $D_x$  as discussed above (see also Table 4.1).

As it is clear from the results presented in Fig. 4.5, Fig. 4.6 and Table 4.2, substantial errors in  $J$  might arise when  $F_w$  variations are ignored for CHP, CAG, Sapflow+ and Tmax. On the contrary, HR appears to be less vulnerable than those as  $E_J$  were always lower than 10 %, independently of species and even considering the whole range of  $\Psi$  shown in Fig. 4.5. The reason behind such higher accuracy lay in both the inverse relationship between  $D_x$  and  $F_w$  ( $D_x$  decrease with increasing  $F_w$  and vice versa when the combination of Eqs. 4.1, 4.5 and 4.8 are considered) and the direct proportionality between  $v_h$  and  $D_x$  (according to the working equation of Burgess et al. (2001)). In this regard, the direct effect of changes in  $F_w$  in Eq. 4.2 is partly compensated by their inverse impact on the calculation of  $v_h$ , resulting in lower errors than those found for CHP, CAG or Sapflow+. Likewise, Tmax exhibited the highest errors because its working equation (Eq. 4.11) establishes an inverse link between  $D_x$  and  $v_h$ , which results in  $F_w$  and  $v_h$  changes going in the same direction.

At this point, the question is how to deal with the variable  $F_w$  when working with heat pulse methods. As conducting multiple core sampling analysis is impractical, a possible alternative is to follow the same approach that in the present study: replace  $F_w$  by  $\Psi$ . However, obtaining desorption curves is time consuming and still requires taking some wood samples.

Moreover, the continuous monitoring of  $\Psi$  in the field is not possible with the extended method of the pressure chamber, which is an issue that may be overcome by using stem psychrometers instead. In this regard, the use of techniques allowing the continuous monitoring of  $F_w$  such as time domain reflectometry (Constant and Murphy 1990) looks appealing but these methods require additional equipment, can be difficult to interpret and struggle to account for the spatial variability of sapwood (Vandegehuchte and Steppe 2012b). On the other hand, when working with CHP sensors, occasional core sampling can be combined with the application of VSH-CHP, which also theoretically allows to continuously monitor  $F_w$  (even under non zero flow conditions), although the accuracy of this methodology is slightly affected by changes in  $R_K$ , which arise again from  $F_w$  variations (López-Bernal et al. 2012). Apart from that, another obvious option is to use HR (using Eq. 4.5 instead of the incorrect Eq. 4.3) whenever possible as it is less affected by  $F_w$  variations than the other heat pulse methods (Fig. 4.5, Fig. 4.6, Table 4.2). Unfortunately, HR is unable to determine high  $J$  (Vandegehuchte and Steppe 2013). As a final remark, the time of day or date in which wood samples are taken for  $F_s$  and  $F_w$  determinations can have practical implications. For instance, if sampling is conducted by midday, the  $E_J$  will be concentrated on periods of low flows (late evening, night and early morning) minimizing the errors in the estimates of daily transpiration.

#### **4.5. Conclusions**

- 1) Large differences in thermal properties were found among the fruit tree species. Differences in anatomical traits and in  $F_s$ ,  $F_w$  and  $F_g$  are also considerable, which explains the variation in thermal properties.

- 2) The use of the classical equations for determining  $D_x$  when applying the HR (Eq. 4.3) and the Tmax (Eq. 4.7) methods might lead to substantial errors (even greater than 10 % according to our results) affecting the accuracy of these heat pulse methods. These errors can be theoretically avoided by combining Eqs. 4.1, 4.5 and 4.8 from  $\rho_d$  and  $F_w$  measurements.
- 3) The semianalytical solution of Knight et al. (2012) seems a promising tool for sap flow research as it can be used to estimate seasonal variations in  $F_w$  and  $D_x$ . Nevertheless, it still deserves further investigation to address the origin of the discrepancies found in this study with the values of  $\rho_c$  and  $D_x$  deduced from  $F_w$  measurements and the application of Eqs. 4.1, 4.5 and 4.8.
- 4) Ignoring seasonal and daily variations in  $F_w$  might result in large errors in calculated sap flux whose extent depends on the species and the heat pulse method. In this regard, the HR presents the lowest loss of accuracy followed by Sapflow+, CHP and CAG while Tmax is the most prone to high errors.

### **Acknowledgements**

This work was funded by the Andalusian Regional Government (Junta de Andalucía, project P10-AGR-6456), by the Spanish Ministry of Natural, Rural and Marine Environment (MMARM, project AGL-2010-20766) and European Regional Development Fund (ERDF). In addition, we thank the Spanish Research Council (CSIC) predoctoral JAE program for the PhD funding granted to the first author. Furthermore, the authors also acknowledge the excellent technical support provided by Mr Rafael del Río, Mr Ignacio Calatrava and Mr José Luis Vazquez.



## References

- Becker P, Edwards WRN (1999) Corrected heat capacity of wood for sap flow calculations. *Tree Physiol* 19:767-768.
- Burgess SSO, Adams MA, Turner NC, Beverly CR, Ong CK, Khan AA, Bleby TM. (2001) An improved heat pulse method to measure low and reverse rates of sap flow in woody plants. *Tree Physiol* 21:589-598.
- Cohen Y, Fuchs M, Green GC (1981) Improvement of the heat pulse method for determining sap flow in trees. *Plant Cell Environ* 4:391-397.
- Constantz J, Murphy F (1990) Monitoring moisture storage in trees using time domain reflectometry. *J Hydrol* 119:31-42.
- Dupleix A, Kusiak A, Hughes M, Rossi F (2013) Measuring the thermal properties of green wood by the transient plane source (TPS) technique. *Holzforschung* 67:437-445.
- Edwards WRN, Warwick NWM (1984) Transpiration from a kiwifruit vine as estimated by the heat pulse technique and the Penman-Monteith equation. *N Z J Agric Res* 27:537-543.
- Gartner BL, Moore JR, Gardiner BA (2004) Gas in stems: abundance and potential consequences for tree biomechanics. *Tree Physiol* 24:1239-1250.
- Griffin DM. (1977) Water potential and wood-decay fungi. *Annu Rev Phytopathol* 15:319-329.
- Griffiths E, Kaye GWC (1923) The measurement of thermal conductivity. *Proc Roy Soc London Ser A* 104:71-98.
- Kluitenberg GJ, Ham JM (2004) Improved theory for calculating sap flow with the heat pulse method. *Agric For Meteorol* 126:169-173.
- Kollmann FFP, Côté WA (1968) Principles of wood science and technology 1, Solid wood. Springer, New York, pp 246-250.

- Knight JH, Kluitenberg GJ, Kamai T, Hopmans JW (2012) Semianalytical solution for dual-probe heat-pulse applications that accounts for probe radius and heat capacity. *Vadose Zone J* 11. doi:10.2136/vzj2011.0112.
- López-Bernal A, Testi L, Villalobos FJ (2012) Using the compensated heat pulse method to monitor trends in stem water content in standing trees. *Tree Physiol* 32:1420-1429.
- Maku T (1954) Studies on heat conduction in wood. Kyoto University, Bulletin of the Wood Research Institute No. 13. pp. 1-80.
- Martínez-Cabrera HI, Jones CS, Espino S, Schenk HJ (2009) Wood anatomy and Wood density in shrubs: responses to varying aridity along transcontinental transects. *Am J Bot* 96:1388-1398.
- Orgaz F, Testi L, Villalobos FJ, Fereres E (2006) Water requirements of olive orchards-II: determination of crop coefficients for irrigation scheduling. *Irrig Sci* 24:77-84.
- Roderick ML, Berry SL (2001) Linking wood density with tree growth and environment: a theoretical analysis based on the motion of water. *New Phytol* 149:473-485.
- Siau JF (1971) Flow in wood. In: Côté WA (ed) Syracuse Wood Science Series. Syracuse University Press, New York, pp131.
- Scholz FG, Bucci SJ, Goldstein G, Meinzer FC, Franco AC, Miralles-Wilhem F (2007) Removal of nutrient limitations by long term fertilization decreases nocturnal water loss in savanna trees. *Tree Physiol* 27:551-559.
- Testi L, Villalobos FJ (2009) New approach for measuring low sap velocities in trees. *Agric For Meteorol* 149:730-734.
- Turrell FM, Austin SW, McNee D, Park WJ (1967) Thermal conductivity of functional citrus tree wood. *Plant Physiol* 42:1025-1034.
- Tyree MT, Yang S (1990) Water-storage capacity of *Thuja*, *Tsuga* and *Acer* stems measured by dehydration isotherms. The contribution of capillary water and cavitation. *Planta* 182:420-426.

Tyree MT, Zimmermann MH (2002) Xylem structure and the ascent of sap. 2<sup>nd</sup> edition. Springer, Berlin. pp. 132-141.

Vandegehuchte MW, Steppe K (2012a) Improving sap flux density measurements by correctly determining thermal diffusivity, differentiating between bound and unbound water. *Tree Physiol* 32:930-942.

Vandegehuchte MW, Steppe K (2012b) Sapflow+: a four-needle heat pulse sap flow sensor enabling nonempirical sap flux density and water content measurements. *New Phytol* 196:306-317.

Vandegehuchte MW, Steppe K (2013) Sap-flux density measurement methods: working principles and applicability. *Funct Plant Biol* 40:213-223.

## **Chapter 5**

### **Low winter temperatures induce a disturbance of water relations in field olive trees**

---

## Chapter 5

### Low winter temperatures induce a disturbance of water relations in field olive trees

#### Summary

A disturbance of water relations in response to chilling have long been observed in potted plants growing under controlled conditions, but information is lacking for field plants. The aim of this study was to assess the effects of winter low temperatures on the water relations of mature olive trees. To this end, water potential, sap flux density, soil temperature and meteorological data were monitored in a hedgerow olive orchard near Córdoba, southern Spain, throughout two consecutive winters. Water stress symptoms were found in terms of midday  $\Psi$  despite adequate water supply and low evaporative demand. These effects were associated with changes in the soil-to-trunk hydraulic resistance ( $R_{\text{root}}$ ), which increased by December-January to much higher values than those previously reported in the literature, particularly in the year of higher fruit load. The contribution of viscosity ( $\eta$ ) to the observed  $R_{\text{root}}$  dynamics was almost negligible as deduced from measurements of soil temperature, so the high winter values of  $R_{\text{root}}$  were likely to have originated from other causes such as reductions in membrane permeability and root growth. The findings of this work raise new major issues that deserve further research such as the impact of the winter water stress on stomatal conductance and photosynthesis rates in mature olive trees.

## **5.1. Introduction**

The olive (*Olea europaea* L.) is an evergreen fruit tree species widely cultivated in the Mediterranean basin, whose climate is characterized by hot dry summers and cool wet winters. As the typical summer drought severely limits yield in traditional rainfed orchards and the water available for irrigated systems is scarce, extensive research has focused on the adaptation of olive trees to water limited conditions (Fernández et al. 1997; Moriana et al. 2003; Connor 2005; Tognetti et al. 2009; Boughalleb and Hajlaoui 2011; Torres-Ruiz et al. 2013). Scientific activity has led to the development of both irrigation scheduling techniques based on the actual water requirements (Orgaz et al. 2006; Testi et al. 2006), deficit irrigation strategies (Moriana et al. 2003; Iniesta et al. 2009) and plant based methods for a precise monitoring of water stress (Fernández and Cuevas 2010; López-Bernal et al. 2010; Fernández et al. 2011; López-Bernal et al. 2012). However, less attention has been paid to water relations beyond the dry season.

Plant responses to low temperatures similar to those induced by water stress have long been reported (Kramer 1940). In addition, a number of studies have also shown that sensitivity to the so-called ‘chilling stress’ differs among species and even among cultivars (Kramer 1942; Aroca et al. 2001; Bloom et al. 2004). Under chilling conditions, temporal imbalances between root water uptake and transpiration take place, resulting in shoot water deficits. These effects are attributed to increased hydraulic resistance of the water pathway from soil to shoots ( $R$ ) as water viscosity ( $\eta$ ) increases with decreasing temperatures (Yamamoto 1995; Hertel and Steudle 1997; Cochard et al. 2000). However, there is also a body of evidence suggesting that this phenomenon is the consequence of an increase in root hydraulic resistance ( $R_{\text{root}}$ ) originating in the radial pathway of water from the soil-

root interface to the xylem (Running and Reid 1980; Ameglio et al. 1990; Wan et al. 2001).

Despite studies assessing the impact of chilling stress on the water relations of trees have been studied for decades (Kramer 1942; Running and Reid 1980; Pavel and Fereres 1998; Norisada et al. 2005), actual observations under natural conditions are still lacking to date. To our knowledge, all studies have been conducted in either lab conditions (e.g. Running and Reid 1980), growth chambers (e.g. Wan et al. 2001) or with plants growing outdoors that are exposed to localized warming or cooling (e.g. Norisada et al. 2005). Furthermore, the reported experiments have always been conducted with young seedlings growing in either pots or hydroponics. This might be inconvenient for extrapolating the results to mature field trees, as both architectural and anatomical root traits can be affected in those artificial conditions. In this regard, it is known that hydroponics can affect the development of root exodermis (Steudle 2000) and that both the morphology and physiology of root systems as well as root-to-shoot ratios are frequently altered in potted trees (Passioura 2006). Further uncertainties arise from the typical short duration of precedent experiments and the way in which trees were chilled. For instance, the chilling stress was frequently induced in previous studies by artificially decreasing the temperature of the soil or mineral solution, which contrasts with the fact that roots are exposed to higher temperatures than the canopy under field conditions. In the light of the above, the occurrence and extent of the chilling stress in mature trees growing in the field remain unknown.

The only studies characterizing the effects of chilling on water relations of olive trees are those conducted with one-year-old potted trees by Pavel and Fereres (1998) and Pérez-López et al. (2010). The former found reductions in both stomatal conductance and stem and leaf water potentials whereas

they encountered increases in  $R_{\text{root}}$  when trees were steadily exposed to soil temperatures below  $6.4 \pm 0.5$  °C. However, they did not observe the phenomenon under low night ( $2.5 \pm 0.4$  and  $5.2 \pm 0.4$  °C) but ambient day ( $16.2 \pm 3.2$  °C) soil temperatures. On the other hand, the study of Pérez-López et al. (2010) reported differences in sensitivity to soil chilling between six cultivars.

This work describes the effects of low temperatures in two consecutive winters on a mature hedgerow olive orchard in Southern Spain. The main goal of this work was to characterize the seasonal patterns of water relations of field olive trees from autumn to spring ascertaining whether the exposure to the low winter temperatures result in similar alterations to those previously observed in young potted plants under controlled conditions or not.

## **5.2. Materials and methods**

### **5.2.1. Experimental site**

The experiments were conducted in two consecutive winters (2011-2012 and 2012-2013) from November to April in an olive (cv. Arbequina) hedgerow orchard located at the CIFA Experimental Station, Córdoba, Spain ( $37.8^{\circ}\text{N}$ ,  $4.8^{\circ}\text{W}$ , 110 m altitude). The olive trees were planted in 1999 and they were renovated by pruning at ground level in 2008. Tree spacing was  $3.5 \text{ m} \times 1.5 \text{ m}$ . During the dry season (period spring-autumn), irrigation was applied with 2.3 L/h drippers supplying enough water to keep maximum evapotranspiration, which was calculated according to the approach of Orgaz et al. (2006). The soil is a Typic Xerofluvent of sandy loam texture exceeding 1.5 m in depth, with upper drained soil water



content limit of  $0.23 \text{ m}^3 \text{ m}^{-3}$  and lower soil water content limit of  $0.07 \text{ m}^3 \text{ m}^{-3}$  (Testi et al. 2004). Five trees in 2011-2012 and four in 2012-2013 were randomly selected for measurements, with 2011 being a year with high fruit load and 2012, one with low fruit load. During the experiment, the height of the canopy was  $3 \pm 0.5 \text{ m}$  and trees presented an average leaf area index of  $1.2 \text{ m}^2 \text{ m}^{-2}$  which was estimated from measurements of diffuse radiation interception performed with a Plant Canopy Analyzer (LAI-2000, Li-Cor, Lincoln, NE, USA). All the fruits of experimental trees were removed in late November before the first measurement date in both years.

### 5.2.2. Measurements

Measurements were performed on sunny days five times per season from late autumn to early spring. November 29, December 23, January 19, February 22 and March 22 in 2011-2012 season and November 28, December 22, January 29, February 15 and April 12 in 2012-2013 were the measurement dates.

Water potential ( $\Psi$ ) was determined using a pressure chamber (Soil Moisture Equipment Corp., Santa Barbara, CA, USA). Values of  $\Psi$  were recorded at predawn and midday in 2011-2012 while for the following winter we included measurements at 1.5 h intervals from 1 hour before sunrise until noon. Four sun-exposed shoots from the canopy top (with 1-3 leaf pairs attached) were sampled per experimental tree in each measurement. In addition,  $\Psi$  of non-transpiring shoots directly attached to the tree trunk or main branches ( $\Psi_{trunk}$ ) were measured at midday (four shoots per tree were covered with aluminum foil five hours before the measurements) in all the experimental trees of 2012-2013 and two of the five trees in 2011-2012.

Experimental trees were instrumented with sap flow sensors (one per tree, always in the trunk at a height of 40 cm from the soil and below a main branch) based on the compensated heat pulse method (Swanson and Whitfield 1981). The probes used were designed and produced in the IAS-CSIC laboratory in Córdoba, Spain and consist of a 4.8 W stainless steel heater of 2 mm diameter and two temperature probes of the same diameter located 10 and 5 mm down- and upstream of the heater, respectively (Testi and Villalobos 2009). Each temperature probe had four embedded Type E (chromel–constantan wire) thermocouple junctions, spaced 10 mm along the needle, that were sampled separately to obtain heat-pulse velocities at 5, 15, 25 and 35 mm below the cambium at 15-min intervals. Sensors were installed at a height of 40 cm from the soil, and the system was controlled by a datalogger (CR1000, Campbell Scientific Inc., Logan, UT, USA). Further details concerning both data processing and sap flow calculations are described in detail in Villalobos et al. (2013).

For the second winter (2012-2013) soil temperature was monitored with Type K (chromel-alumel) thermocouples. Temperature was recorded at 15-min intervals and the equipment was controlled by a datalogger (CR1000, Campbell Scientific Inc., Logan, UT, USA). Three thermocouples were installed at 75 mm depth around one of the experimental trees: one close to the tree trunk (20 cm apart), another in the middle point between trees in a row (75 cm apart) and the last one in the central point of the alley between four trees. The averaged value was used to derive the seasonal course of root sap  $\eta$  from a:

$$\eta = \frac{1.95 \cdot 10^8}{T^7} \quad (1)$$

where  $T$  is the liquid temperature in K and  $\eta$  is in  $\text{MPa s}^{-1}$  (Roderick and Berry et al. 2001).

Meteorological data was recorded at 10-min intervals in an automated weather station placed 500 m from the orchard.

### 5.2.3. Determination of stomatal conductance

Midday values of canopy stomatal conductance ( $G_s$ , mol m<sup>-2</sup> s<sup>-1</sup>) were calculated by inversion of the imposed evaporation equation:

$$G_s = \frac{E_p P}{VPD} \quad (2)$$

where  $E_p$  (mol m<sup>-2</sup> s<sup>-1</sup>) is the transpiration rate per m<sup>2</sup> of soil (deduced from sap flow records and tree spacing),  $P$  is atmospheric pressure (kPa) and VPD is vapour pressure deficit (kPa).

### 5.2.4. Determination of hydraulic resistances

Apparent resistance ( $R$ , MPa m<sup>2</sup> s mol<sup>-1</sup>) of the whole soil-plant continuum was deduced using Ohm's law analogy from transpiration rate normalized by cross-sectional trunk area ( $Q_n$ , mol m<sup>-2</sup> s<sup>-1</sup>) and water potential gradient at midday in MPa:

$$R = \frac{(\Psi_{soil} - \Psi)}{Q_n} \quad (3)$$

where predawn shoot  $\Psi$  was used as a surrogate of  $\Psi_{soil}$  under the assumption that the former had equilibrated with the latter by that time (Dichio et al. 2013). On the other hand,  $Q_n$  measurements were used as estimates of transpiration. Similarly, apparent  $R_{root}$  (MPa m<sup>2</sup> s mol<sup>-1</sup>) was computed as:

$$R_{root} = \frac{(\Psi_{soil} - \Psi_{trunk})}{Q_n} \quad (4)$$

where  $\Psi_{trunk}$  values were taken from the midday  $\Psi$  measurements in non-transpiring shoots directly attached to trunks.

### **5.2.5. Water balance**

A monthly water balance was applied to assess the occurrence of drought stress during the experiments. Changes in soil water content (*SWC*) were calculated as:

$$\Delta SWC = P_{\text{eff}} + I - ET \quad (5)$$

where  $P_{\text{eff}}$  is effective precipitation,  $I$  is the amount of irrigation applied and  $ET$  represents the orchard evapotranspiration. The first was calculated using the U.S. Bureau of Reclamation method from monthly rainfall values recorded by the meteorological station while the approach of Orgaz et al. (2006) was applied to estimate the later. The calculations were performed from January 2011 to the end of the experiments (May 2013) assuming that our soil was in the upper limit in the former. Such assumption was justified by the huge amount of rainfall recorded in December 2010 (> 300 mm).

Once *SWC* was computed, it was expressed in relative terms for each month as:

$$RSWC = \frac{SWC - SWC_u}{SWC_u - SWC_l} \quad (6)$$

with  $SWC_u$  and  $SWC_l$  being the soil water content in the upper and lower limit, respectively.

### **5.26. Statistics**

The statistical treatment of the data was performed with the Statistix program (Statistix 9 for Windows, Analytical Software, Tallahassee, FL, USA). The occurrence of significant variations in  $\Psi$ ,  $Q_n$  and R along each

measurement season was explored through a conventional analysis of variance (ANOVA), using the LSD test at  $P < 0.05$  for mean comparisons. For those cases in which the assumptions of ANOVA could not be fulfilled, the Kruskal-Wallis test was employed.

### 5.3. Results

The two winters showed contrasting meteorological conditions. The first one (2011-2012, Fig. 5.1A) was particularly dry, with 189 mm of rainfall mainly concentrated in the beginning and end of the November-April period. Mean temperature was 10.7 °C and up to 27 days with minimum temperatures below 0 °C were recorded for the same period (18 of these days on February). By contrast, the winter 2012-2013 was characterized by abundant and more uniformly-distributed precipitation and warmer temperatures with 760 mm of rainfall, 11.9°C of mean temperature and only 6 days with frost in the November-April period (Fig. 5.1B).

The evaporative demand was rather low for both winters as indicated by the course of midday VPD presented in Figure 5.2A-B. In this regard, marked differences between years were only evident by March. Values of midday VPD were lower in 2013, probably due to the abundant rainfall events recorded that month (Fig. 5.1B). Figure 5.2A-B also illustrates the results of the water balance by showing the values of *RSWC* at the beginning of each month. In general, high values were estimated throughout the two seasons, with *RSWC* remaining above 0.60 most of the time. Lower values were estimated only by 1-March-2012 (*RSWC* = 0.45) and 1-Apr-2012 (*RSWC* = 0.54).

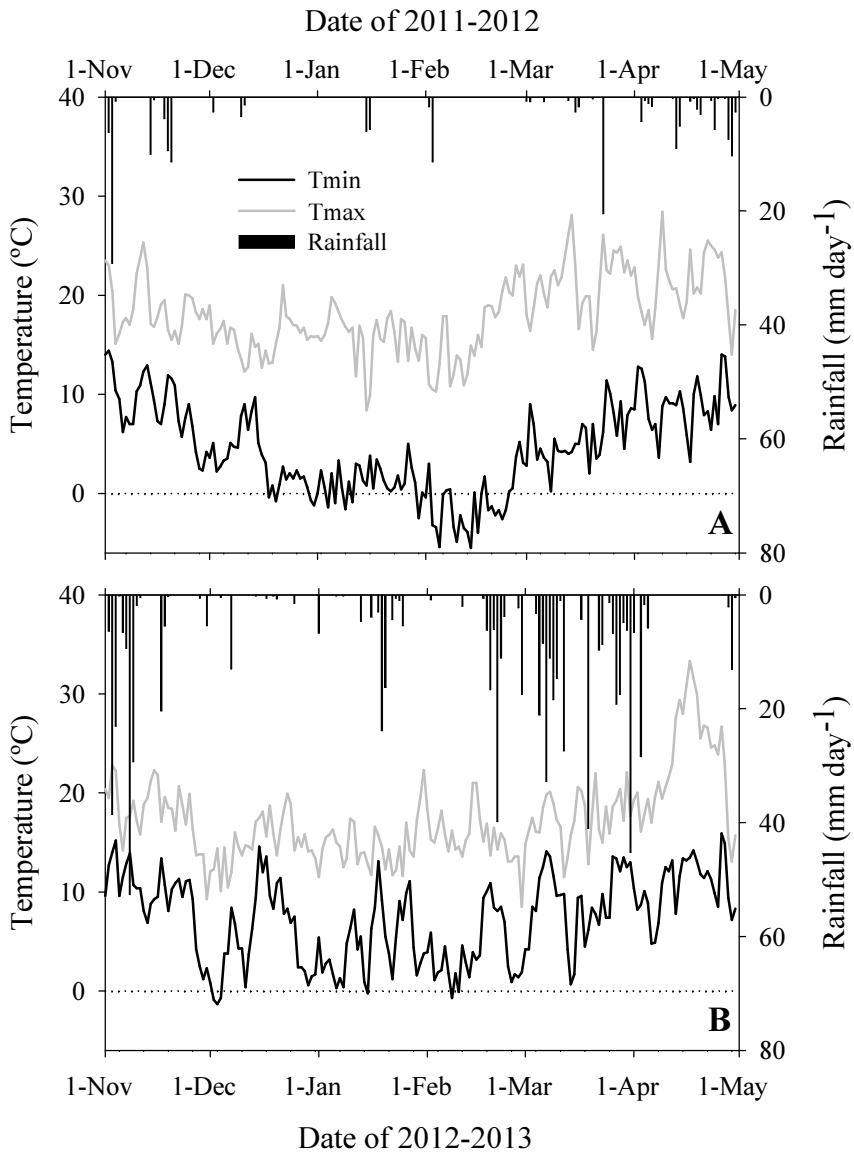


**Figure 5.1.** Maximum ( $T_{max}$ ) and minimum ( $T_{min}$ ) daily temperatures and daily precipitation recorded by a meteorological station during the experiments in 2011-2012 (A) and 2012-2013 (B) winters.

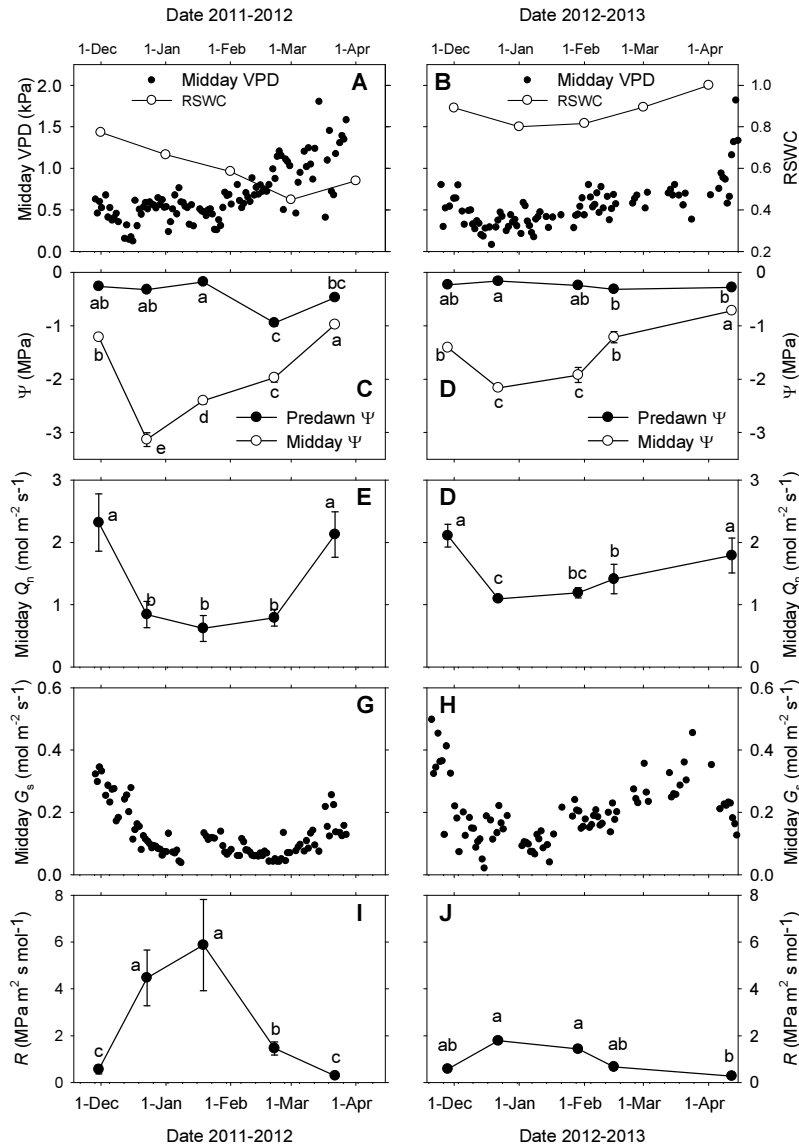


**Figure 5.2.** Patterns of midday vapor pressure deficit (VPD; solid line) and relative soil water content (RSWC; dotted line with circles) (A and B), predawn (closed symbols) and midday (open symbols) stem water potentials ( $\Psi$ ; C and D), sap flow rate normalized by cross-sectional sapwood area ( $Q_n$ ; E and F), midday bulk canopy stomatal conductance ( $G_s$ ; G and H), and calculated hydraulic resistances ( $R$ ; I and J)  $\rightarrow$

for the days of measurement in both the winters 2011-2012 (left panels) and 2012-2013 (right panels). The complete time course is presented for both  $G_s$  and VPD panels excluding those days with rainfall  $>0.3$  mm. In  $\Psi$ ,  $Q_n$  and  $R$  panels, data are means  $\pm$  standard errors ( $n=5$  in 2011-2012 and  $n=4$  in 2012-2013) of all monitored trees. Lowercase letters in panels A, B, C, D, I and J denote statistically significant ( $P < 0.05$ ) differences between dates.

The courses of predawn and midday  $\Psi$  during both 2011-2012 and 2012-2013 winters are shown in Figure 5.2C-D. As compared to spring values (March 2012, April 2013), midday  $\Psi$  was significantly lower in the beginning of both winters (December-January), clearly below  $-2$  MPa. In fact, values lower than  $-3$  MPa were reached in the first season. Such low winter midday  $\Psi$  was not apparently accompanied by decreases in predawn  $\Psi$ . In fact, it remained  $> -0.35$  MPa for both the whole experimental period in 2012-2013 and for the period between November and January in the first winter. Rather more negative predawn  $\Psi$  were measured in February 2012 ( $-0.97$  MPa) and March 2012 ( $-0.49$  MPa), which was in accordance with the aforementioned trends of RSWC. In the former case, the low predawn  $\Psi$  might also be indirectly associated with the particularly low temperatures at the time of the measurements (air temperature was  $-1.7$  °C).

Both midday  $Q_n$  (Fig. 5.2E-F) and  $G_s$  (Fig. 5.2G-H) were also lower in the central and colder period of the winter, when VPD was low (Fig. 5.2A-B). For both  $Q_n$  and  $G_s$ , the transition from the low winter values to the high ones in spring was found to occur earlier in 2012-2013 than in 2011-2012. The final decrease in  $G_s$  observed in 2012-2013 (Fig. 5.2H) coincided with a period of high temperatures (Fig. 5.1B) and evaporative demand (note also the final rise in VPD in Fig. 5.2B).

The courses of midday  $Q_n$ , midday  $\Psi$  and predawn  $\Psi$  resulted in a peaked pattern for the computed  $R$  (Fig. 5.2I and 5.2J, bottom panels). For both



years, maximum values occurred in December and January but the maximum averaged values measured in 2011-2012 ( $5.9 \text{ MPa m}^2 \text{ s mol}^{-1}$ ) were several-fold greater than those found in 2012-2013 ( $1.78 \text{ MPa m}^2 \text{ s mol}^{-1}$ ). Interestingly, these maximum values did not perfectly coincide with the coldest periods of winter revealing that the time series of air and soil temperature were not clearly in phase with those of  $R$  (see Figures 5.1 and 5.5). For instance, by mid February both  $R$  and midday  $\Psi$  decreased to values similar to those determined in late November despite the temperatures in the former month being similar or colder (especially in 2012) than those of December or January (Fig. 5.1A and 5.1B), when  $R$  was the highest. Likewise, the periods with low predawn  $\Psi$  (Fig. 5.2C) and low  $RSWC$  (Fig. 5.2A) in February-March 2012 were not in phase with the peak of  $R$  recorded earlier (December-January) that winter.

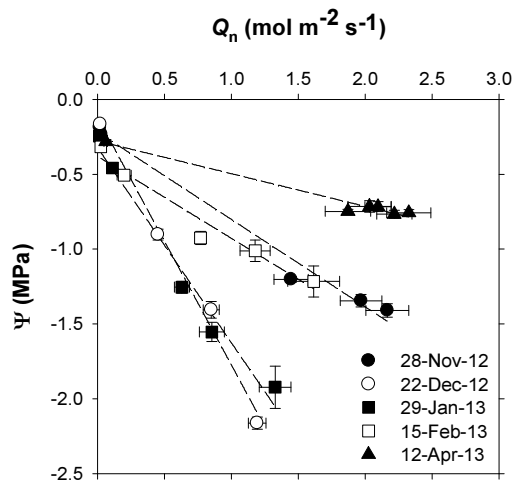


**Figure 5.3.** Daily shoot water potential ( $\Psi$ ) as a function of sap flow rate normalized by cross-sectional sapwood area ( $Q_n$ ) for the five days of measurement in the 2012-2013 season. The points represent the averaged values of the four instrumented trees for each simultaneous measurement of  $Q_n$  and  $\Psi$ . Vertical and horizontal error bars correspond to standard errors.

Concerning the variability among individuals shown by the error bars in Fig. 5.2, trees behaved in a similar way in terms of predawn and midday  $\Psi$  (average CV close to 10 % in all cases) while differences in  $Q_n$  were slightly higher (average CV of 22 % in 2011-2012 and 17 % in 2012-2013). Obviously, the variability in both  $\Psi$  and  $Q_n$  led to large differences in  $R$  between individuals (CV=64 % in 2011-2012 and 20% in 2012-2013), but the differences between winter and spring values were still significant.

The higher  $R$  values in winter were also evident analyzing the diurnal dynamics of  $\Psi$  conducted in the 2012-2013 season (Fig. 5.3). Computing  $R$  as the slope of the relationships  $Q_n$  vs.  $\Psi$  yielded similar values to those calculated from midday measurements and followed the same pattern, with the slope being the steepest in absolute terms for December 22<sup>nd</sup> (1.74 MPa m<sup>2</sup> s mol<sup>-1</sup>) and the lowest for April 12<sup>th</sup> (0.23 MPa m<sup>2</sup> s mol<sup>-1</sup>). Moreover, significant correlations ( $P < 0.01$ ) and good fits ( $r^2 > 0.90$ ) between  $Q_n$  and  $\Psi$  were always found independently of both the tree and the date.

Figure 5.4 presents the diurnal trends of  $\Psi$ ,  $Q_n$  and  $G_s$  for two dates, one representing early winter (29 January 2013, when the estimates of  $R$  were high) and the other spring conditions (12 April 2013, when low values of  $R$  were deduced). Although predawn  $\Psi$  values (the first point in Fig. 5.4A) were high ( $> -0.3$  MPa) and similar between the two compared dates, a sharp decline in  $\Psi$  was observed for the winter date in relation to that of spring. In terms of  $Q_n$ , lower values were found in winter throughout the daytime, but they may be related to the lower evaporative demand in that date (the daytime average VPD was 0.57 kPa in the winter date and 1.03 kPa in the spring one). Finally, the trends of  $G_s$  differed between the two dates in early morning but were rather similar in the afternoon.

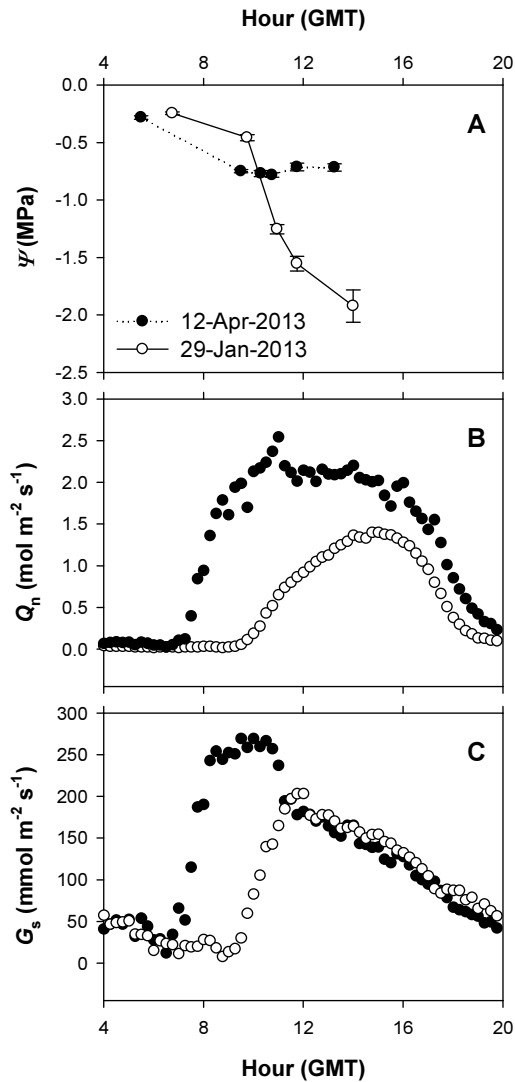


**Figure 5.4.** Diurnal course of shoot water potential ( $\Psi$ ; A), sap flow rate normalized by cross-sectional sapwood area ( $Q_n$ ; B) and bulk canopy stomatal conductance ( $G_s$ ; C) for both a winter (29-January-2013, closed symbols) and a spring date (12-April-2013, open symbols). Values are the averaged values of the four instrumented trees. Standard errors are represented by the error bars in the case of A and avoided in the rest for the sake of clarity.

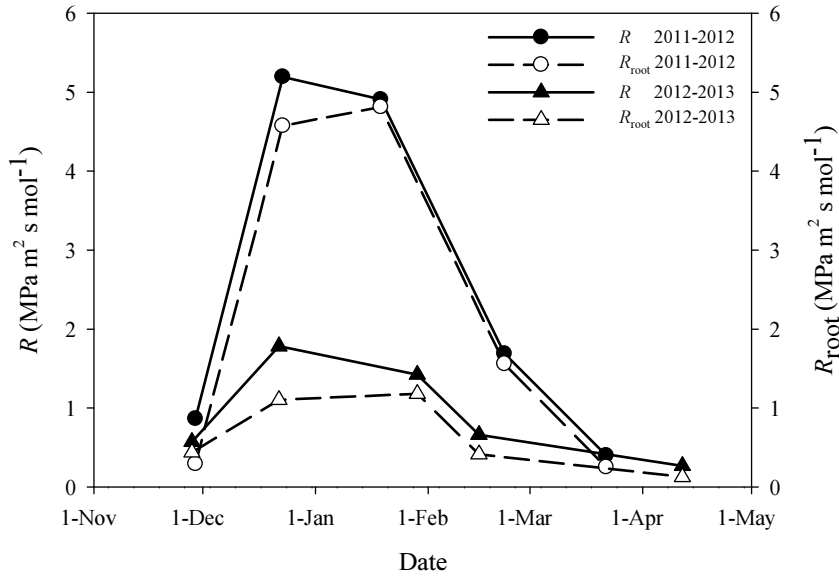


**Figure 5.5.** Temporal variation of both the whole soil-plant continuum hydraulic resistance ( $R$ ; solid lines, closed symbols) and the soil-to-trunk hydraulic resistance ( $R_{\text{root}}$ ; dashed lines, open symbols) in 2011-2012 (circles) and 2012-2013 (triangles) seasons. In the former season the results correspond to the average of the two trees in which measurements of  $\Psi$  were performed in non-transpiring shoots.

The measurements of  $\Psi$  in covered shoots followed the same trends as those of sun-exposed shoots in both seasons with lower values in early winter than at the end of the measurement periods. As a consequence, the computed  $R_{\text{root}}$  (Eq. 4) exhibited peaked patterns similar to those of  $R$ , but reaching slightly lower values throughout the two measurement seasons (Fig. 5.5). In relation to  $R_{\text{root}}$ , the trunk to shoot hydraulic resistance (i.e. the difference between  $R$  and  $R_{\text{root}}$ ) presented little seasonal variations, despite showing slightly higher values by December in both years. Comparing the maximum winter values with the minimum spring ones, relative changes in

$R$  ( $\Delta R$ ) of 20.8-fold and 6.7-fold were registered while those of  $R_{\text{root}}$  yielded 19.2-fold and 9.2-fold for 2011-2012 and 2012-2013 seasons, respectively. By contrast, the estimated seasonal changes in root sap  $\eta$  ( $\Delta\eta$ ) in the second year were of a lesser magnitude, as illustrated in Figure 5.6. For instance, comparing the same pairs of dates  $\eta$  decreased from  $1.32 \cdot 10^{-9}$  in winter to  $1.02 \cdot 10^{-9}$  MPa s in spring. Therefore, the estimated  $\Delta\eta$  (i.e. 1.29-fold changes using again spring values as the reference) was rather low as compared to those of  $\Delta R_{\text{root}}$  (Fig. 5.5).

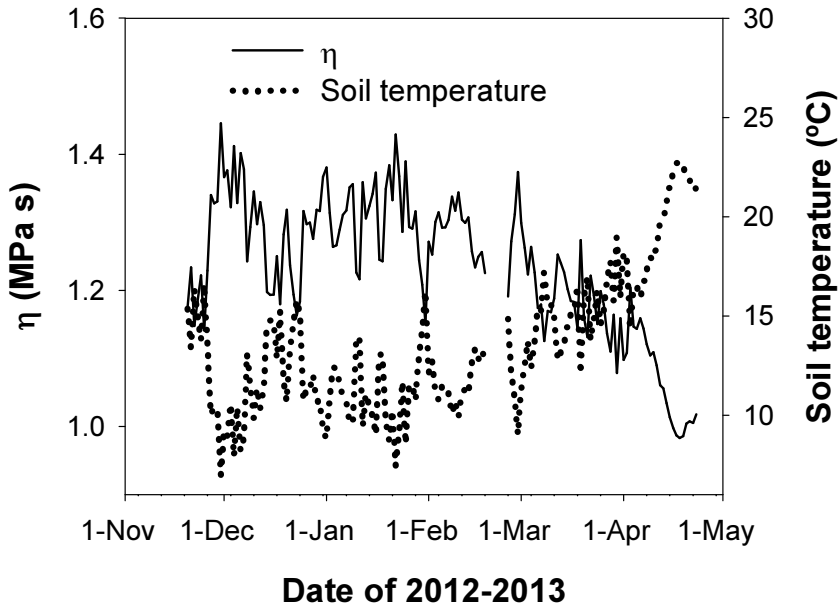


**Figure 5.6.** Time course of apparent root sap viscosity ( $\eta$ , solid line) and midday soil temperature (dotted line) through the 2012-2013 season.

#### **5.4. Discussion**

The results of the present work show that low winter temperatures result in a disturbance of water relations in mature olive trees. Regardless of the year, such disturbance was particularly evident in early winter (December-January). By that time, our measurements of midday  $\Psi$  revealed lower values (below -2 MPa, Fig. 5.2C-D) than those usually found in well irrigated olive cv. Arbequina trees in summer (down to -1.5 MPa according to Iniesta et al. 2009), even though evaporative demand is substantially lower in winter. By contrast, the values of *RSWC* estimated from the water balance were fairly high ( $> 0.6$  in December-January, Fig. 5.2A-B) in relation to the critical threshold from which a water stress-induced decrease in transpiration is expected for olive trees (0.45 according to Allen et al. 1998). It is noteworthy that this threshold *RSWC* is reported for conditions of high evaporative demand and hence, its value is expected to be even lower in winter (Allen et al. 1998). In the same line, the predawn  $\Psi$  measurements yielded high values ( $> -0.35$  MPa, Fig. 5.2C-D) in December-January, which were comparable to those found by other authors in well-irrigated olive trees in summer (Angelopoulos et al. 1996; Tognetti et al. 2009). Lower values of *RSWC* (0.45) and predawn  $\Psi$  (-0.95 MPa) were also observed in February 2012, probably as a consequence of the scant precipitation recorded that winter (Fig. 5.1A), but midday  $\Psi$  was not as low as in the precedent period (Fig. 5.2C). All this body of evidence indicates that the observed disturbance of water relations occurred under non-limiting soil water conditions and can be mainly attributed to the effect of early winter chilling temperatures.

Our observations of low midday  $\Psi$  may indicate tissue dehydration which would be to some extent in consonance with the experiments of Charrier and Ameglio (2011) and Charrier et al. (2013). These authors worked with

two-years-old walnut trees and found that the low temperatures of winter induced a decrease in stem water content in relation to cold-deprived plants. Earlier reports about chilling responses in potted plants (e.g. Kramer 1940; Running and Reid 1980) have suggested that the alteration in water relations is triggered by changes in  $R$  leading to imbalances between transpiration and water uptake. Such circumstance was also observed in our study (Fig. 5.2I-J). Apart from that and agreeing with the observations of Pavel and Fereres (1998) in 1-year old olive trees growing in pots, our measurements provided evidence that the  $\Delta R$  took place mainly in the soil-root-trunk water pathway (Fig. 5.5). But, what was the actual cause of changes in  $R_{\text{root}}$  in winter?

The literature shows that  $\Delta\eta$  is one of the main factors triggering  $\Delta R_{\text{root}}$  under chilling stress conditions (Kramer 1940; Cochard et al. 2000; Norisada et al. 2005). In this study, midday soil temperatures and the concomitant estimated root sap  $\eta$  differed little among the measurement dates of the second season (maximum  $\Delta\eta$  around 1.4-fold; Fig. 5.6) as compared to  $R_{\text{root}}$  ( $\Delta R_{\text{root}}$  of 9.2-fold; Fig. 5.5). Therefore, our results suggest that the contribution of  $\eta$  to either  $\Delta R$  or  $\Delta R_{\text{root}}$  was negligible, which is in agreement with the findings of other authors (Ameglio et al. 1990; Pavel and Fereres 1998; Murai-Hatano et al. 2008; see also Table 5.1). This analysis and its conclusions may be criticized because of the shallow depth at which the soil temperature measurements shown in Figure 5.6 were conducted (75 mm), which does not represent the whole root system temperature. Nevertheless, our results are unlikely to underestimate the role of  $\eta$  because soil temperature variations (and hence those of  $\eta$ ) are increasingly mitigated at greater soil depths. Furthermore, the contribution of  $\eta$  to the observed  $\Delta R$  should be of minor importance from a theoretical point of view: in a hypothetical and exaggerated situation in which root sap temperature changed from 0 °C in winter to 30 °C in spring, the winter

value of  $\eta$  would hardly be twice the spring one, which is still far from the observed 11.4-fold  $\Delta R_{\text{root}}$ .

**Table 5.1.** Maximum increases in hydraulic resistance ( $\Delta R$ , in n-folds increases) observed in the literature for woody species exposed to different temperature treatments. Equation 5.1 was applied to deduce the viscosity increments ( $\Delta\eta$ , in n-folds). Data from the present study are presented in the last two rows allowing comparisons. Values of  $\eta$  for the 2012-2013 season were estimated from midday soil temperature measurements.

Study	Species	Temperature range (°C)	$\Delta R$ (n-folds)	$\Delta\eta$ (n-folds)
Running and Reid (1980)	<i>Pinus contorta</i>	20.0-0.0	4.4	1.6
Pavel and Fereres (1998)	<i>Olea europaea</i>	11.5-4.6	3.6	1.2
Cochard et al., (2000) **	<i>Quercus robur</i>	20.0-2.0	1.9	1.6
Wan et al., (2001) *	<i>Populus tremuloides</i>	20.0-5.0	3.0	1.4
Norisada et al., (2005) *	<i>Cryptomeria japonica</i>	33.2-5.0	2.2	2.0
This experiment (2011-2012)	<i>Olea europaea</i>		20.8	
This experiment (2012-2013)	<i>Olea europaea</i>	21.5-10.7	6.7	1.3

\*  $\Delta R$  measured in detopped root systems using pressure chambers (i.e.  $\Delta R = \Delta R_{\text{root}}$ )

\*\*  $\Delta R$  measured in either root or shoot systems using the high flow pressure method

Leaving aside the contribution of  $\eta$ , the most widespread hypothesis in the literature explaining the reported chilling-induced  $\Delta R_{\text{root}}$  lies in biological



and metabolic changes in the radial water pathway from the soil-root interface to the xylem. Those changes can be associated with either membrane permeability, through aquaporin activity (Murai-Hatano et al. 2008; Aroca et al. 2011) and/or suberin deposition in the root endodermis (Lee et al. 2005). The experiments of Pavel and Fereres (1998) in young olive trees showed  $\Delta R_{\text{root}}$  occurring in less than three days, sustaining the hypothesis of reduced membrane permeability as suberin deposition should take longer (Enstone and Peterson 1997). Nevertheless, they found much lower  $\Delta R$  than those presented in this work (Table 5.1) which may point to additional factors (beyond both the cellular level and the short term) playing a role in our conditions. In this regard, the results observed in this study may be associated with alterations in root growth dynamics as they are affected by temperature as well (Kramer 1940; Wan et al. 1999; Pregitzer et al. 2000). In other words, low soil temperatures in winter may hinder root proliferation limiting the amount of absorbing roots, which, in turn, would lead to an increase in  $R_{\text{root}}$ . This hypothesis is to some extent supported by the observations of Fernández et al. (1992), who, working with mature olive trees subjected to different irrigation treatments, found decreases in root density of variable magnitude (depending on the treatment and point of measurement) during the winter months. As a final remark, cavitation in root xylem vessels might have played a role in the observed  $\Delta R_{\text{root}}$  but there seem to be few arguments to support this explanation under our experimental conditions. On the one hand, freeze-thaw-induced embolisms were unlikely because periods of frost (Fig. 5.1) were infrequent, mild (air temperatures not much below 0 °C), short in time (hours), and, above all, they should have affected distal shoots and branches rather than trunks or roots, whose temperature must be closer to that of the soil. On the other hand, one could argue that the low  $\Psi$  measured in winter might have originated cavitations in the large vessels of main roots and

trunks, but it should also have occurred in main branches and again translated into increases in the trunk to shoot  $R$  (i.e. the difference between  $R$  and  $R_{\text{root}}$  in Fig. 5.5) which were not clearly observed.

An interesting result of the present study is the huge variability found in the degree of disturbance of water relations between winters. Thus, values of both minimum midday  $\Psi$  and  $\Delta R$  were significantly lower and higher, respectively, in December 2011 - January 2012 than for the same months of 2012-2013 (Fig. 5.2 and 5.5). It should be stressed again that such differences appeared under non-limiting soil water conditions as evidenced by both the high  $RSWC$  and high predawn  $\Psi$  recorded for both years (rather low  $RSWC$  and predawn  $\Psi$  were evident by February 2012, but it did not correspond to the period with the highest  $\Delta R$ ; Fig. 5.2). Apart from that, the differences between winters in the December/January temperatures were not very marked (on average the second winter was 1.4 °C warmer in December-January, Fig. 5.1), which also points to a minor role of  $\eta$  as a cause for such observations. However, it is unknown whether such small difference in temperature leads to an equally small difference in membrane permeability or not. In this regard, many studies (e.g. Running and Reid 1980; Ameglio et al. 1990) have shown that  $R_{\text{root}}$  increases exponentially when root temperature falls below a threshold. Therefore, under certain circumstances, a small temperature decrease might result in a large  $\Delta R_{\text{root}}$ . Unfortunately, the relationship between  $R_{\text{root}}$  and root temperature is unknown in the case of olive, so it is not possible to quantify if the temperature differences between winters lead to significant differences in  $R_{\text{root}}$ . Finally, a reasonable hypothesis linking the inter-year differences in  $\Delta R_{\text{root}}$  with the alternate bearing behavior of olive trees can also be formulated. The higher fruit load in the first year (16.5 t ha<sup>-1</sup> in terms of fresh weight) could have resulted in lower carbon availability for root

turnover during winter, leading to the development of higher  $R_{\text{root}}$  and lower  $\Psi$  in relation to the second one (when the yield was lower, 5.2 t ha<sup>-1</sup>).

Regardless of the year being considered, our results revealed higher  $\Delta R$  than those previously reported (Table 5.1). The fact that our estimated  $\Delta R$  were higher than those reported by Pavel and Fereres (1998) in young olive plants suggests that the exposure to low temperatures might cause different effects between potted and field olive trees and underline that the reported responses with chilled young plants growing in controlled conditions are not necessarily the same that take place under natural conditions. Such discrepancies might be ascribed to differences in structural patterns (e.g. root architecture) or in the duration and conditions of experiments. For instance, Pavel and Fereres (1998) measured  $\Delta R$  in less than three days after trees were exposed to low soil temperatures, so long-term responses to chilling such as a decrease in the amount of absorbing roots, and suberization of endodermal cells are not expected to be captured. Moreover, additional factors typically absent in young trees but present in our experimental conditions (e.g. presence of fruits) might also play a role.

Another intriguing observation arises when the patterns of  $R$  or  $R_{\text{root}}$  (Fig. 5.5) are compared with those of air or soil temperatures (Fig. 5.1 and 5.6). Under similar temperature conditions, both  $R$  and  $R_{\text{root}}$  decreased significantly by February in relation to December-January. This phenomenon may be associated with acclimation processes allowing the trees to cope better with the low temperatures of the end of winter. In this context, it is well known that certain exposure to low temperatures provides protection against freeze and chilling stresses through changes in metabolism, most of them related to membrane lipids and proteins, and possibly including aquaporins (Fennel and Markhart 1998; Ahamed et al. 2012).

Finally, this study shows that the water relations in mature olive trees are altered during winter through increased  $R$ , but it remains unclear if such alterations can affect canopy conductance and gas exchange. Figure 5.2G-H shows a decline in  $G_s$  in winter which apparently supports the hypothesis of the direct effects on stomatal aperture. Nevertheless, the low winter  $G_s$  found in this work may be related to different factors. For instance, photosynthesis rates could be limited by the low temperatures of winter inducing stomata to close, which would concur with the delay in the recovery of  $G_s$  in 2011-2012 versus 2012-2013.

## **5.5. Conclusions**

This study show for the first time that winter low temperatures lead to a disturbance of water relations in field olive trees. Chilling induced an increase in  $R$  that resulted in midday  $\Psi$  falling to lower values than those expected for well-irrigated trees in summer, despite evaporative demand being substantially lower during our experiments. Apparently, measurements of predawn  $\Psi$  and estimates of  $RSWC$  indicated that this phenomenon took place under non-limiting conditions of soil water availability. Besides that, our estimated chilling-induced increases in either  $R$  were higher than those previously reported for young potted trees growing under controlled conditions. This, along with additional findings, such as differences in the chilling effects between winters or the lags between the peaks of  $R$  and temperature suggest that the phenomenon is more complex and involves a greater number of factors in the case of mature trees.



### **Acknowledgements**

This work was funded by the Spanish Ministry of Science and Innovation (MICINN, project AGL-2010-20766) and European Regional Development Fund (ERDF). We thank the Spanish Research Council (CSIC) predoctoral JAE program and the aforementioned project for providing the Ph.D. scholarship granted to the first and second author, respectively. We are grateful both to Ms Julie Newton for helpful assistance with language editing and to Mr Rafael del Río, Mr Ignacio Calatrava and Mr José Luis Vazquez for the excellent technical support provided.

## References

- Ahamed A, Murai-Hatano M, Ishikawa-Sakurai J, Hayashi H, Kawamura Y, Uemura M (2012) Cold stress-induced acclimation in rice is mediated by root-specific aquaporins. *Plant Cell Physiol* 53: 1445-1456.
- Allen RG, Pereira JS, Raes D, Smith M (1998) Crop evapotranspiration: guidelines for computing crop water requirements. FAO Irrigation and Drainage Paper, 56. Food and Agriculture Organization of the United Nations, Rome 300 pp.
- Améglio T, Morizet J, Cruiziat P, Martignac M (1990) The effects of root temperature on water flux, potential and root resistance in sunflower. *Agronomie* 10: 331-340.
- Angelopoulos K, Dichio B, Xiloyannis C (1996) Inhibition of photosynthesis in olive trees (*Olea europaea* L.) during water stress and rewatering. *J Exp Bot* 47:1093-1100.
- Aroca R, Porcel R, Ruiz-Lozano JM (2011). Regulation of root water uptake under abiotic stress conditions. *J Exp Bot* 63: 43-57.
- Aroca R, Tognoni F, Irigoyen JJ, Sánchez-Díaz M, Pardossi A (2001) Different root low temperature response of two maize genotypes differing in chilling sensitivity. *Plant Physiol Bioch* 39: 1067-1073.
- Bloom AJ, Zwieniecki MA, Passioura JB, Randall LB, Holbrook NM, Clair DAST (2004) Water relations under root chilling in a sensitive and tolerant tomato species. *Plant Cell Environ* 27: 971-979.
- Boughalleb F, Hajlaoui H (2011) Physiological and anatomical changes induced by drought in two olive cultivars (cv Zalmati and Chemlali). *Acta Physiol Plant* 33:53-65.
- Charrier G, Améglio T (2011) The timing of leaf fall affects cold acclimation by interactions with air temperature through water and carbohydrate contents. *Environ Exp Bot* 72: 351-357.

- Charrier G, Poirier M, Bonhomme M, Lacoïnte A, Améglio T (2013) Frost hardiness in walnut trees (*Juglans regia* L.): How to link physiology and modeling? *Tree Physiol* 33: 1229-1241.
- Cochard H, Martin R, Gross P, Bogeat-Triboulot MB (2000) Temperature effects on hydraulic conductance and water relations of *Quercus robur* L. *J Exp Bot* 51: 1255-1259.
- Connor DJ (2005) Adaptation of olive (*Olea europaea* L.) to water-limited environments. *Aust J Agr Res* 56: 1181-1189.
- Dichio B, Montanaro G, Sofo A, Xiloyannis C (2013) Stem and whole-hydraulics in olive (*Olea europaea*) and kiwifruit (*Actinidia deliciosa*). *Trees* 27: 183-191.
- Enstone DE, Peterson CA (1997) Suberin deposition and band plasmolysis in the corn (*Zea mays* L.) root exodermis. *Can J Bot* 75: 1188-1199.
- Fennell A, Markhart AH (1998) Rapid acclimation of root hydraulic conductivity to low temperature. *J Exp Bot* 49: 879-884.
- Fernández JE, Cuevas MV (2010) Irrigation scheduling from stem diameter variations: a review. *Agr Forest Meteorol* 150: 135-151.
- Fernández JE, Moreno F, Girón IF, Blázquez OM (1997) Stomatal control of water use in olive tree leaves. *Plant Soil* 190: 179-192.
- Fernández JE, Moreno F, Martín-Aranda J, Fereres E (1992) Olive-tree root dynamics under different soil water regimes. *Agr Med Vol* 122:225-235.
- Fernández JE, Moreno F, Martín-Palomo MJ, Cuevas MV, Torres-Ruiz JM, Moriana A (2011) Combining sap flow and trunk diameter measurements to assess water needs in mature olive orchards. *Environ Exp Bot* 72: 330-338.
- Hertel A, Steudle E (1997) The function of water channels in *Chara*: The temperature dependence of water and solute flows provide evidence for composite membrane transport and for a slippage of small organic solutes across water channels. *Planta* 202: 324-335.



- Iniesta F, Testi L, Orgaz F, Villalobos FJ (2009). The effects of regulated and continuous deficit irrigation on the water use, growth and yield of olive trees. *Eur J Agron* 30: 258-265.
- Kramer PJ (1940) Root resistance as a cause of decreased water absorption by plants at low temperatures. *Plant Physiol* 15: 63-79.
- Kramer PJ (1942) Species differences with respect to water absorption at low soil temperatures. *Am J Bot* 29: 828-832.
- Lee SH, Chung GC, Steudle E (2005) Gating of aquaporins by low temperature in roots of chilling-sensitive cucumber and chilling-tolerant figleaf gourd. *J Exp Bot* 56: 985-995.
- López-Bernal A, Alcantara E, Testi L, Villalobos FJ (2010) Spatial sap flow and xylem anatomical characteristics in olive trees under different irrigation regimes. *Tree Physiol* 30: 1536-1544.
- López-Bernal A, Testi L, Villalobos FJ (2012) Using the compensated heat pulse method to monitor trends in stem water content in standing trees. *Tree Physiol* 32: 1420-1429.
- Moriana A, Orgaz F, Pastor M, Fereres E (2003) Yield responses of a mature olive orchard to water deficits. *J Am Soc Hortic Sci* 128: 425-431.
- Murai-Hatano M, Kuwagata T, Sakurai J, Nonami H, Ahmed A, Nagasuga K, Matsunami T, Fukushi K, Maeshima M, Okada M (2008) Effect of low root temperature on hydraulic conductivity of rice plants and the possible role of aquaporins. *Plant Cell Physiol* 49: 1294-1305.
- Norisada M, Hara M, Yagi H, Tange T (2005) Root temperature drives winter acclimation of shoot water relations in *Cryptomeria japonica* seedlings. *Tree Physiol* 25: 1447-1455.
- Orgaz F, Testi L, Villalobos FJ, Fereres E (2006) Water requirements of olive orchards-II: determination of crop coefficients for irrigation scheduling. *Irrigation Sci* 24, 77-84.
- Passioura JB (2006) The perils of pot experiments. *Funct Plant Biol* 33, 1075-1079.

- Pavel EW, Fereres E (1998) Low soil temperatures induce water deficits in olive (*Olea europaea*) trees. *Physiol plantarum* 104: 525-538.
- Pérez-López D, Gijón MC, Mariño J, Moriana A (2010) Water relation response to soil chilling of six olive (*Olea europaea* L.) cultivars with different frost resistance. *Span J Agric Res* 8: 780-789.
- Pregitzer KS, King JS, Burton AJ, Brown SE (2000) Responses of tree fine roots to temperature. *New Phytol* 147: 105-115.
- Roderick ML, Berry SL (2001) Linking wood density with tree growth and environment: a theoretical analysis based on the motion of water. *New Phytol* 149: 473-485.
- Running SW, Reid CP (1980) Soil temperature influences on root resistance of *Pinus contorta* seedlings. *Plant Physiol* 65: 635-640.
- Steudle E (2000) Water uptake by roots: effects of water deficit. *J Exp Bot* 51:1531-1542.
- Swanson RH, Whitfield WA (1981) A numerical analysis of heat pulse velocity theory and practice. *J Exp Bot* 32: 221-239.
- Testi L, Villalobos FJ (2009) New approach for measuring low sap velocities in trees. *Agr Forest Meteorol* 149: 730-734.
- Testi L, Villalobos FJ, Orgaz F (2004) Evapotranspiration of a young irrigated olive orchard in southern Spain. *Agr Forest Meteorol* 121: 1-18.
- Testi L, Villalobos FJ, Orgaz F, Fereres E (2006) Water requirements of olive orchards: I simulation of daily evapotranspiration for scenario analysis. *Irrigation Sci* 24: 69-76.
- Tognetti R, Giovannelli A, Lavini A, Morelli G, Fragnito F, d'Andria R (2009) Assessing environmental controls over conductances through the soil-plant-atmosphere continuum in an experimental olive tree plantation of southern Italy. *Agr Forest Meteorol* 149: 1229-1243.
- Torres-Ruiz JM, Diaz-Espejo A, Morales-Sillero A, Martin-Palomo MJ, Mayr S, Beikircher B, Fernandez JE (2013) Shoot hydraulic

characteristics, plant water status and stomatal response in olive trees under different soil water conditions. *Plant Soil* 373: 77-87.

Villalobos FJ, Testi L, Orgaz F, García-Tejera O, López-Bernal A, González-Dugo MV, Ballester-Lurbe C, Castel JR, Alarcón-Cabañero JJ, Nicolás-Nicolás E, Girona J, Marsal J, Fereres E (2013) Modelling canopy conductance and transpiration of fruit trees in Mediterranean areas: a simplified approach. *Agric For Meteorol* 171:93-103.

Wan X, Landhäusser SM, Zwiazek JJ, Lieffers VJ (1999). Root water flow and growth of aspen (*Populus tremuloides*) at low root temperatures. *Tree Physiol* 19: 879-884.

Wan X, Zwiazek JJ, Lieffers VJ, Landhäusser SM (2001) Hydraulic conductance in aspen (*Populus tremuloides*) seedlings exposed to low root temperatures. *Tree Physiol* 21: 691-696.

Yamamoto R (1995) Dependence of water conductivity on pressure and temperature in plant stems. *Biorheology* 32: 421-430.





## **Chapter 6**

### **General discussion and final remarks**

---

## Chapter 6

### General discussion and final remarks

#### 6.1. General discussion

Because of their capacity to determine tree transpiration ( $E_p$ ), sap flow methods are increasingly drawing attention from scientists belonging to different disciplines, including hydrology, ecology, forestry and agronomy. Apart from their suitability as research tools, in an agronomical context they are expected to play a central role in the development of smart irrigation control systems (Fernández et al. 2001). Therefore, understanding the limitations and exploring the full potential of these techniques have become of paramount importance. In this regard, the results presented in this thesis show that sap flow methods have a huge potential but they still face many challenges that should be better addressed.

Many studies have focused on the effects of water stress on  $E_p$  and the possibility of using sap flow methods to derive indicators of water status (Jones 2004; Tognetti et al. 2004; Nadezhdina et al. 2007; Tognetti et al. 2009; López-Bernal et al. 2010; Cuevas et al. 2013) and they have been also employed to quantify stomatal conductance ( $G_s$ ) (Villalobos et al. 2013). The aim of Chapter 2 was to go one step further and propose a methodology to estimate net assimilation ( $A$ ) combining the information provided by sap flow methods and meteorological data. The measurement of  $A$  is of paramount interest, particularly for agronomists, because it represents a direct indicator of the biomass accumulation rate. Despite its importance, the existing measurement techniques are not easy to use. On the one hand, both leaf cuvette gas analyzers (Moriani and Fereres 2002) and large canopy chambers (Pérez-Priego et al. 2010; Villalobos et al. 2012) are labour-intensive and time-consuming measuring devices. Besides

that, the former is challenged because scaling-up the measurements to the canopy-level is tricky, while the later requires complex instrumentation and its use is unwieldy under certain conditions (e.g. tall trees, hedgerow orchards). As an alternative, the eddy covariance technique allows for the monitoring of net ecosystem exchange (NEE, which integrates the balance between both raw assimilation and soil and plant respiration at the orchard-level) and is suitable for automation, but it relies on strong assumptions on the turbulence structure and can only be applied for large, uniform and flat plots (Pérez-Priego 2011). In this context, the methodology described in Chapter 2 overcomes the aforementioned handicaps, as it is automatable and easy to implement, works at the canopy-level and does not require special orchard or tree characteristics. Furthermore, the results of our field experiments were promising: a close agreement was found between the estimates of  $A$  and independent measurements of NEE (Fig. 2.3), which suggests that the method is reliable to monitor, at least, rough estimates of  $A$ . The ‘at least’ in the previous sentence comes from the fact that our approach is not entirely flawless, as it both requires accurate  $E_p$  records and is prone to errors in those species exhibiting marked variations in the intercellular  $\text{CO}_2$  concentration ( $C_i$ ) in response to changing water status. The development of user-friendly calibration procedures for sap flow methods and further research on the species-specific effects of water stress on  $C_i$  are, therefore, the two foundations for improving the accuracy and extending the validity of the proposed methodology in the future.

Chapter 4 covered a mixture of issues and could be actually divided into two separate parts. On the one hand, a first section (Experiment 1) focused on the characterization of sapwood thermal properties for a number of fruit tree species. Thermal properties were determined through different methodologies including the model of Siau (1971) and its recently improved version (Vandegehuchte and Steppe 2012a) as well as two



thermometric methods based on the use of dual-probe sap flow sensors: the Tmax method (Cohen et al. 1981; Kluitenberg and Ham 2004) and the semi-analytical solution of Knight et al. (2012). Regardless of the methodology employed, large differences in thermal properties were found between species (Fig. 4.2), which were ascribed to differences in the physical and anatomical characteristics of sapwood (Fig. 4.1). From a practical viewpoint, however, the most transcendental result of this section laid in the differences observed between the methods employed for determining thermal properties, because both the Tmax (Cohen et al. 1981; Kluitenberg and Ham 2004) and the heat ratio methods (HR, Burgess et al. 2001) require an estimate of thermal diffusivity in the axial direction ( $D_x$ ) to proceed with the calculation of convective heat velocity ( $v_h$ ). In the former heat pulse method,  $D_x$  is calculated under zero flow conditions through Eq. 4.7 while the later typically estimates it applying the model of Siau (1971). Both approaches –and also that of Knight et al. (2012)– exhibited moderate deviations in relation to the most theoretically correct approach (i.e. the model by Vandegehuchte and Steppe (2012a)) (Fig. 4.3, Table 4.1). Such differences indicate, therefore, that the accuracy of both the Tmax and HR might be fairly compromised by the approach followed to determine  $D_x$ .

On the other hand, both the second part of Chapters 4 (Experiment 2) and Chapter 3, dealt with the practical importance of measuring sapwood water content ( $F_w$ ) for sap flow research. Apart from its value as an indicator of water status (Nadler et al. 2003; Nadler et al. 2006; Hernández-Santana et al. 2008; Chapter 3),  $F_w$  is important because it is a prerequisite in the conversion from  $v_h$  to sap flux density ( $J$ ) in all heat-pulse methods (Eq. 1.1). Moreover, an estimate of  $F_w$  is needed to apply the models of Siau (1971) (Eqs. 4.3 and 4.4) and Vandegehuchte and Steppe (2012a)

(Eqs. 4.5 and 4.6), which, as mentioned above, represents a previous step in the calculation of  $v_h$  by HR (Burgess et al. 2001).

The available techniques for determining  $F_w$  in trees include gamma-ray attenuation (Edwards and Jarvis 1983), nuclear magnetic resonance (Byrne et al. 1986; Van As et al. 2009), electrical conductivity (Nadler and Tyree 2008; Nadler et al. 2008), time domain reflectometry (TDR, Constantz and Murphy 1990; Wullschleger et al. 1996) and the traditional gravimetric approach based on core sampling. While the first three show serious drawbacks that make them impractical for field measurements, TDR only yields sound results in expert hands and struggle to account for the spatial variability of sapwood. As a consequence, the labour-intensive core sampling method remains as the most widespread technique. Unfortunately, the harmful nature of this technique have led the users of heat pulse methods to perform a limited number of  $F_w$  determinations (typically only one) during the measurement period, which implies disregarding its possible variations. These circumstances have led several research teams to develop new techniques aimed to employ sap flow sensors for indirectly estimating  $F_w$ . Until now, three methodologies have been reported in the literature including those described in Vandegehuchte and Steppe (2012b), Knight et al. (2012) and the one presented in the Chapter 3 of this thesis. Their main strengths and weaknesses are discussed below and summarized in Table 6.1.

Vandegehuchte and Steppe (2012b) presented a new heat pulse sap flow method referred to as Sapflow+. At the cost of a greater number of needles (four) per sensor, Sapflow+ allows for estimating simultaneously  $v_h$ , volumetric specific heat ( $\rho c$ ) and thermal conductivities in both axial ( $K_x$ ) and tangential ( $K_y$ ) directions. Once  $\rho c$  is known, the value of  $F_w$  can be deduced from Eq. (4.8). However, the methodology has not yet been tested

in standing trees and the results of a finite element modelling exercise demonstrated that accurate estimates of  $F_w$  are only yielded under low flow conditions (Vandegehuchte and Steppe 2012b).

**Table 6.1.** Strengths and weaknesses of the available methods for estimating  $F_w$  using sap flow sensors.

Method	Strengths	Weaknesses
Sapflow+ (Vandegehuchte and Steppe 2012b)	- Theoretically sound	- Complex sensors - Not valid for high $v_h$ - Tests on living trees lacking
Semi-analytical solution (Knight et al. 2012)	- Applicable to any heat pulse sap flow system - Theoretically sound	- Only valid when $v_h = 0$ - Questionable reliability (Chapter 4)
VSH-CHP (Chapter 3)	- Theoretically valid for any value of $v_h$	- Do not provide absolute values unless independent calibration is performed - Poor reliability for large $F_w$ variations

Knight et al. (2012) derived a semi-analytical solution that, accounting for probe radius and heat capacity, allows the calculation of sapwood thermal properties (including  $\rho c$ , from which  $F_w$  can be deduced) using dual heat pulse probes. This methodology is, therefore, applicable to any heat-pulse sap flow method (provided that absolute temperatures are measured for each temperature probe), and considers for the first time in sap flow research that the finite volume occupied by probes present different heat capacity than that of the sapwood into which they are installed. By contrast,

the semi-analytical solution is limited by the fact that it was derived for zero-flow conditions. Chapter 4 (Experiment 1) shows the first tests of this methodology in living plants, restricting the determinations to the hours previous to dawn to ensure zero or negligible flows. In relation to gravimetric approaches, the Knight et al. (2012)'s approach overestimated the values of  $\rho c$ , and hence of  $F_w$  (Table 4.1). Although our results were not encouraging, it should be indicated that the discrepancies found might be attributed to low nocturnal sap flow rates, small misalignments of probes and/or actual differences in  $F_w$  between the points chosen for core sampling and those where probes were installed.

Finally, the VSH-CHP method described in Chapter 3 was developed to use compensated heat pulse (CHP) sensors for concurrently measuring  $F_w$  and  $v_h$ . Both lab and field experiments evidenced that VSH-CHP was suitable for monitoring relative variations in  $F_w$ . On the contrary, it was unable to provide absolute  $F_w$  values (Fig. 3.2), which is a serious limitation because calibration would require carrying out additional determinations through core sampling or TDR. Also, our lab experiments raised concerns about the reliability of the method on species with large temporal fluctuations in  $F_w$ . Finally, a further issue arises due to the fact that the working equation (Eq. 3.6) of VSH-CHP includes the anisotropy ratio ( $R_K$ , i.e. the ratio of  $K_x$  to  $K_y$ ) as a constant, while both Siau (1971) and Vandegehuchte and Steppe (2012a) models predict changes in  $R_K$  with  $F_w$ . Fortunately, this theoretical flaw is very likely to have a minimal impact on the accuracy of the method because both the expected variations of  $F_w$  in most living trees are generally small (Nadler and Tyree 2008) and it is the square root of  $R_K$  ( $\delta$ ) which actually appears in Eq. 3.6.

The three methods can be considered great technical advances in sap flow research, all being promising approaches to monitor seasonal changes in  $F_w$

and hence in water status. By contrast, none of them seem practical for continuously providing accurate  $F_w$  values, which, as indicated above, would be of major interest for achieving a more correct calculation of  $J$ . Perhaps a combination of gravimetric determinations with the VSH-CHP method may be a suitable alternative when working with CHP sensors, but it still deserves further research. Consequently, most users of heat pulse methods will continue measuring  $F_w$  through core sampling and assuming it constant for  $J$  calculations in forthcoming years.

In this context, the second part of Chapter 4 (Experiment 2) provides an experimental assessment of the errors arising from ignoring the natural variations in  $F_w$ . To do so, desorption curves of sapwood were constructed for four fruit tree species from core samples (Fig. 4.4), enabling us to predict the relative errors in the calculation of  $J$  ( $E_J$ ) as a function of varying water potential ( $\Psi$ ) (Fig. 4.5), whose measurement pose lesser problems and is more extended and repeatable. As illustrated in both Figures 4.5 and 4.6 and Table 4.2, substantial  $E_J$  were deduced, and their magnitude depended on the heat pulse method and species considered. For instance, HR was the least vulnerable heat pulse method followed by Sapflow+, CHP and CAG, while Tmax was the one with the highest sensitivity to  $\Psi$  or  $F_w$  variations. Likewise, considering the same  $\Psi$  change, the predicted  $E_J$  were lower for almond than for olive, fig and orange (Fig. 4.5).

In short, the results of Chapter 4 (Experiment 2) suggest that the accuracy of heat pulse methods is significantly hindered by the assumption of constant  $F_w$ , even at daily scales (Table 4.2). As discussed in the final paragraph of section 4.4.3, several alternatives can be undertaken to cope with the  $E_J$  associated to  $F_w$  variations, but neither of them is actually free from drawbacks. At least, the errors in the daily estimates of  $E_p$  can be

substantially minimized if core sampling is conducted by midday because  $E_J$  will concentrate in periods of low flows (late evening, night and early morning).

Finally, Chapter 5 presents a practical example of how sap flow sensors can improve our understanding of water relations. In particular, this chapter was devoted to study the dynamics of water status in mature olive trees over the course of two winters. Previous studies (Kramer 1940; Running and Reid 1980; Pavel and Fereres 1998; Wan et al. 2001) conducted under controlled conditions with young plants of a number of species (including olive) had shown that the exposure to chilling soil temperatures frequently resulted in water stress symptoms, even in the absence of soil water deficits. Nevertheless, there was no evidence that the phenomenon took place at field conditions so far. Such gap in the literature was probably associated with the difficulties of measuring sap flow ( $Q$ ) in field plants under low evaporative demand conditions. This challenge was overcome in our study by the use of CHP sensors applying the calibrated average gradient procedure (CAG, Testi and Villalobos 2009).

The results of Chapter 5 confirmed the occurrence of water stress symptoms in the absence of soil water deficits by early winter (Fig. 5.2). This was mainly evidenced by midday  $\Psi$  reaching lower values than those typically found in irrigated trees of the same cultivar in summer under a much higher evaporative demand (see e.g. Iniesta et al. 2009). In accordance with previous studies (Running and Reid 1980; Pavel and Fereres 1998; Wan et al. 2001; Aroca et al. 2011), the disturbance of water relations was attributed to an increase in the hydraulic resistance of the soil-to-shoot continuum ( $R$ ). Also, Figure 5.4 indicated that the largest proportion of such increase apparently occurred in the soil-to-trunk water pathway, which points to changes in membrane permeability and root

growth dynamics as the most likely causes behind it. Apart from these general observations, our study yielded some intriguing results that raise new questions about chilling stress responses in field trees. For example, Figures 5.2 and 5.4 illustrate that there was an enormous difference in the disturbance of water relations between the two years of study, and Table 5.2 shows that, regardless of the year considered, our estimated increases in  $R$  were higher than any previously published report. These facts suggest that the reported effects of chilling on young potted trees may differ from those actually occurring in orchards. Another interesting result was the lag found between the maximum  $R$  values and the minimums of air and soil temperatures (Figures 5.1, 5.5), which might be indicative of acclimation processes allowing the trees to cope better with the low winter temperatures after a prolonged exposure to stressful conditions.

To sum up, Chapter 5 provides the first evidences of chilling stress in mature olive trees and opens the door for further research on this topic in olive and other perennial fruit tree species. Some relevant questions to answer in future investigations include: What are the actual factors triggering the low temperature-induced  $\Delta R$  in field trees? What is originating the inter-annual differences? Do field (olive) trees experience a real acclimation to low temperatures? Has the chilling stress a significant effect on gas exchange during winter? Are other perennial fruit tree species vulnerable to chilling stress?

## **6.2. Conclusions**

1. A combined use of meteorological data and sap flow methods can provide a user-friendly alternative to determine canopy net assimilation in tree species. Nevertheless, the reliability of the proposed procedure is

uncertain for species with marked variations in leaf intercellular CO<sub>2</sub> concentration in response to changing water status and is constrained by the availability of accurate input data.

2. Applying the methodology developed in Chapter 2, compensated heat pulse sensors can concurrently provide information about sapwood water content and sap flow dynamics. Although our lab and field experiments demonstrated the suitability of the method to monitor relative changes in sapwood water content, accurate absolute values cannot be obtained unless independent calibration is conducted. Besides that, the reliability of our approach is uncertain for those species exhibiting large temporal fluctuations in sapwood water content.

3. The use of the classical equations for determining sapwood thermal diffusivity in the axial direction when applying the heat ratio and the T<sub>max</sub> heat pulse techniques might lead to deviations affecting the accuracy of these heat pulse methods. These errors can be theoretically avoided by using the model of Vandegehuchte and Steppe (2012a) from measurements of basic density and water content of sapwood.

4. The accuracy of heat pulse methods is compromised by natural changes in sapwood water content. Ignoring seasonal and daily variations in sapwood water content might result in large errors in calculated sap flux density whose extent depends on the species and the heat pulse method. In this regard, the heat ratio method presents the lowest loss of accuracy followed by Sapflow+, compensated heat pulse and calibrated average gradient, while T<sub>max</sub> is the most prone to high errors.

5. The low temperatures of winter result in a disturbance of water relations in mature olive trees under non-limiting conditions of soil water content. Such disturbance was evidenced by unforeseen low midday water potential



and triggered by an increase in the hydraulic resistance of the water pathway from soil to shoots.

6. Compared to previous studies, our estimated increases in the soil-to-shoot hydraulic resistance were higher than those found for young potted trees growing under controlled conditions. This, along with additional results such as the different chilling stress in the two years or the apparent lags between the peaks of soil-to-shoot hydraulic resistance and temperature suggest that the phenomenon is more complex and involves a greater number of factors in the case of mature trees.

## **References**

- Aroca R, Porcel R, Ruiz-Lozano JM (2011) Regulation of root water uptake under abiotic stress conditions. *J Exp Bot* 63:43-57.
- Burgess SSO, Adams MA, Turner NC, Beverly CR, Ong CK, Khan AA, Bleby TM (2001) An improved heat pulse method to measure low and reverse rates of sap flow in woody plants. *Tree Physiol* 21:589-598.
- Byrne GF, Fenn MD, Burgar MI (1986) Nuclear magnetic resonance studies of water in tree sections. *Agric For Meteorol* 38:307-317.
- Cohen Y, Fuchs M, Green GC (1981) Improvement of the heat pulse method for determining sap flow in trees. *Plant Cell Environ* 4:391-397.
- Constantz J, Murphy F (1990) Monitoring moisture storage in trees using time domain reflectometry. *J Hydrol* 119:31-42.
- Cuevas MV, Martín-Palomo MJ, Díaz-Espejo A, Torres-Ruiz JM, Rodríguez-Dominguez CM, Perez-Martin A, Pino-Mejías R, Fernández JE (2013) Assessing water stress in a hedgerow olive orchard from sap flow and trunk diameter measurements. *Irrig Sci* 31:729-746.
- Edwards WRN, Jarvis PG (1983) A method for measuring radial differences in water content of intact tree stems by attenuation of gamma radiation. *Plant Cell Environ* 6:255-260.
- Fernández JE, Palomo MJ, Díaz-Espejo A, Clothier BE, Green SR, Girón IF, Moreno F (2001) Heat-pulse measurements of sap flow in olives

- for automating irrigation: tests, root flow and diagnostics of water stress. *Agric Water Manag* 51:99-123.
- Hernández-Santana V, Martínez-Fernández J, Morán C, Cano A (2008) Response of *Quercus pirenaica* (melojo oak) to soil water deficit: a case study in Spain. *Eur J Forest Res* 127:369-378.
- Iniesta F, Testi L, Orgaz F, Villalobos FJ (2009). The effects of regulated and continuous deficit irrigation on the water use, growth and yield of olive trees. *Eur J Agron* 30:258-265.
- Jones HG (2004) Irrigation scheduling: advantages and pitfalls of plant-based methods. *J Exp Bot* 55:2427-2436.
- Kluitenberg GJ, Ham JM (2004) Improved theory for calculating sap flow with the heat pulse method. *Agric For Meteorol* 126:169-173.
- Knight JH, Kluitenberg GJ, Kamaï T, Hopmans JW (2012) Semianalytical solution for dual-probe heat-pulse applications that accounts for probe radius and heat capacity. *Vadose Zone J* 11. doi:10.2136/vzj2011.0112.
- Kramer PJ (1940) Root resistance as a cause of decreased water absorption by plants at low temperatures. *Plant Physiol* 15:63-79.
- López-Bernal A, Alcántara E, Testi L, Villalobos FJ (2010) Spatial sap flow and xylem anatomical characteristics in olive trees under different irrigation regimes. *Tree Physiol* 30:1536-1544.
- Moriana A, Fereres E (2002) Plant indicators for scheduling irrigation of young olive trees. *Irrig Sci* 21:83-90.

*General discussion and final remarks*

Nadezhdina N, Nadezhdin V, Ferreira MI, Pitacco A (2007) Variability with xylem depth in sap flow in trunks and branches of mature olive trees. *Tree Physiol* 27:105-113.

Nadler A, Raveh E, Yemiyahu U, Green SR (2003) Evaluation of TDR use to monitor water content in stem of lemon trees and soil and their response to water stress. *Soil Sci Soc Am J* 67:437-488

Nadler A, Raveh E, Yemiyahu U, Green SR (2006) Stress induced water content variations in mango stem by time domain reflectometry. *Soil Sci Soc Am J* 70:510-520.

Nadler A, Tyree MT (2008) Substituting stem's water content by electrical conductivity for monitoring water status changes. *Soil Sci Soc Am J* 72:1006-1013.

Nadler A, Raveh E, Yermiyahu U, Lado M, Nasser A, Barak M, Green SR (2008) Detecting water stress in trees using stem electrical conductivity measurements. *Soil Sci Soc Am J* 72:1014-1024.

Pavel EW, Fereres E (1998) Low soil temperatures induce water deficits in olive (*Olea europaea*) trees. *Physiol plantarum* 104:525-538.

Pérez-Priego O, Testi L, Orgaz F, Villalobos FJ (2010) A large closed canopy chamber for measuring CO<sub>2</sub> and water vapour exchange of whole trees. *J Exp Bot* 68:131-138.

Pérez-Priego O (2011) El secuestro del carbono y la productividad del agua en el olivar. Tesis doctoral, Universidad de Córdoba, 120 pp.

Testi L, Villalobos FJ (2009) New approach for measuring low sap velocities in trees. *Agric For Meteorol* 149:730-734.

- Running SW, Reid CP (1980) Soil temperature influences on root resistance of *Pinus contorta* seedlings. *Plant Physiol* 65:635-640.
- Siau JF (1971) Flow in wood. In: Côté WA (ed) Syracuse wood science series. Syracuse University Press, New York, pp 131.
- Tognetti R, d'Andria R, Morelli G, Calandrelli D, Fragnito F (2004) Irrigation effects on daily and seasonal variations of trunk sap flow and leaf water relations in olive trees. *Plant Soil* 263:249-264.
- Tognetti R, Giovanelli A, Lavini A, Morelli G, Fragnito F, d'Andria R (2009) Assessing environmental controls over conductances through the soil-plant-atmosphere continuum in an experimental olive tree plantation of southern Italy. *Agric For Meteorol* 149:1229-1243.
- Van As H, Scheenen T, Vergeldt FJ (2009) MRI of intact plants. *Photosynth Res* 102:213-222.
- Vandegheuchte MW, Steppe K (2012a) Improving sap flux density measurements by correctly determining thermal diffusivity, differentiating between bound and unbound water. *Tree Physiol* 32:930-942.
- Vandegheuchte MW, Steppe K (2012b) Sapflow+: a four-needle heat pulse sap flow sensor enabling nonempirical sap flux density and water content measurements. *New Phytol* 196:306-317.
- Villalobos FJ, Perez-Priego O, Testi L, Morales A, Orgaz F (2012) Effects of water supply on carbon and water exchange of olive trees. *Eur J Agron* 40:1-7.
- Villalobos FJ, Testi L, Orgaz F, García-Tejera O, López-Bernal A, González-Dugo MV, Ballester-Lurbe C, Castel JR, Alarcón-

*General discussion and final remarks*

Cabañero JJ, Nicolás-Nicolás E, Girona J, Marsal J, Fereres E (2013) Modelling canopy conductance and transpiration of fruit trees in Mediterranean areas: a simplified approach. *Agric For Meteorol* 171:93-103.

Wan X, Zwiazek JJ, Lieffers VJ, Landhäuser SM (2001) Hydraulic conductance in aspen (*Populus tremuloides*) seedlings exposed to low root temperatures. *Tree Physiol* 21: 691-696.

Wullschleger SD, Hanson PJ, Todd DE (1996) Measuring stem water content in four deciduous hardwoods with a time-domain reflectometer. *Tree Physiol* 16:809-815.



## Other scientific contributions

Other scientific contributions derived from the Doctoral Thesis are listed below:

### Peer reviewed publications in international journals

**López-Bernal A**, Alcántara E, Testi L, Villalobos FJ (2010) Spatial sap flow and xylem anatomical characteristics in olive trees under different irrigation regimes. *Tree Physiol* 30:1536-1544.

Villalobos FJ, Testi L, Orgaz F, García-Tejera O, **López-Bernal A**, González-Dugo MV, Ballester-Lurbe C, Castel JR, Alarcón-Cabañero JJ, Nicolás-Nicolás E, Girona J, Marsal J, Fereres E (2013) Modelling canopy conductance and transpiration of fruit trees in Mediterranean areas: a simplified approach. *Agric For Meteorol* 171:93-103.

Tejado I, Vinagre BM, Torres D, **López-Bernal A**, Villalobos FJ, Testi L, Podlubny I. Fractional approach for estimating sap velocity in trees. *Fract Calc Appl Anal* 18:479-494.

**López-Bernal A**, García-Tejera O, Vega V, Hidalgo JC, Testi L, Orgaz F, Villalobos FJ. Using sap flow measurements to estimate the effects of water stress on net assimilation in fruit orchards. *Irrig Sci*, under review.

### Communications at conferences

Villalobos FJ, Alcántara E, Testi L, **López-Bernal A** (2010) Spatial sap flow and xylem anatomical characteristics in olive trees under different irrigation regimes. *XXVIII International Horticultural Congress*, Lisbon, Portugal, 22-27 August 2010.

**López-Bernal A**, Testi L, Villalobos FJ (2012) Using the compensated heat pulse method to monitor the stem water content in standing trees. *XII Congress of the European Society for Agronomy*, Helsinki, Finland, 20-24 August 2012.

Villalobos FJ, Tejado I, **López-Bernal A**, Torres D, Testi L, Vinagre BM, Podlubny I (2013) Measurement of sapwood water content using the



compensated heat pulse technique. *IXth International Workshop on Sap Flow*, Ghent, Belgium, 4-7 June 2013.

**López-Bernal A**, Testi L, Villalobos FJ (2013) Oscillations in transpiration in young potted olive trees. *IXth International Workshop on Sap Flow*, Ghent, Belgium, 4-7 June 2013.

Tejado I, HosseinNia SH, Torres D, Vinagre BM, **López-Bernal A**, Villalobos FJ, Testi L, Podlubny I (2014) Fractional models for measuring sap velocities in trees. *International Conference on Fractional Differentiation and its Applications (ICFDA14)*, Catania, Italy, 23-25 June 2014.

García-Tejera O, **López-Bernal A**, Orgaz F, Villalobos FJ, Testi L (2014) Root distribution under different irrigation regimes. *XIIIth Congress of the European Society for Agronomy*, Debrecen, Hungary, 20-24 August 2014.

**López-Bernal A**, García-Tejera O, Orgaz F, Testi L, Villalobos FJ (2014) Olive bud dormancy is induced by low temperatures. *XIIIth Congress of the European Society for Agronomy*, Debrecen, Hungary, 20-24 August 2014.



